A STUDY OF GAS FLOW PATTERN, UNDERCUTTING AND TORCH MODIFICATION IN VARIABLE POLARITY PLASMA ARC WELDING

John C. McClure, Haihui (Ron) Hou

Department of Metallurgical and Materials Engineering

University of Texas at El Paso, El Paso, Texas 79968

Final Report for Contract # NAS8-39602

August 31, 1994

SUMMARY

A study on the plasma and shield gas flow patterns in variable polarity plasma arc (VPPA) welding was undertaken by shadowgraph techniques. Visualization of gas flow under different welding conditions was obtained.

Undercutting is often present with aluminum welds. The effects of torch alignment, shield gas flow rate and gas contamination on undercutting were investigated and suggestions made to minimize the defect.

A modified shield cup for the welding torch was fabricated which consumes much less shield gas while maintaining the weld quality.

The current torch was modified with a trailer flow for Al-Li welding, in which hot cracking is a critical problem. The modification shows improved weldability on these alloys.

1. INTRODUCTION

Plasma arc welding (PAW) is similar to gas tungsten arc (TIG) welding in that both processes use the same power supplies and the same non-consumable tungsten electrode. The major difference is that PAW uses a constricted nozzle which dramatically increases the plasma jet velocity and thus the energy density as well. Figure 1 shows the differences between the TIG and PAW welding process.

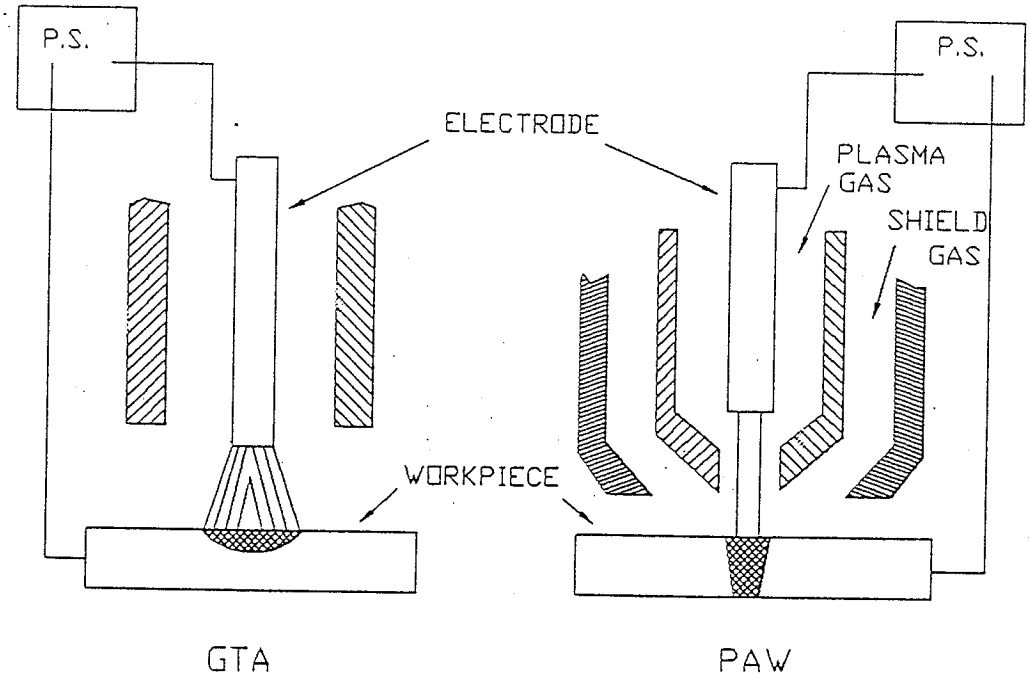

Figure 1 Comparison of TIG and PAW Welding Process

Plasma arc welding can be carried out in two modes: cover pass and keyhole. Less penetration is obtained in cover pass mode because of the relatively lower plasma jet velocity and smaller energy input. This mode is usually used to fill grooved joints or repair the joints after an initial pass. In keyhole mode the plasma

jet penetrates through the workpiece, forming a hole which then closes behind the plasma jet as a result of the surface tension and gravity. The major advantages of keyhole mode are better efficiency in terms of fewer weld passes and better quality because of the flushing action which purges the gases and contaminants that otherwise would be entrapped in the weld. Figure 2 is a schematic of the VPPA welding torch.

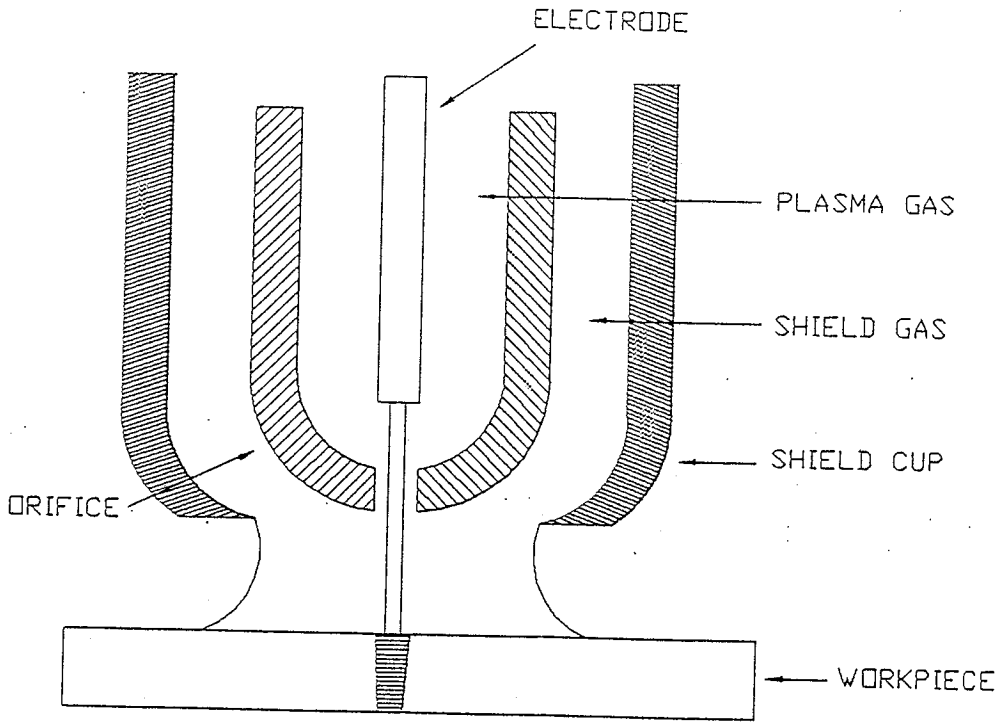

Figure 2 Schematic of Welding Torch in VPPA Welding

The electrode in Variable Polarity Plasma Arc Welding (VPPAW) alternates between positive and negative polarity. While the electrode is negative, which is called straight (or DCEN) polarity mode, the electrons in the plasma are accelerated toward the workpiece (anode) with a high velocity. Since the electrons carry the bulk

of the current, most of the heat is released on the workpiece and the workpiece is melted. At the same time, the positive ions drift much more slowly toward the electrode, and electrode deterioration is minimal.

During the reverse polarity mode (DECP), in which the electrode is positive, the massive positive ions move toward the workpiece. These ions clean the workpiece surface by so called cathodic cleaning.

Since the late 1960s, when it was first developed at the Boeing Company, the VPPA process has become commercially feasible. It is successfully used by NASA on the Space Shuttle external tank on aluminum 2219 with zero rejectable internal defects[1].

2. OBJECTIVES

In VPPA welding, the plasma gas transfers the energy to the workpiece. The shield gas is used to protect the weld pool from the atmosphere and can influence the stability of the arc, the occurrence of porosity and undercutting, and the metallurgical quality of the weld. The shape of these plasma and shield gas flows is a very important and interesting issue. A knowledge of these flows will help to understand the gas behavior during welding and is also a stepping stone for exploring the fundamental mechanisms affecting this behavior. A few investigators have visualized the shield gas flow during TIG and MIG with shadowgraph or schlieren techniques[2,3]. However, no similar research has been done in the VPPA process. The first objective of this work is to visualize the plasma and shield gas flow patterns

in VPPA welding.

Since undercutting can reduce load carrying capacity and produce stress risers that impair impact, fatigue or low-temperature service, undercutting is a serious defect. Finding the relation between torch alignment, undercutting, and different shielding conditions will be the second objective of this work.

The final objective is to modify the present welding torch design. The modification will help to improve the process performance and minimize welding defects such as undercutting and hot cracking especially in Al-Li welds.

3. INTRODUCTION TO SHADOWGRAPHY

Shadowgraphy is a standard flow visualization technique. A light beam is transmitted through a fluid field, and the visual pattern depends on the variation of the refractive index of the fluid.

The variation of the refractive index is caused by changes in fluid density. Density and index of refraction are correlated in the Gladstone-Dale relation:

$$n-1=K\rho$$

where n is the refractive index, ρ is the fluid density, and k is defined as the Gladstone-Dale constant, which has the dimension of $1/\rho$ and depends on the molar weight and resonant frequency as well as on the frequency of the gas and the wavelength of the light used.

The G-D equation can also be applied to mixtures, but ρ will be the density of the mixture, and k is the weighted constant for the mixture,

$$k = k_i w_i / w$$

where (w_i/w) equals the mass fractions of the components in the gas mixture.

In general, variations of the refractive index remain invisible to the naked eye and require certain optical methods to make such changes visible.

When a light beam passes through the test field with an inhomogeneous distribution of the refractive index, it will be altered. The changes with respect to the undisturbed case without flow are of two types: (1) the light is deflected from its original direction and (2) the phase of the disturbed light wave is shifted with respect to that of the undisturbed beam. Both these changes can be used to visualize the refractive index change. Shadowgraphy uses the first phenomenon to visualize flow pattern. Another visualization method, termed schlieren, employs the second one.

Considering Figure 3, when light passes through a test field with an inhomogeneous refractive index (density), the individual light rays are refracted and bent out of their original path. A particular deflected light ray can be traced and arrives at a point Q* of the recording plane instead of a point Q, so that the distribution of light intensity in that plane is altered with respect to the undisturbed cases, e.g., Q* receives more light than before, while no light arrives at Q, which can be regarded as the shadow of the respective object point. Therefore an image of the test field can be generated by imaging the displacement QQ^*.

Assuming that $I(x,y)$ denotes the light intensity distribution in the recording plane for the undisturbed case, whereas $I^*(x^*,y^*)$ is the intensity for the disturbed case, one can obtain[4]

$$\frac{I^*-I}{I}=\frac{\Delta I}{I}=l\int_{z1}^{z2}\left(\frac{\partial^2}{\partial x^2}+\frac{\partial^2}{\partial y^2}\right)(\ln n)\,dz$$

By applying the G-D formula which was introduced at the beginning of this section, it becomes evident that the shadowgraph is sensitive to changes in the second derivative of the gas density. In other words, if the refractive index in the test section is uniform, the screen will be uniformly illuminated. If there is a constant gradient of the refractive index, all rays will be equally deviated and there will be no change in the illumination of the screen. If, however, the gradient of n varies in space, i.e., if there is a second derivative of the refractive index, there will be variations in the illumination of the screen. For this reason, shadowgraphy is not a method suitable for quantitative measurement of the fluid density. Owing to its simplicity, however, shadowgraphy is a convenient method for obtaining a survey of flow fields with varying fluid density.

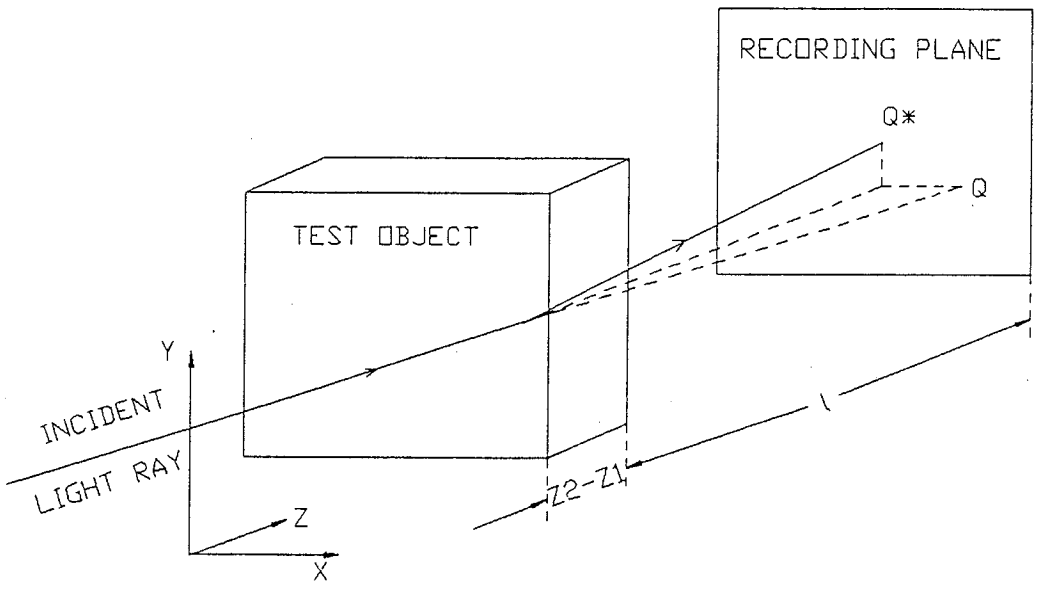

Figure 3 Deflection of a Light Ray in an Inhomogeneous Test Object.

A typical optical setup for shadowgraphy is shown in Figure 4. The elements include a light source, collimator which generates parallel light, test object, and recording plane. In order to avoid the use of too large a photographic plate, the recording plane can be focused by means of a camera lens onto a film or plate of reduced size.

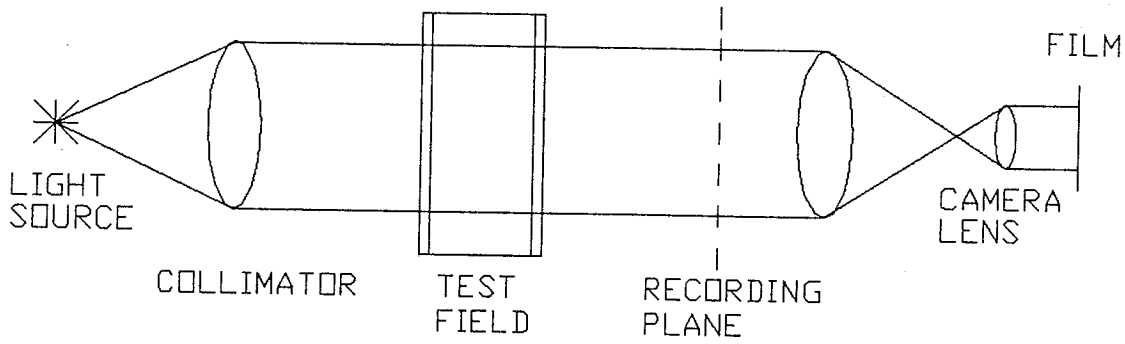

Figure 4 Shadowgraph System with Parallel Light through the Test Field.

4. SHADOWGRAPHYSYSTEM IN THIS WORK

In this experiment, a system similar to that shown in Figure 4 was used. The light source was a 10-mW He-Ne laser beam with a low divergence of 1.2 mrad. The beam of the laser tube (0.68mm in diameter) was made divergent by a spatial filter made up of a well corrected positive lens and a pinhole placed at the focus of that lens. This spatial filter assembly could produce a divergent point source of 25 microns in diameter with a smooth, nearly ideal intensity profile. By means of a plano-convex lens, the divergent beam was converted to a round parallel beam of a

diameter of 47mm.

For permanent recording of the shadows a PENTAX 35mm camera was used with a shutter time up to 1/1000 second. However, the regular lens of the camera is designed for forming the images of divergent light emitted from objects. The invisible gaseous flow will only deviate the light instead of emitting divergent light when a parallel beam is applied to the flow field. Then the outer rays at the periphery can be blocked by the aperture of the lens or the aperture diaphragm, and one does not obtain a complete image of the field.

This problem was solved by using of an extra positive lens (combination of three Promaster Spectrum 7 close-up lenses $+1, +4,$ and $+4$ diopters) placed in front of the camera. This lens converged the beam in such a way that no ray was obstructed by either the aperture of the lens or the aperture diaphragm. A schematic of this optical arrangement is drawn in Figure 5.

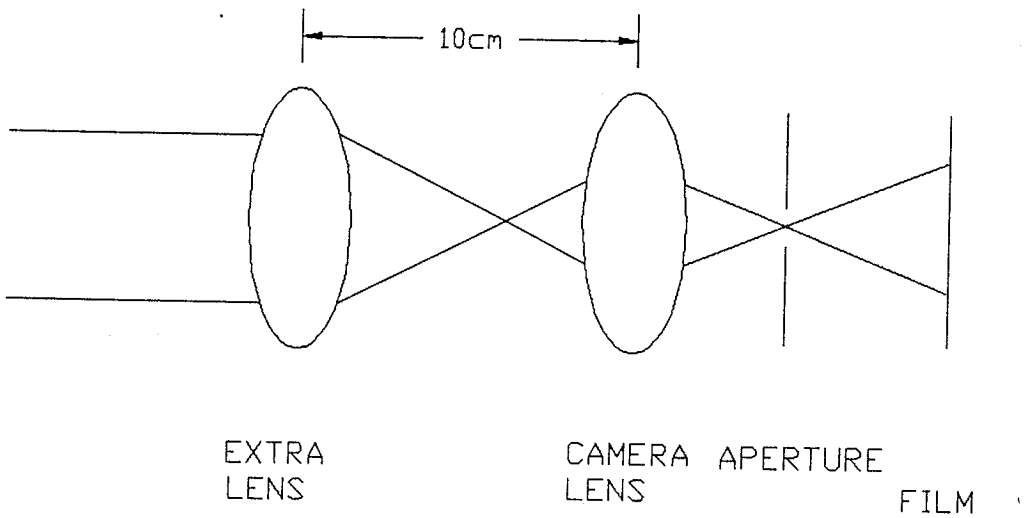

Figure 5 Schematic of an Optical Arrangement for Shadowgraph Image Recording.

5. PRELIMINARY TESTS

As a preliminary test, the shadowgraph system was first used to visualize a propane flame from a Weller high performance brazing torch. This portable torch contained high-pressure propane gas and could generate a flame with temperature as high as 1982°C (3600°F). The image of this flame by shadowgraphy is shown in Figure 6.

A similar test was carried out with a heat gun, where a glass funnel was used to cover the gun to produce a stream. The temperature of the gas was about 80°C and the flow is clearly seen in Figure 7.

The same visualization method was also applied to argon gas, using a VPPA welding torch. The argon gas bottle was connected to the plasma and shield gas inlets of the torch. At first, the test was made at room temperature and no flow pattern was recorded on the film. It was later found that the refractive index of argon is almost same as that of air at room temperature so a furnace was installed between the argon cylinder and the torch to heat the gas before it entered the torch as shown in Figure 8. With this modification the argon flow patterns were successfully obtained as seen in Figure 9 through Figure 11. Figure 9 demonstrates the free jet, and Figure 11 shows the pattern when a board simulating the workpiece (see Figure 10) was placed in front of the torch. The gas temperature in these cases was about 100°C and flow rate was 1400l/hr (50CFH). Note the large amount of turbulence in this case because of the relatively large Reynolds number.

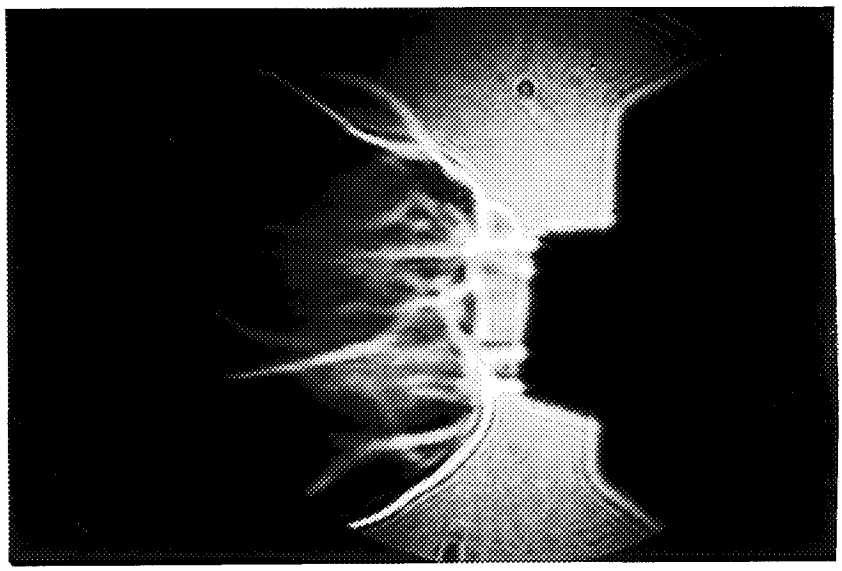

Figure 6 Image of Propane Flame by Shadowgraphy.

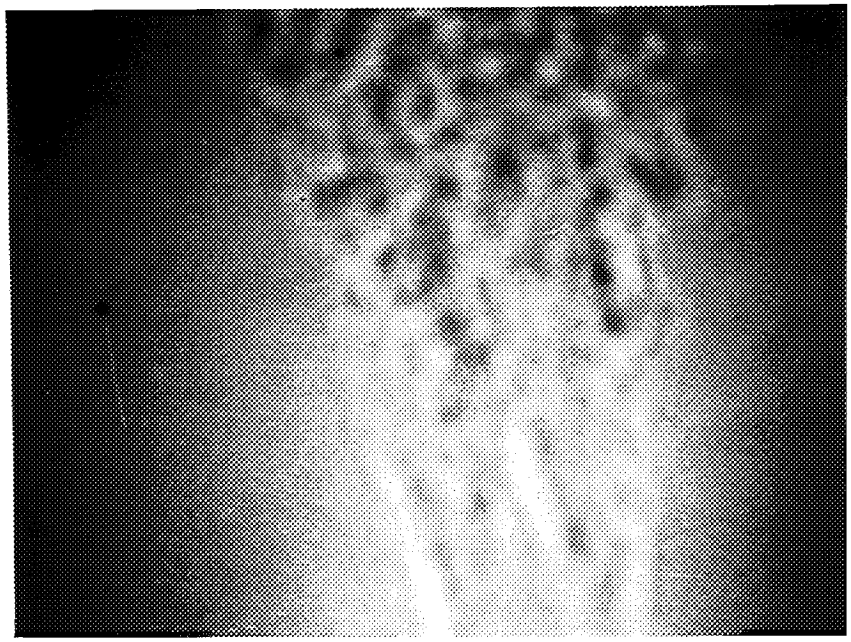

Figure 7 Shadowgraph Image of Hot Air Jet.

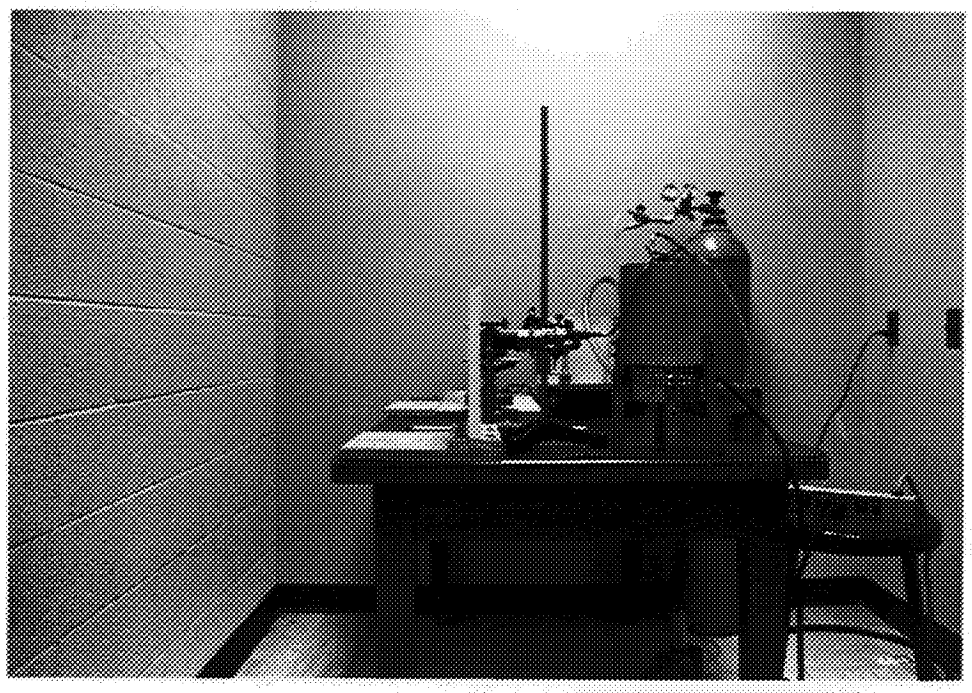

Figure 8 A Setup for Obtaining Heated Argon Gas Flow Pattern.

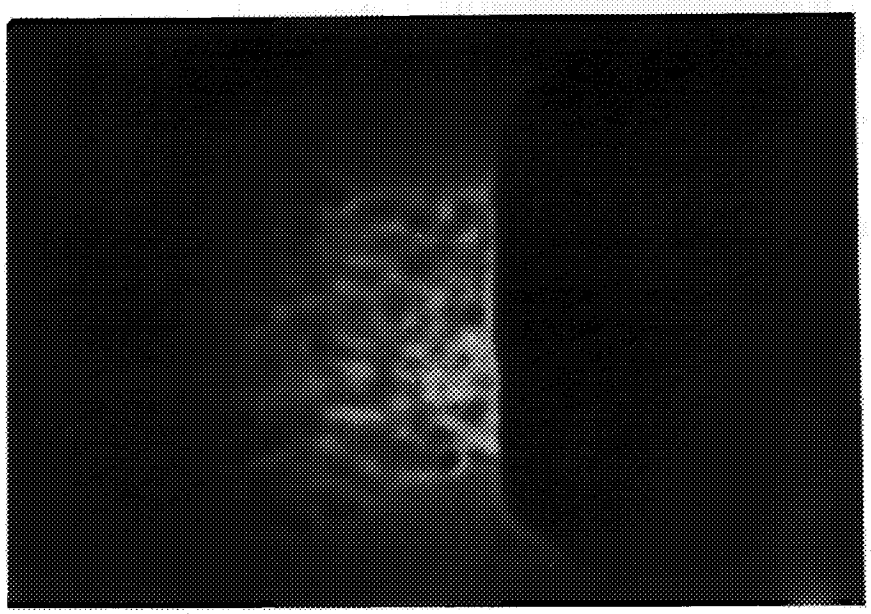

Figure 9 Heated Argon Gas from a Welding Torch.

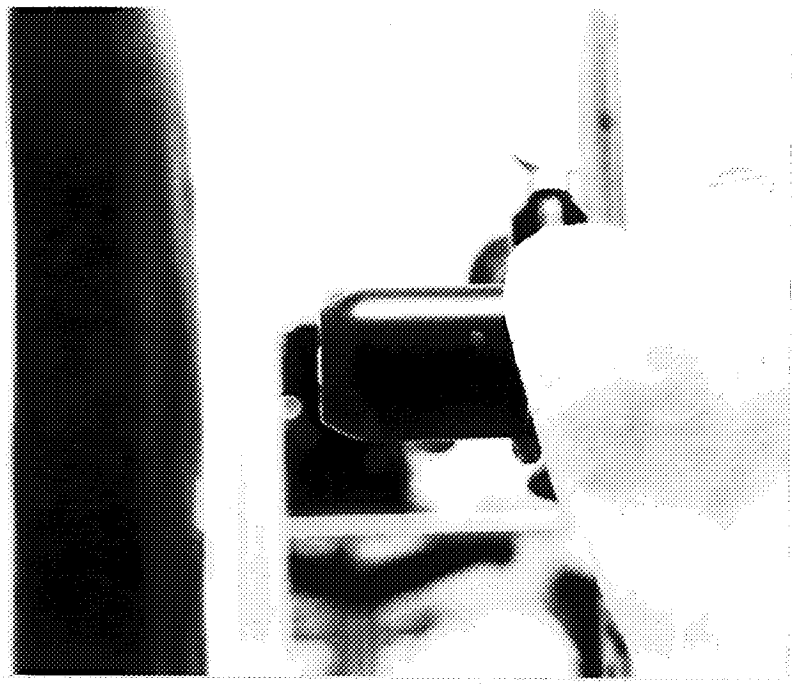

Figure 10 A Board for Simulating Workpiece in Front of the Torch.

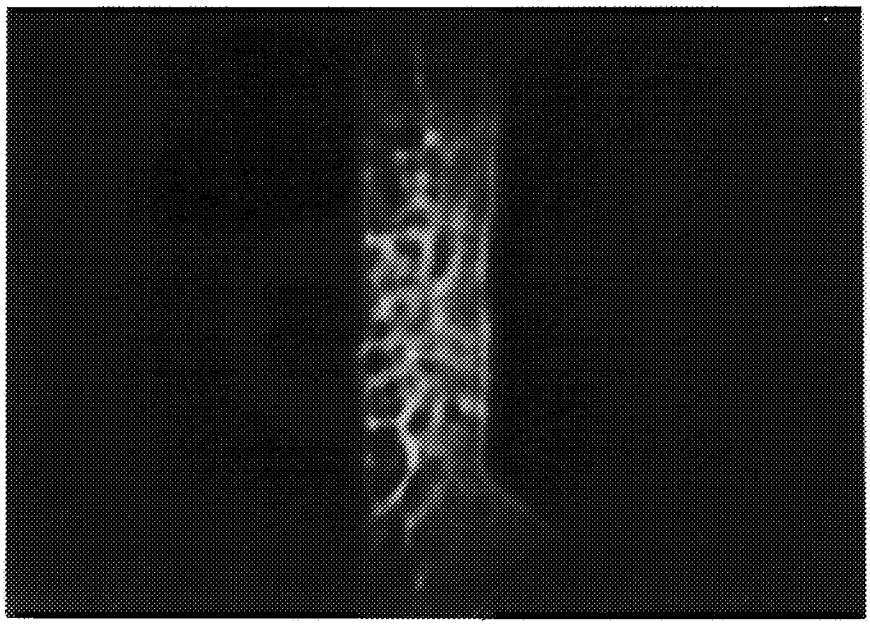

Figure 11 Heated Argon Gas from a Welding Torch by Shadowgraphy (with a board).

6. SHADOWGRAPHY APPLIED TO VPPA WELDING

After these pre-tests were performed, the shadowgraph optical system was mounted to the VPPA welding setup. The whole experimental setup is shown in Figure 12.

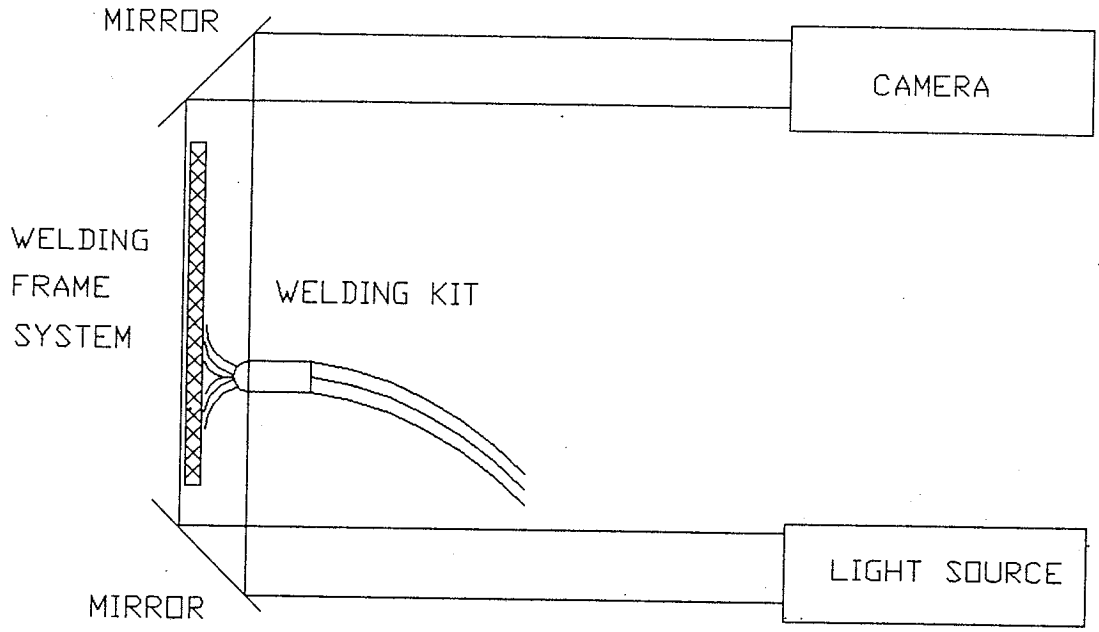

Figure 12 Experimental Setup for Flow Pattern Visualization in VPPA Welding.

In this experiment, a variable polarity plasma arc welding system purchased from the Hobart Brothers Company, Troy, Ohio, was used. The system consisted of a variable polarity 300 series power supply, control console, and water chiller. A welding torch from the B & B Company, Owens Crossroads, Alabama, was used.

The welding frame assembly was composed of three components: the frame itself, a heat sink and clamping system, and a welding kit (torch and its holder). The

welding frame was made of 5.0cm (2") X 5.0cm (2") rectangular steel tubing, and measured 100cm (74") high by 147cm (58") wide. The frame was bolted to the floor through anti-vibration pads. A third vertical piece of the same tubing was installed and divided the frame into two parts. The left part was used for this portion of the work.

One stainless steel linear bearing (with diameter of 1.8cm or 0.7") was fixed to each vertical frame by a flange. A smaller frame made of round (for the two sides) and rectangular (for the top and bottom) tubing moved along this vertical shaft driven by a BUGO-2004 motorized carriage. The smaller frame was balanced by a counter weight through a pulley. Figure 13 illustrates the frame system.

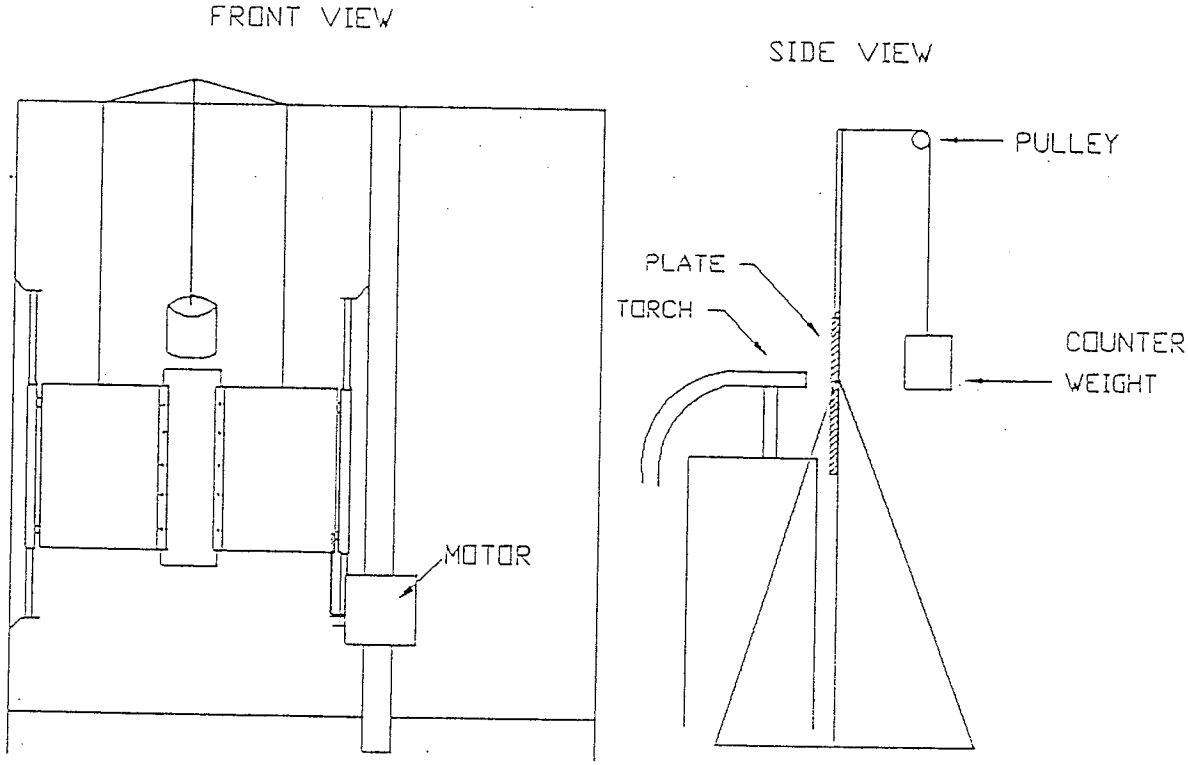

Figure 13 Schematic of Welding Frame.

Two heat sinks, 40.6cm (16") X 12.7cm (5") X 3.8cm (1.5"), made of 6061 aluminum plate, were bolted to the smaller frame. The purpose of the clamping and heat sinking systems was to eliminate test plate warpage during the welding. The clamping system, which is shown in Figure 14, was comprised of the 1.27cm (0.5") thick aluminum heat sinks, and two pieces of 0.635cm (0.25") thick rectangular aluminum stock, and ten 0.635cm (0.25") nuts and bolts.

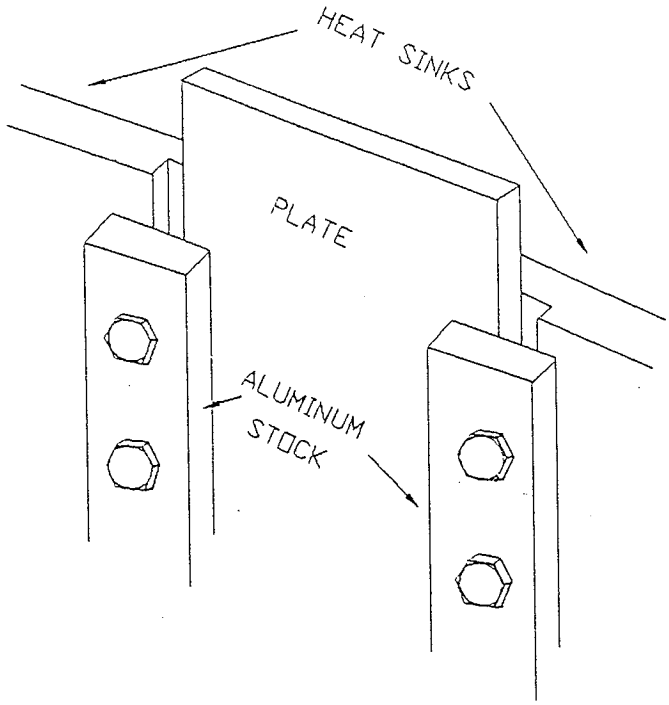

Figure 14 Clamping System.

The welding kit, which consisted of a welding torch and a BUGO-9472 two motion torch support group with a CON-1020 swivel mount, was bolted on a 1.27cm (0.5") thick aluminum plate with 38.74cm (15.25") X 10.16cm (4") wide. The aluminum plate was bolted vertically to another steel bracket which was welded to a heavy table in front of the welding frame. A schematic of the welding kit is shown

in Figure 15.

During welding, the torch is stationary and the weld plate moves downward and no changes in the optical system were necessary during a weld run.

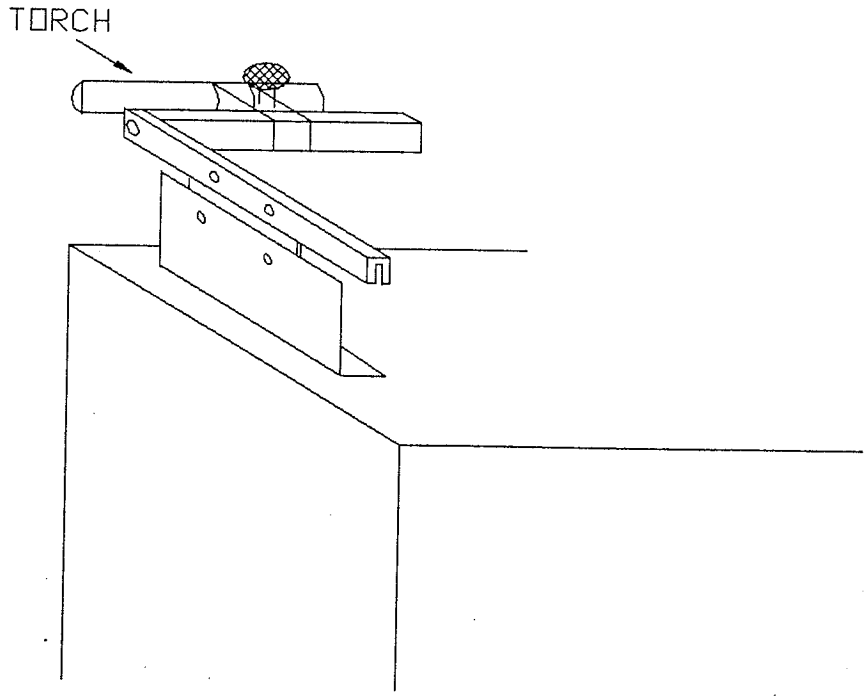

Figure 15 Schematic of Welding Kit.

7. OPTICAL SYSTEM

Two 45° mirrors were used to conveniently place the laser source and the camera. The mirrors were fastened on a steel tube which was placed behind the welding frame. One was on the bottom, for switching the light from the source to the test field, the other was on the top, for switching the beam to the camera. The distance between them was about 89cm (35"). Figure 16 is a schematic of the optical system.

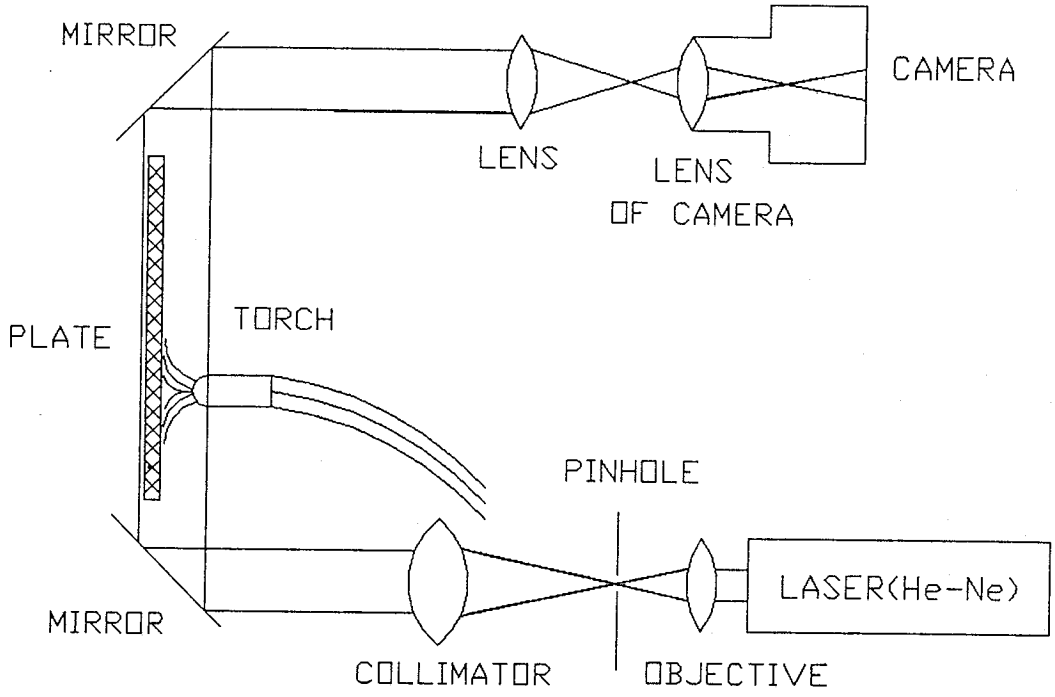

Figure 16 Schematic of Optical System.

8. VPPA GAS FLOW PATTERNS

To initiate welding a pilot arc is generated between the electrode and the nozzle by a high frequency circuit. Then the torch is moved toward the workpiece. When the electric field intensity is high enough, the plasma gas will be ionized and the main arc (plasma arc) will is produced. Flow patterns at different stages of the welding process will now be shown. First, the images of the plasma jet gas were taken. In this case, no shield gas was used and no weld plate was mounted. Only the pilot arc was on. The results with plasma flow rates from 56l/hr (2CFH) to 140l/hr (5CFH) are shown in Figure 17.

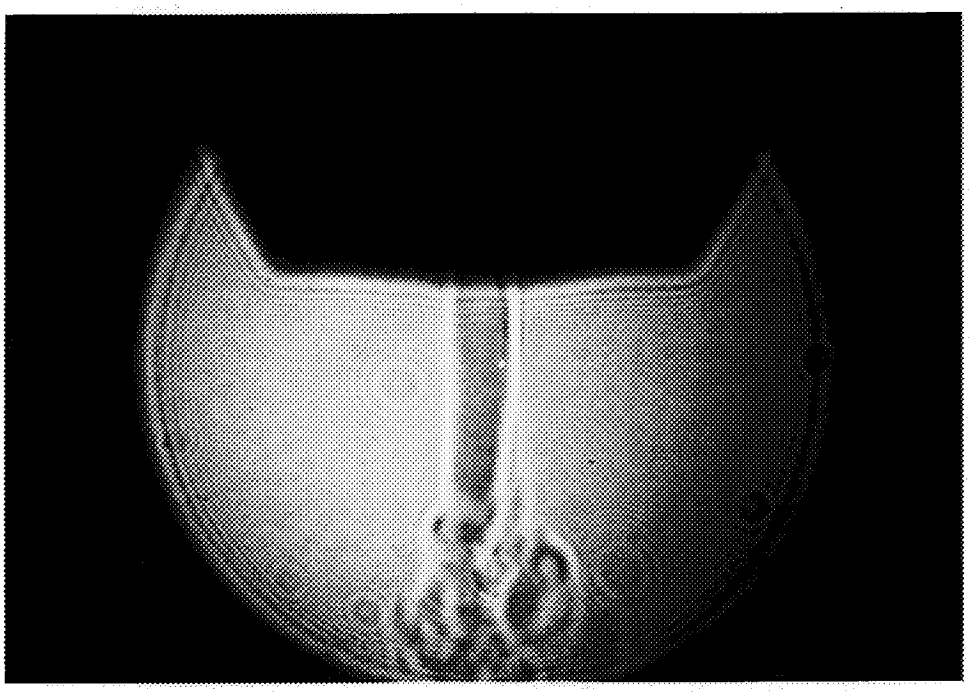

(a)

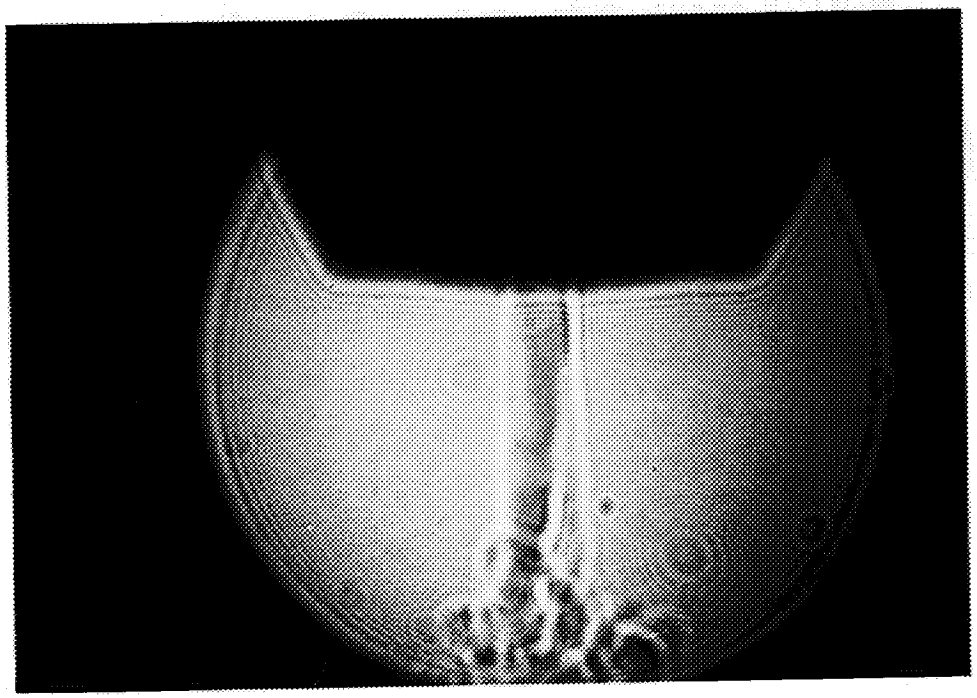

(b)

Figure 17 Plasma Gas Flow Patterns, Flow Rate 2CFH(a), 3CFH(b).

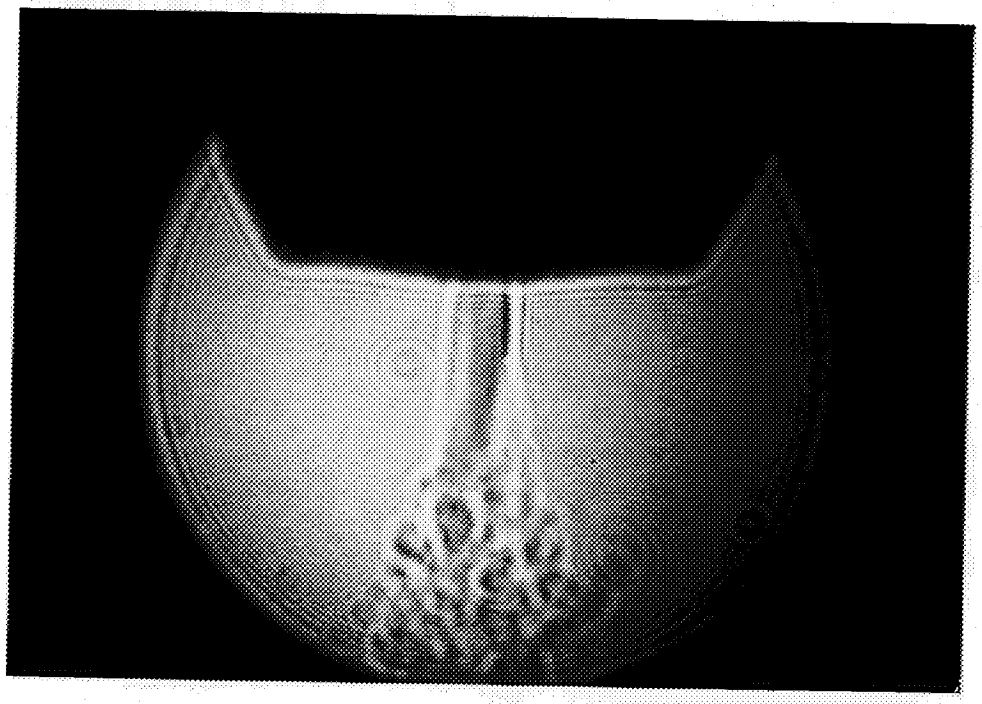

(c)

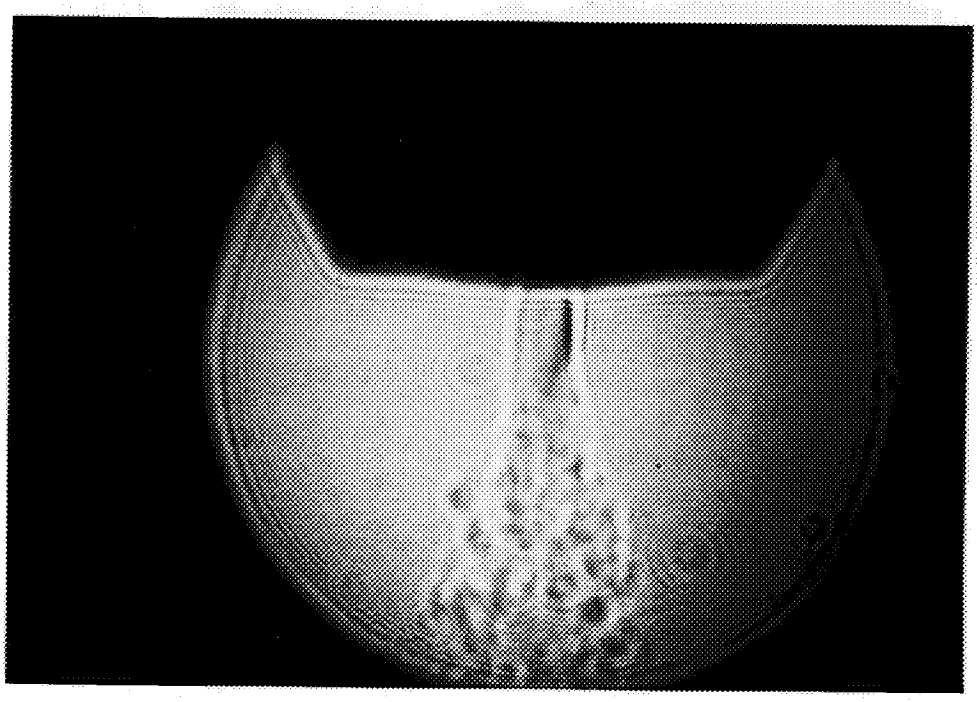

(d)

Figure 17 (continued) Plasma Gas Flow Patterns, Flow Rate 4CFH(c), 5CFH(d).

The Reynolds Number was estimated by

$$Re = Vm\rho d/\mu$$

The velocity of the fluid Vm could be calculated from the continuity equation

$$\rho VmA = \rho_0 V_0$$

where A is the cross area of the orifice and ρ_0 and V_0 are density and volume flow rates of argon at s.t.p. A velocity of about 3.4m/s was estimated when the flow rate was 56l/hr (2CFH) and the temperature was
500K. The velocity will increase rapidly when temperature is raised because of the decrease in gas density.

Assuming the temperature was 227°C (500K), for argon gas, a density of $0.961 Kg/m^3$ and a viscosity of $341.6 \times 10^{-7} N \cdot s/m^2$ were used to calculate Re[5]. If the characteristic length d was chosen as 1 cm, which is the order of the standoff in VPPA welding, Reynolds numbers from 950 to 2375 were obtained in the above cases. With an increase of the plasma flow rate, the velocity and Reynolds number increase. The turbulent flows also show an increase.

Figure 18 displays the flow patterns with both the plasma and shield gas. The results indicate that turbulent flow originally generated by plasma gas is suppressed by the shield gas. This is attributed to the interaction of the relatively slow shield gas with the plasma gas. This suppression becomes more complete with higher shield flow rate.

Next the weld plate was mounted, but only the pilot arc was on. The results for different flow rates and standoffs are shown in Figure 19 and Figure 20

respectively.

The flow pattern changes slightly when the shield flow rate changes, but more significant changes can be observed when the plasma flow rate is raised from 2CFH to 4CFH. Plasma flow is evidently dominant in the overall flow patterns due to its high gas velocity. Note that the patterns become less discernable when the standoff is decreased because of the limited flow path for the gases and the increased spatial temperature gradient.

Finally the plasma (main) arc was ignited, the images obtained are shown in Figure 21 and 22. Figure 21 shows the center and edge area of the welding torch when a standard cover pass weld was produced. Figure 22 is for a keyhole weld.

It is found that the image appears less interpretable when the plasma arc is introduced. It is thought that the images may represent a combination of electron, ion, and neutral gas density distribution which will be discussed in detail below.

9. DISCUSSION

As is shown above, it is difficult to interpret the gas flow patterns when the plasma arc is on. This difficulty is further shown in Figure 23. This was initially unexpected and some reasons will be discussed here.

For an ionized monatomic gas, the ionized gas mixture consists of neutral atoms, ions, and free electrons. The degree of ionization, α_1, is the mass fraction of ions in the mixture, and the mass fraction of the electrons may be neglected. The Gladstone-Dale relation for ionized gas is then written as

$$n-1=\rho\{(1-\alpha_1)K_A+\alpha_1 K_I\} + NeKe$$

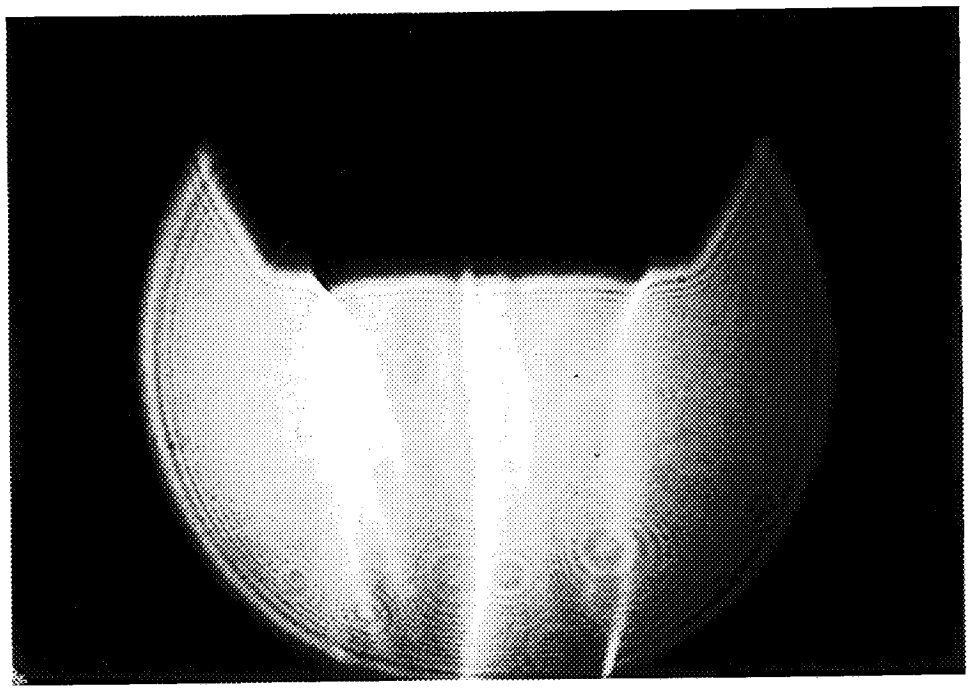

(a)

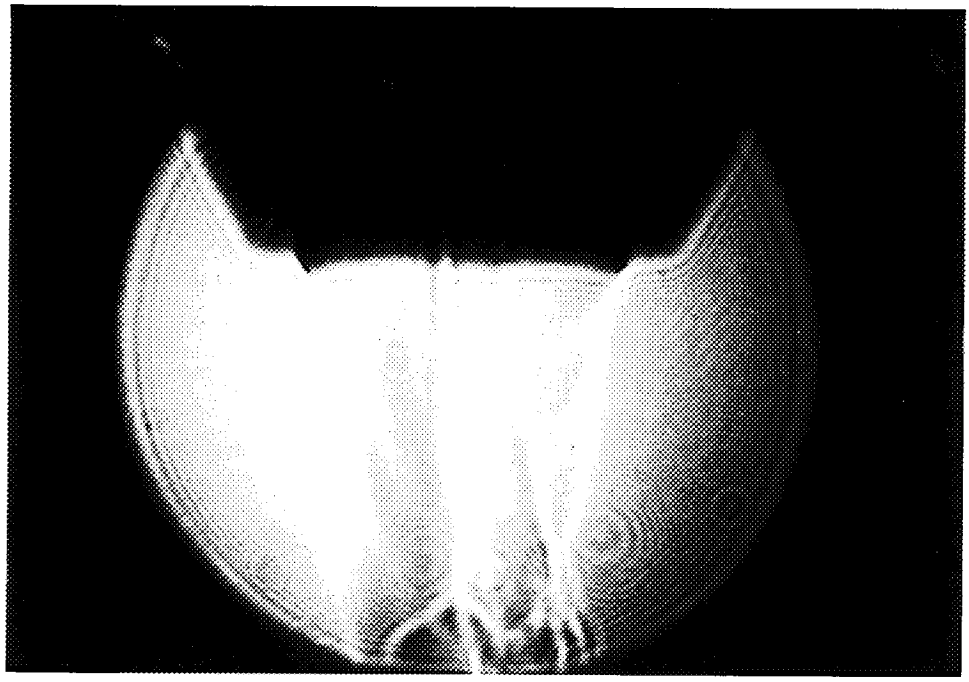

(b)

Figure 18 Gas Flow Patterns of Plasma and Shield Gas (without Workpiece), Plasma and Shield Flow Rate, 2 and 40CFH(a), 5 and 40CFH(b).

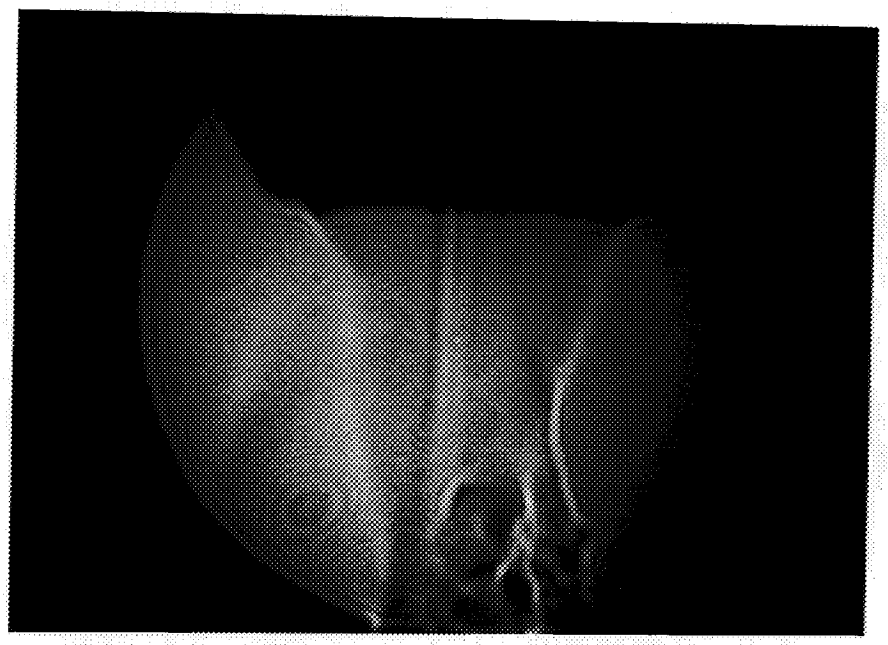

(c)

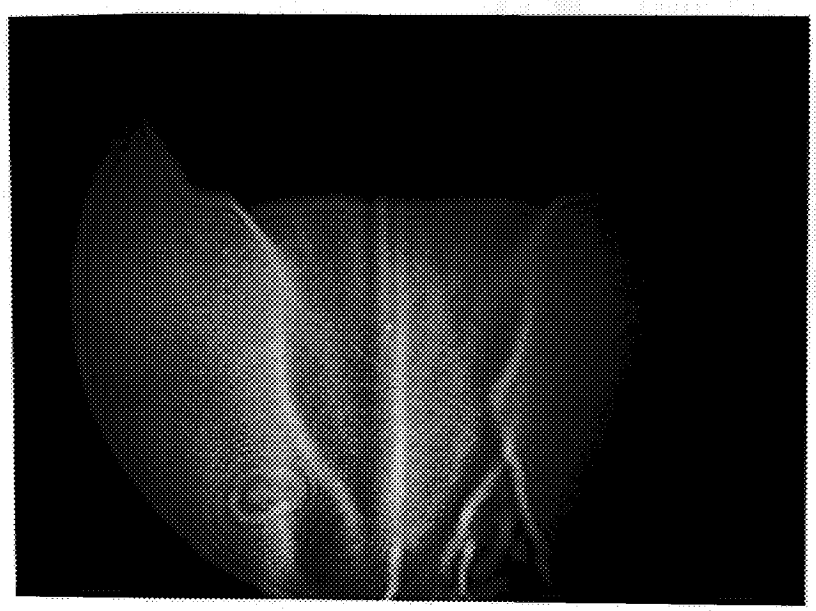

(d)

Figure 18 (continued) Gas Flow Patterns of Plasma and Shield Gas (without Workpiece), Plasma and Shield Flow Rate, 4 and 30CFH(c), 4 and 45CFH(d).

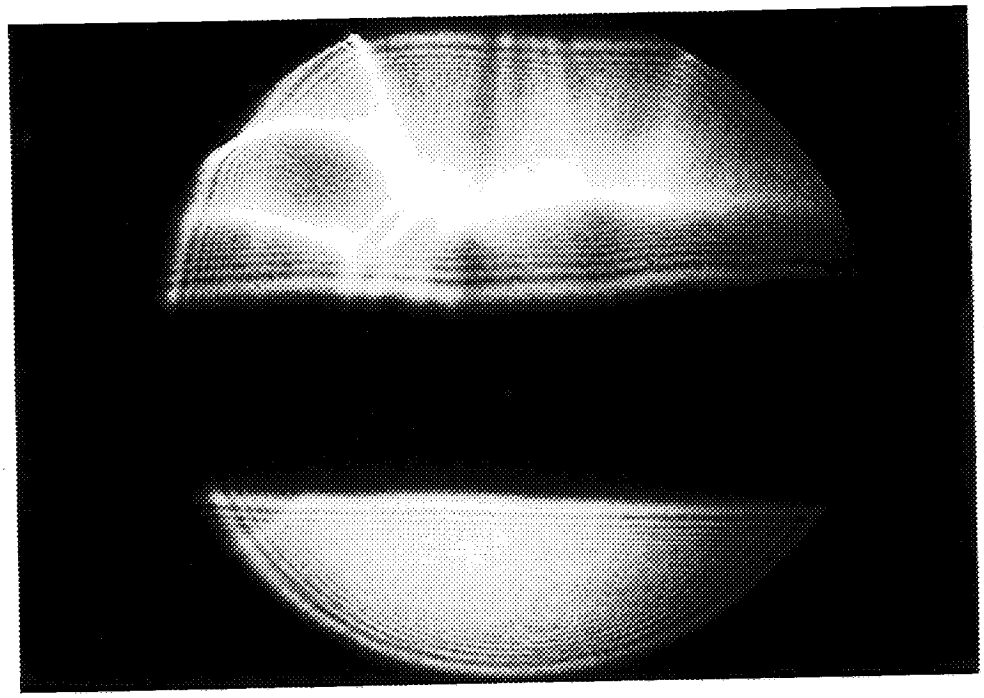

(a)

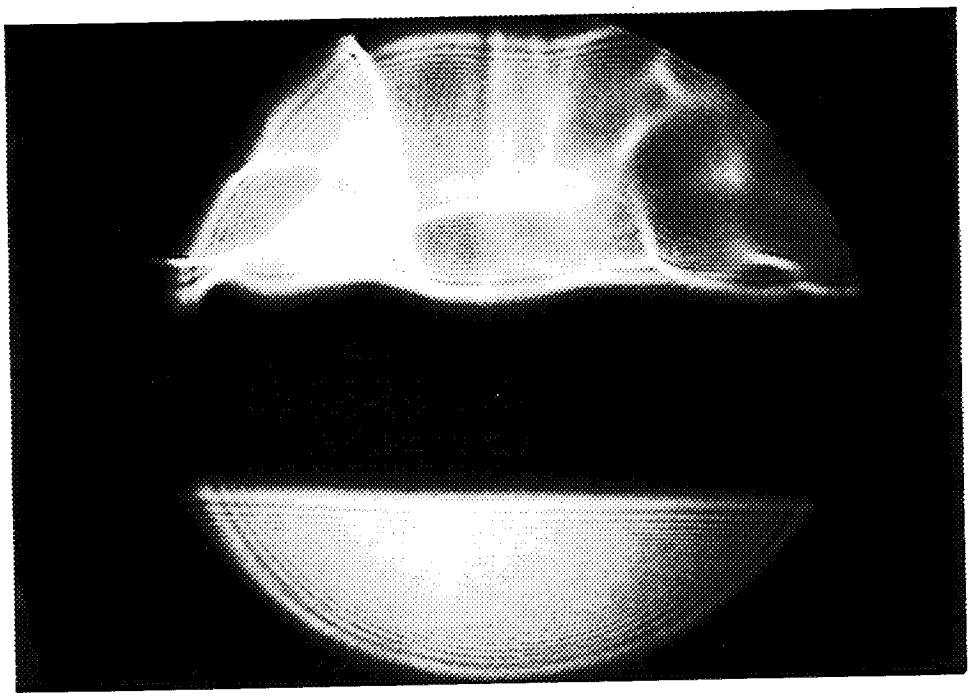

(b)

Figure 19 Flow Patterns with Workpiece but no Plasma Arc, Plasma and Shield Flow Rate, 2 and 20CFH(a), 2 and 40CFH(b).

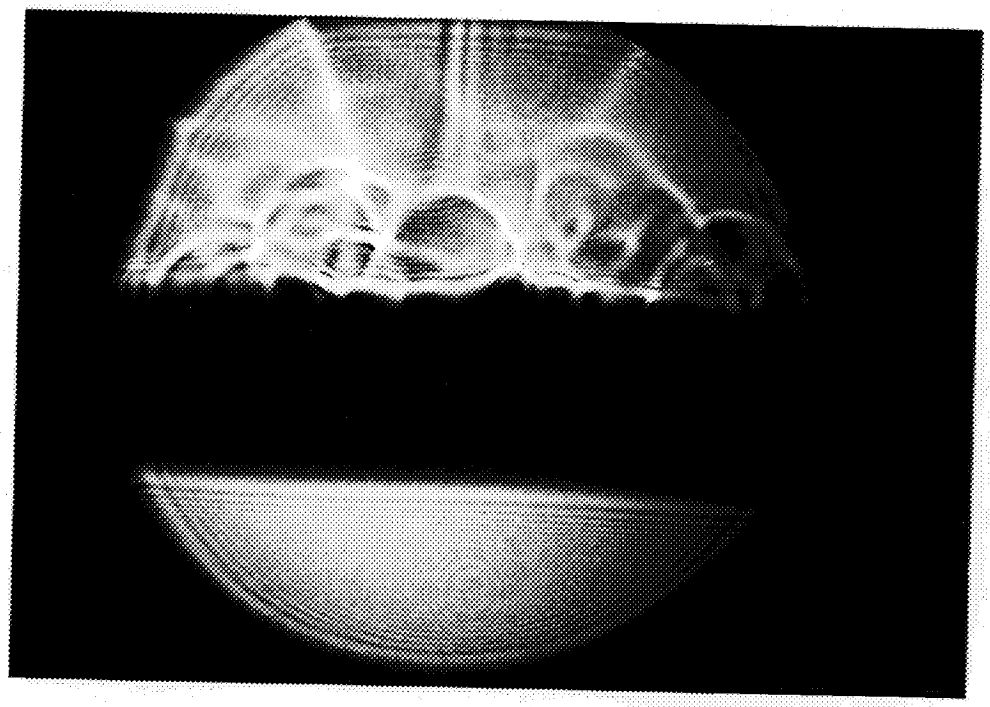

(c)

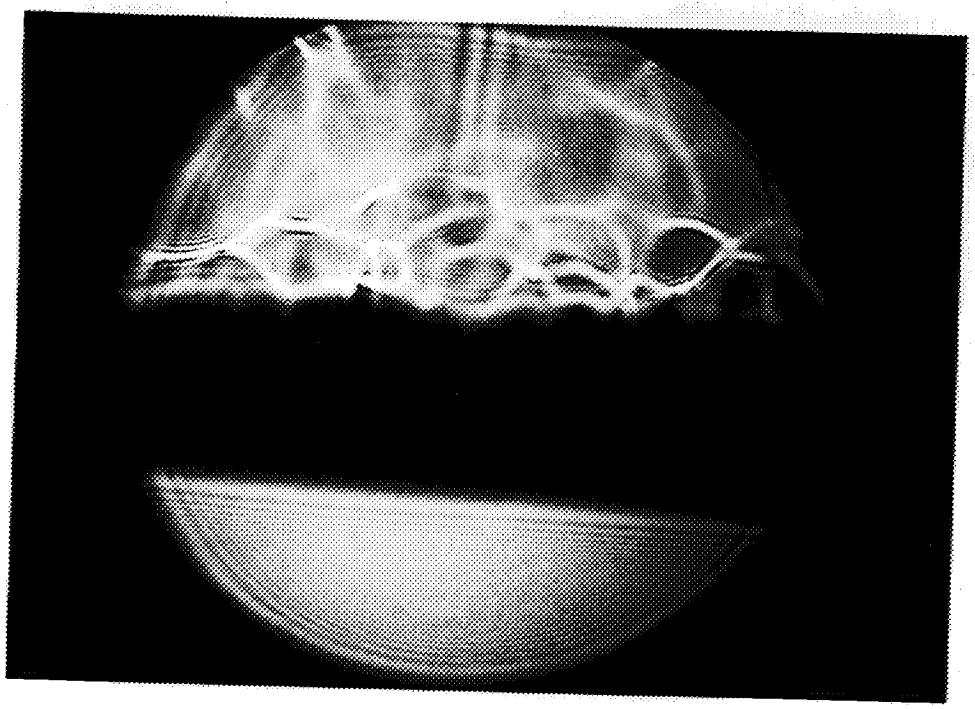

(d)

Figure 19 (continued) Flow Patterns with Workpiece but no Plasma Arc, Plasma and Shield Flow Rate, 4 and 20CFH(c), 4 and 40CFH(d).

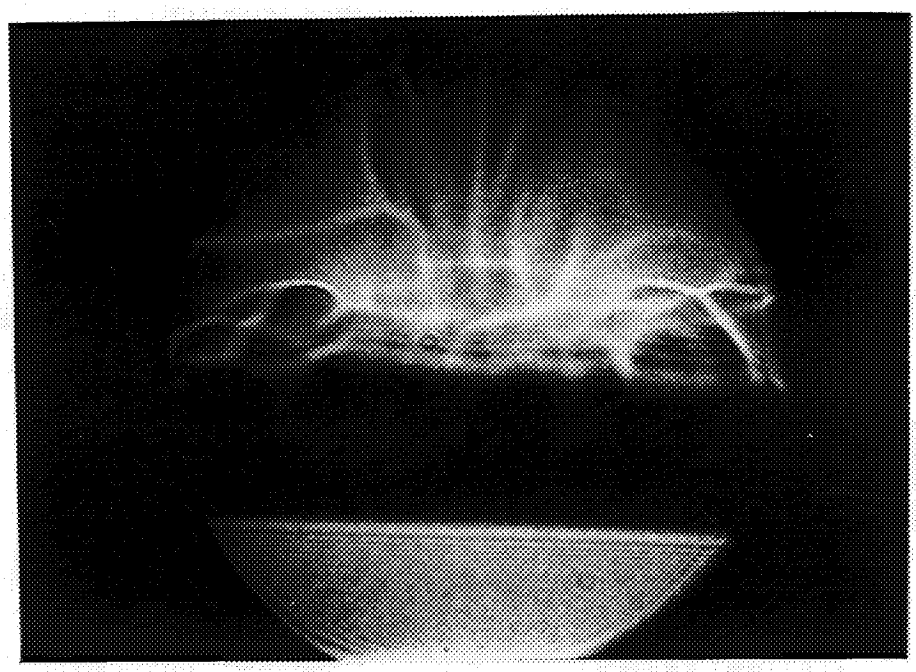

(a)

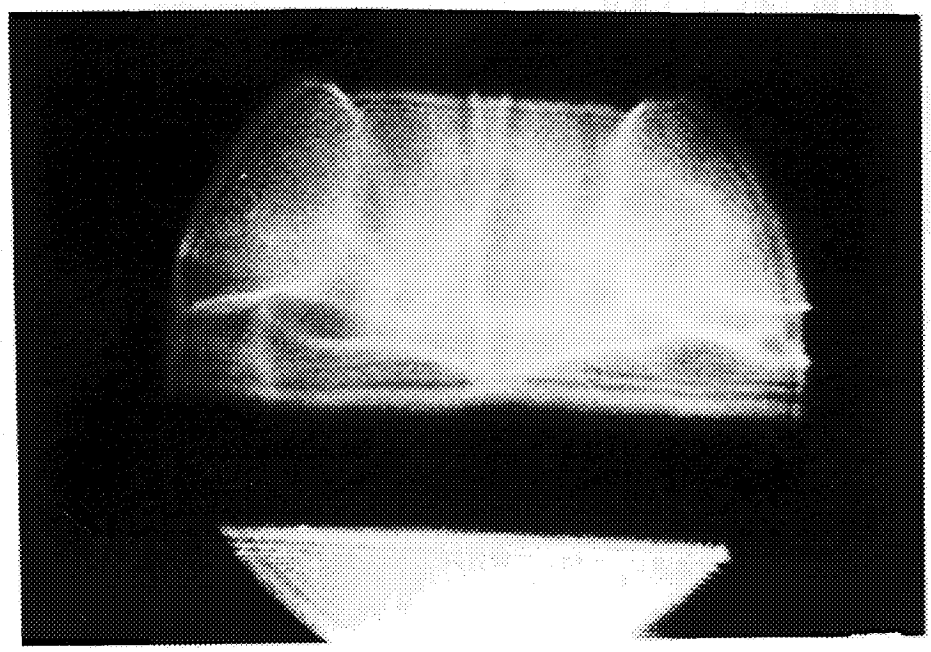

(b)

Figure 20 Comparison of Flow Patterns with different Standoffs (Plasma Flow Rate 2CFH and Shield Flow Rate 40 CFH), 35mm(a), 13mm(b).

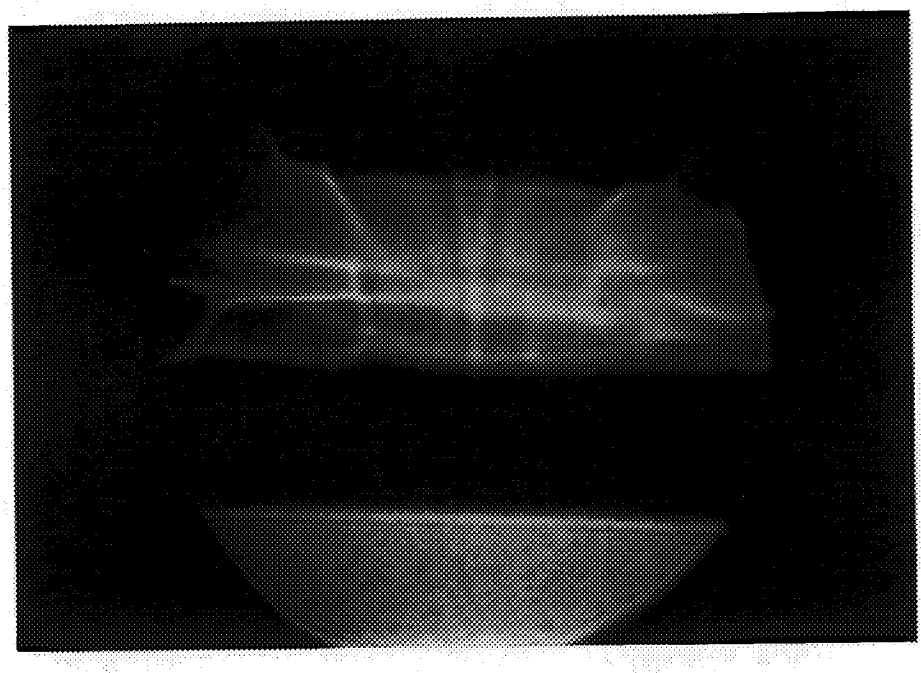

(c)

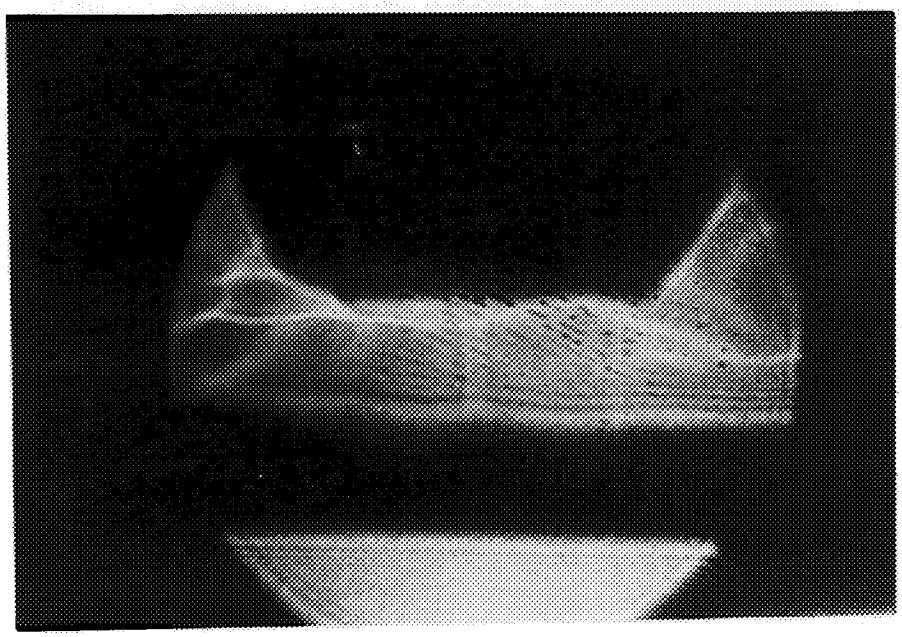

(d)

Figure 20 (continued) Comparison of Flow Patterns with different Standoffs (Plasma Flow Rate 2CFH and Shield Flow Rate 40 CFH), 10mm(c), 7mm(d).

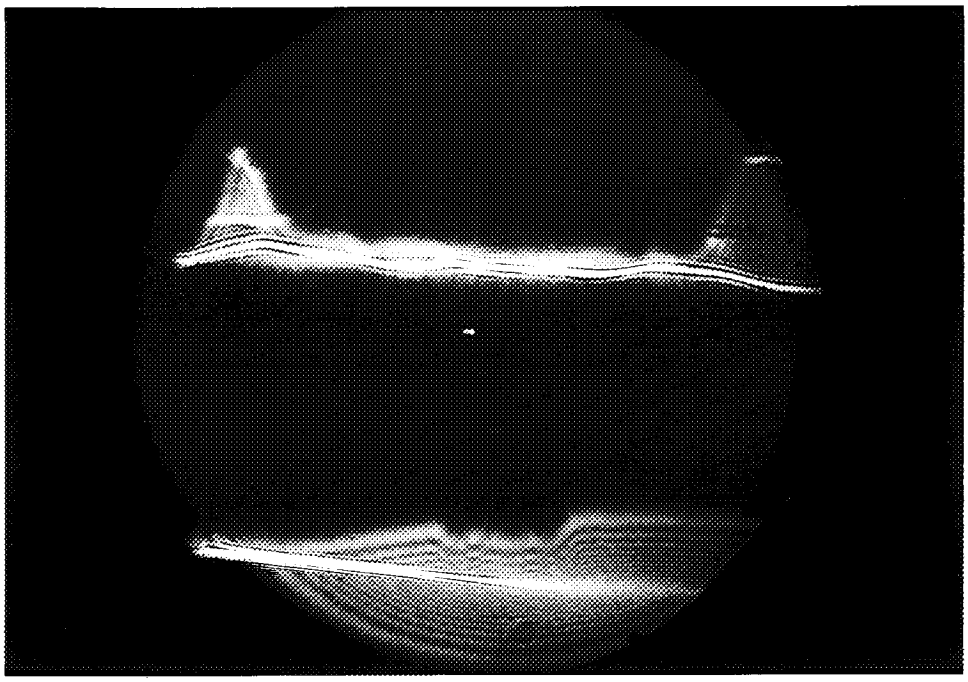

(a)

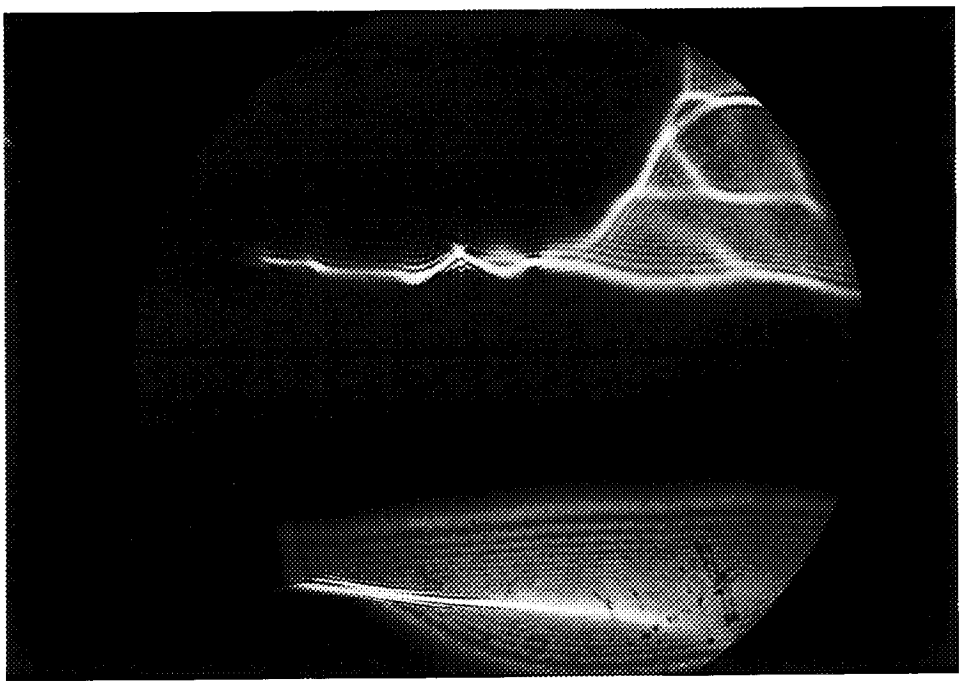

(b)

Figure 21 Flow Patterns with Plasma Arc (Cover Pass Mode Weld), Center Area(a) and Edge Area(b).

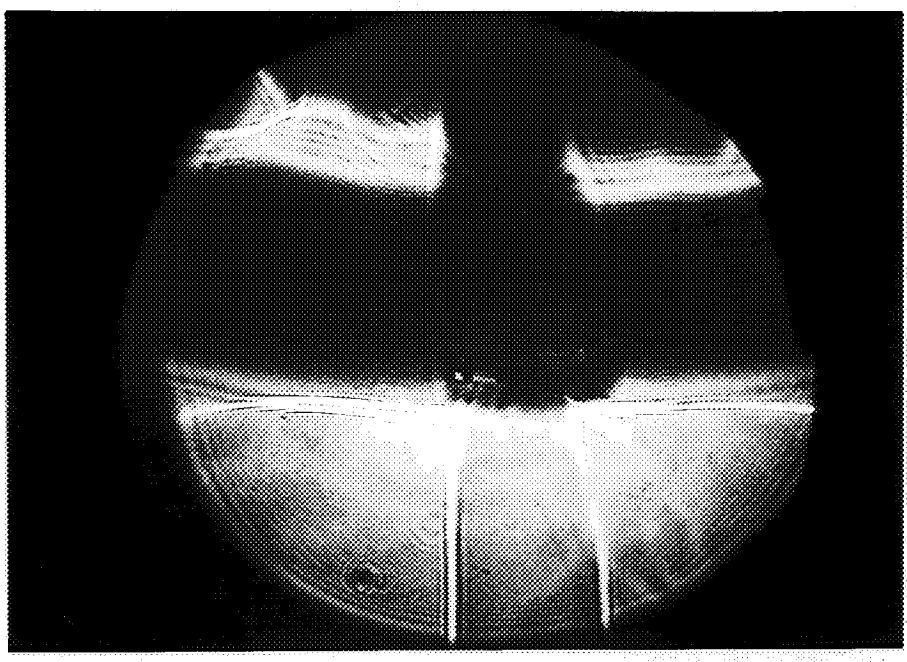

(a)

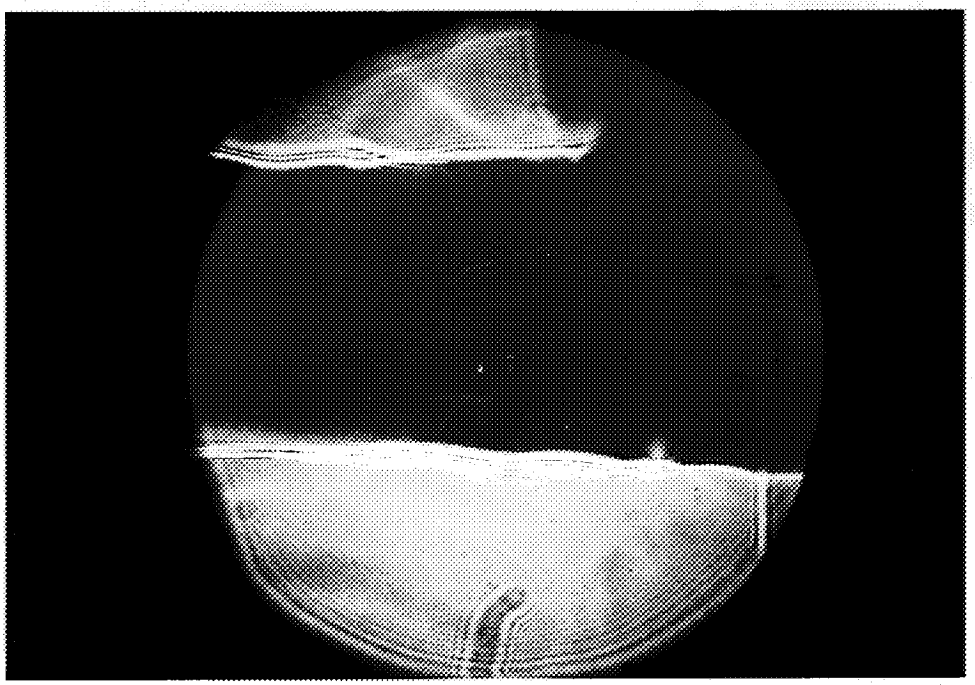

(b)

Figure 22 Flow Patterns with Plasma Arc (Keyhole Mode Weld), Center Area(a) and Edge Area(b).

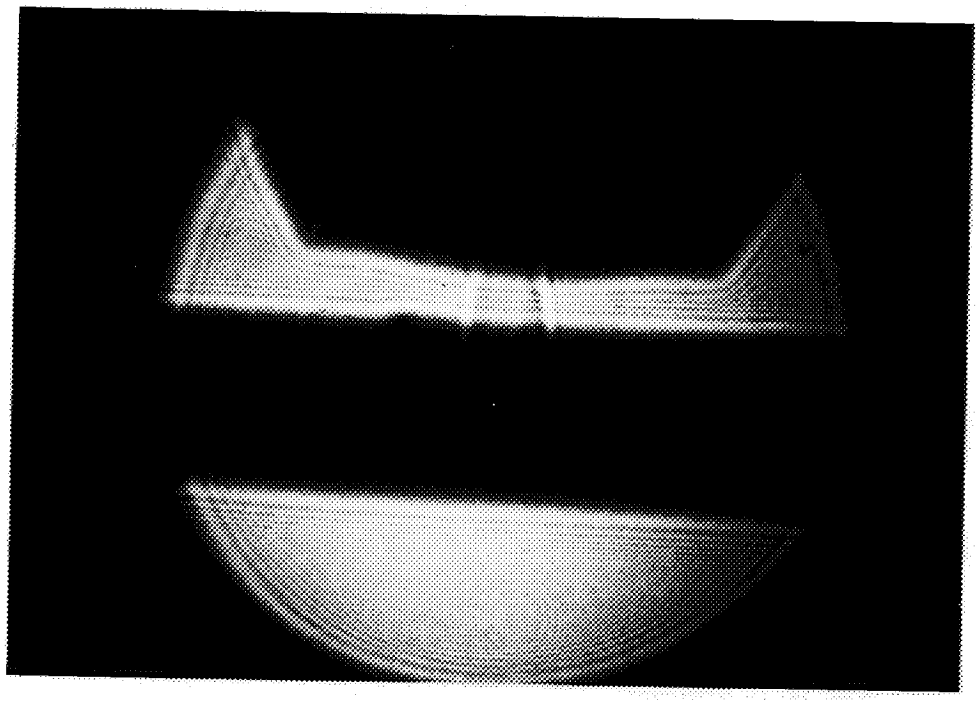

(a)

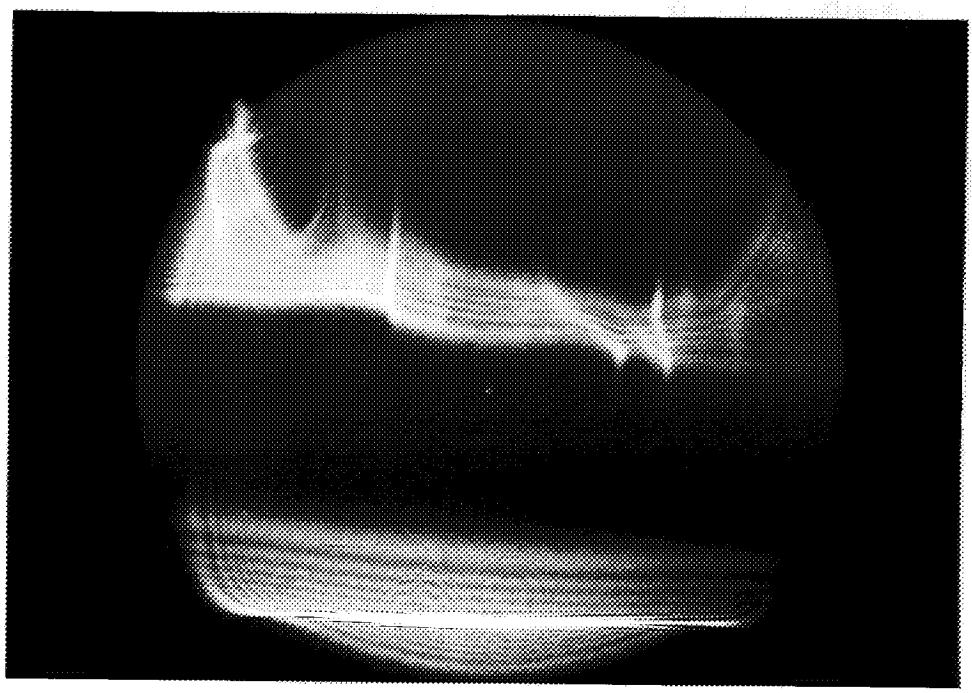

(b)

Figure 23 Comparison of Flow Patterns with and without Plasma Arc, Plasma and Shield Flow Rate, 2 and 0CFH, without Plasma Arc(a), with Plasma Arc(b).

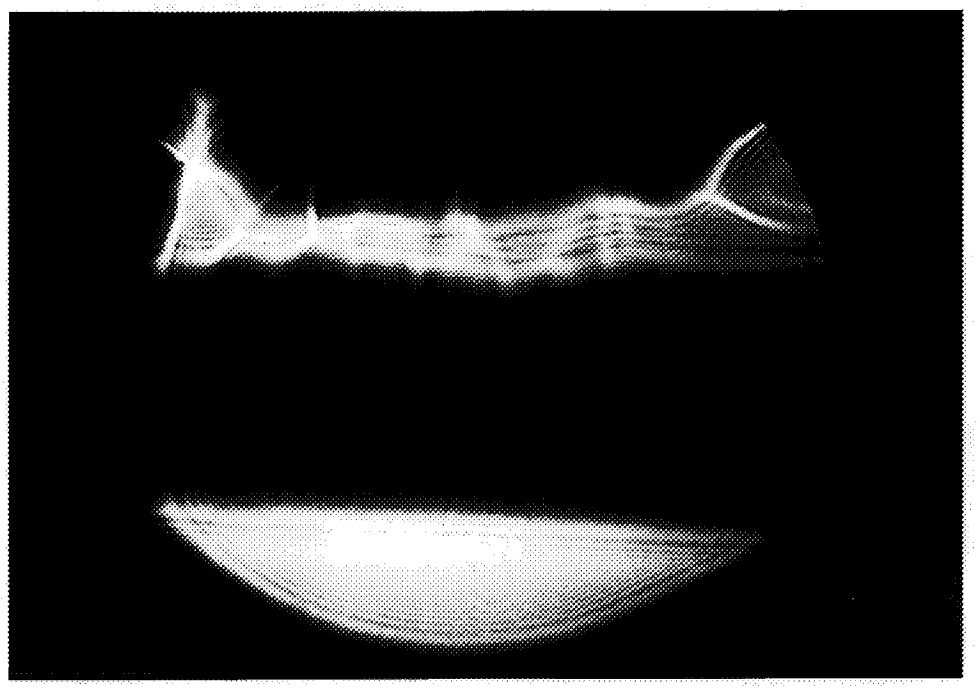

(c)

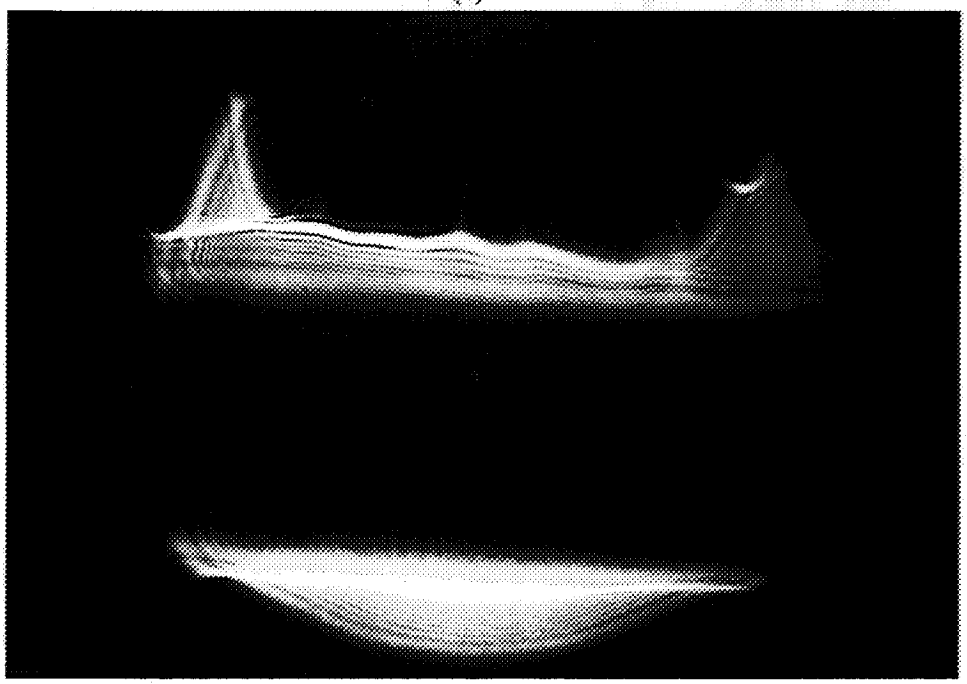

(d)

Figure 23 (continued) Comparison of Flow Patterns with and without Plasma Arc, Plasma and Shield Flow Rate, 2 and 40CFH, without Plasma Arc(c) and with Plasma Arc(d).

where K_A and K_I are the Gladstone-Dale constants of the atom gas and of the ion gas, respectively; Ne is the electron number density(i.e., the number of electrons per unit volume); and the Gladstone-Dale constant of the electron gas is Ke'. According to Alpher and White[6], for argon $K_I = 2/3\ K_A$. From plasma theory it follows that the refractive index n_e of an electron gas is[7]

$$n_e-1=-(\lambda^2 N_e e^2)/(2\pi m_e c^2)$$

with e being the charge and m_e the mass of an electron; c, the velocity of light in vacuum; and λ the wavelength of the light transmitted through the gas mixture. If λ is measured in centimeters, the index will be

$$n_e-1=-4.46X10^{-14}\lambda^2 N_e$$

indicating that the Gladstone-Dale constant of the electron gas, Ke', is negative and strongly dispersive.

Comparing, at a given wavelength, the Gladstone-Dale relation for the electron gas with that for the neutral atom gas, it is seen that the specific refractivity (n-1) per electron is greater than the specific refractivity per atom by more than one order of magnitude. The optical behavior of an ionized gas is therefore dominated by the presence of free electrons, even at a low ionization level. Since the Gladstone-Dale constant of the electron gas is negative, the optical response to density changes is opposite to the response in the neutral gas. In plasma arc welding, the degree of ionization is above 10%. Therefore in VPPA welding, when the plasma arc is present, the shadowgraph will reflect the density of electrons as well as the plasma gas. Different regions near the torch have varying electron and neutral

gas densities, so the pattern will be very complicated.

Some other factors that might affect the image are the smaller standoff and higher velocity of the plasma. In VPPA welding the standoff, which is the distance from the torch to the workpiece, is less than 1cm and the plasma gas has a velocity on the order of 400m/s[8]. In addition, the directions of electrons and ions change due to the changing polarity. Within the photographic exposure time (1/1000 second), the recorded image might be an average.

Additionally, the welding plate is at high temperature during the welding. This will produce convection away from the weld torch but still in the test volume and may cause additional shadows.

10. CONCLUSIONS ON FLOW PATTERN VISUALIZATION

1. The plasma gas plays a dominant role on the overall flow pattern.

2. The shield gas can reduce turbulence caused by the plasma gas and improve the stability of the plasma arc.

3. The presence of a high density of electrons in the plasma arc as well as other factors greatly affects the appearance of flow pattern.

11. INTRODUCTION TO UNDERCUTTING

The weld defects most commonly present in aluminum and aluminum alloy welds include: crater cracks, longitudinal cracks, incomplete fusion, incomplete penetration, porosity, and undercutting.

The term "undercutting" is used to describe a groove melted into the base metal adjacent to the toe of a weld and left unfilled by the weld metal. It also describes the melting away of the sidewall of a welding groove at the edge of a layer or bead. This melting away of the groove forms a sharp recess in the sidewall where the next layer or bead must fuse as is shown in Figure 24.

Undercutting is a particularly undesirable defect in that the parent metal at the undercutting point is thinner. The weld bead may be deposited correctly and have sufficient strength, but the reduction in the cross sectional area along the side of the weld bead creates a weak point in the weld. If several passes are carried out in a weld, the undercutting in prior passes can introduce defects such as porosity or incomplete fusion into the weld.

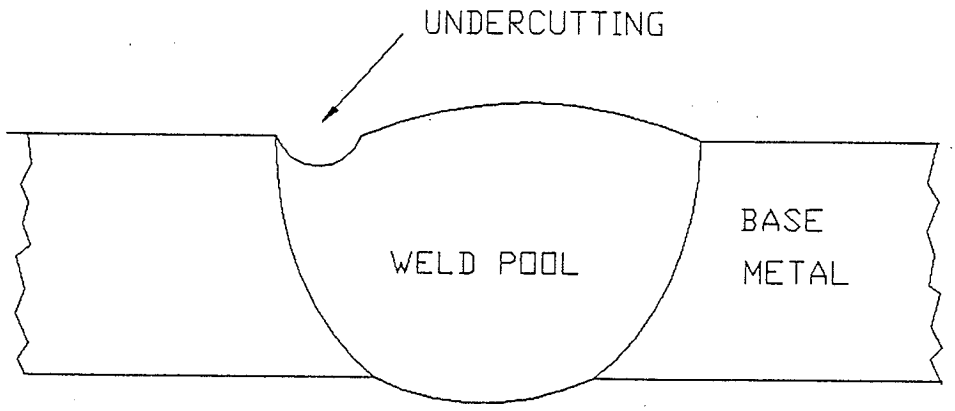

Figure 24 Schematic of Undercutting.

Undercutting is usually more serious in keyhole mode welding. In this mode, the force tending to form and maintain the keyhole is the arc pressure. Forces tending to close the keyhole are the gravitational pressure and surface tension[9].

Undercutting is produced during the solidification of the weld pool so the surface tension can be considered to be an important factor causing the defect.

Surface tension and its temperature dependence play a major role in weld pool flow. It has been shown that surface tension driven fluid flow (Marangoni) convection is responsible in many cases for the fluid flow pattern produced in weld pools[10]. For example, the fluid flow pattern formed in a thin layer of fluid heated uniformly from below (Benard convection) is determined by surface tension driven fluid flow, not convection from buoyancy effects[11].

Aluminum and its alloying elements have a high surface tension in the vicinity of their melting points, i.e., much higher than mercury at ambient temperature, as shown in Table 1. An obvious example of the effect of surface tension in welding is the stable suspension of the molten pool without any backing system in full penetration welding of the plates.

Most solute elements, particularly non-metals such as oxygen, are highly surface active in liquid metals. It is reported that radially outward surface motion velocities of 80-150cm/s could be produced in liquid tin by blowing a low velocity jet of oxygen vertically onto the center of a pool of tin in a crucible, while a surface motion of less than 5cm/s was produced when argon rather than oxygen was used[13].

Due to the effects of dissolved elements or the asymmetric profile of temperature in the weld pool, the gradient of surface tension ($d\sigma^*/dT$) from the center to the edge may become asymmetric in the weld pool. On the side with the

higher gradient, faster Marangoni convection can produce the undercutting. Changes in weld pool flow can result in undercutting: an estimated 40cm/s velocity change is all that is required to produce the observed undercutting[14].

Table 1 Surface Tensions σ of Pure Liquid Metals at Their Melting Points and Mercury at 298K[12]

Metal	σ (mNm^{-1})	$d\sigma/dT$ ($mNm^{-1}K^{-1}$)
Li	398	-0.14
Mg	559	-0.35
Al	914	-0.35
Si	865	-0.13
Cu	1303	-0.23
Zn	782	-0.17
Hg	485	-0.20

So the factors which can induce the changes of $d\sigma^*/dT$ are suspected to affect the occurrence of undercutting. Among these factors the welding torch tilt angle, shield gas flow rate and gas contamination will be studied in this report.

12. UNDERCUTTING EXPERIMENTS

The same welding system described above was used in this study. In addition to this system, a protractor (Figure 25) was made to control the welding torch tilt

angle more accurately. The tilt angle can be controlled to within 0.5°. Figure 26 is a schematic of the torch and the protractor. The center of the protractor circle is coincident with the projection point of the torch rotation axis on the protractor plane. This position is fixed and marked beforehand. Whenever the torch is to be tilted, the torch must be restored to this marked position and the torch is rotated. The tilt angle is read on the protractor by an indicator which is attached to the torch body.

The 6.35mm (1/4") thick 2219 and 6061 Al alloy plates were used in the experiments. They were cleaned with dilute nitric acid and methyl ethyl ketone (MEK) prior to welding. Keyhole mode welds were performed with the standard welding parameters[15]. After welding, a small piece was sectioned from each weld, mounted, and polished to 1μm finish. Finally it was etched with Keller's etch and the cross section of each weld was examined optically at low magnification.

The welding torch tilt angle is defined as the angle between the torch symmetry axis and the direction perpendicular to the welding plate in a plane perpendicular to the torch travel direction (shown as in Figure 27). The degree of undercutting is represented by the groove depth (Figure 27). Shadowgraph pictures showing the gas flow patterns when the torch is tilted left from 0 to 3 degree are shown in Figure 28, in which only the pilot arc was on. In these experiments, the torch was always tilted to the left resulting in undercutting to the left.

Figure 25 Protractor.

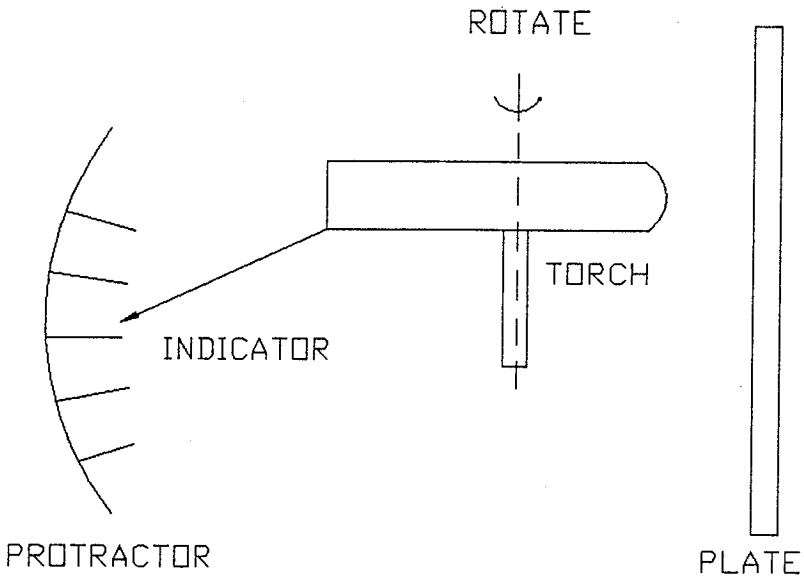

Figure 26 Schematic of Torch and Protractor.

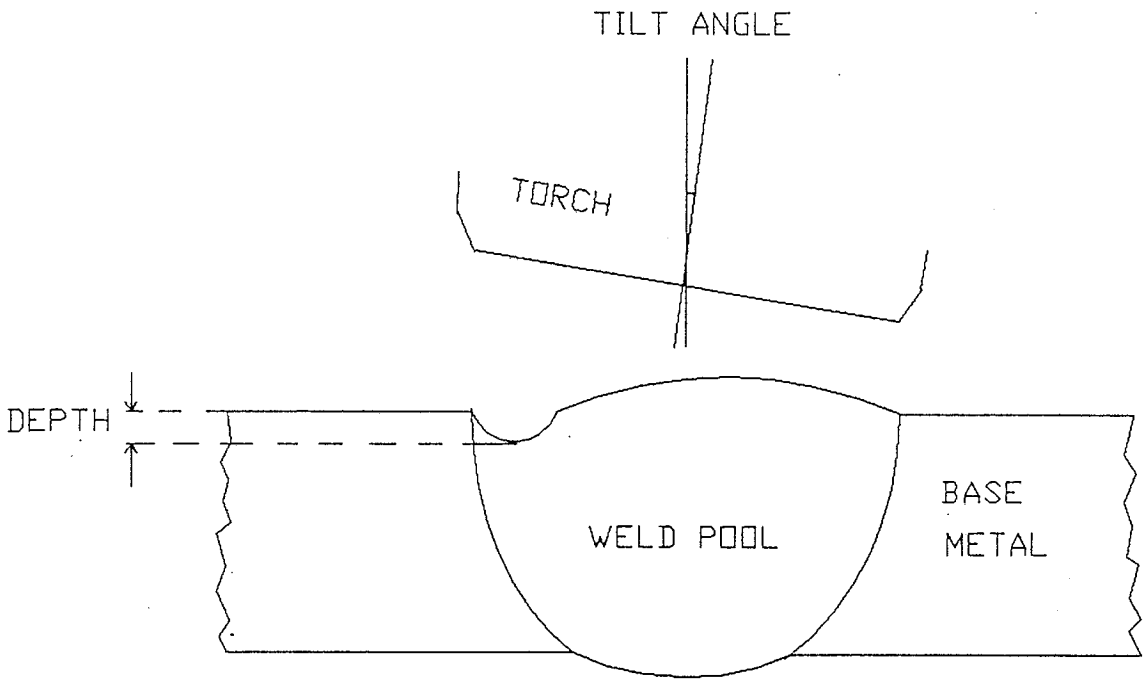

Figure 27 Definition of Tilt Angle and Degree of Undercutting.

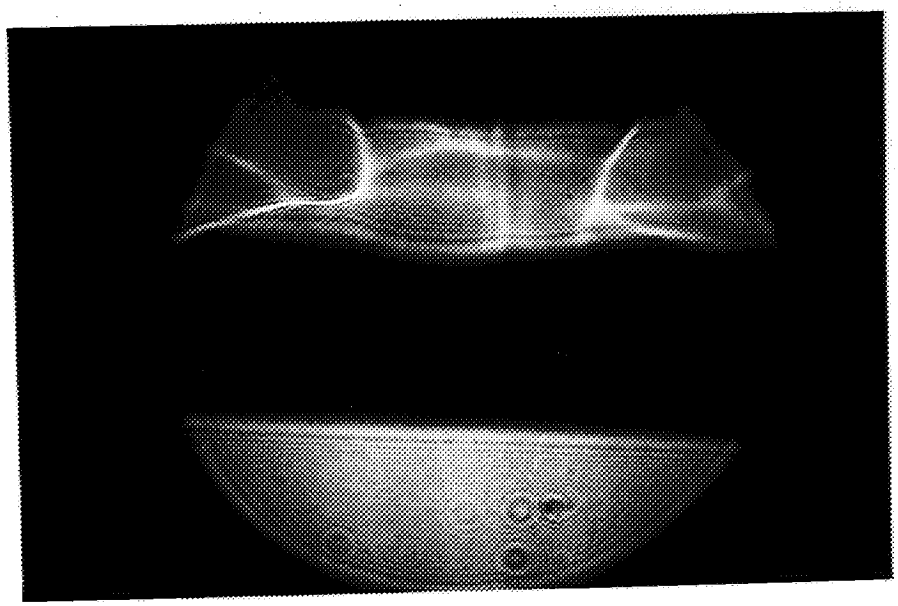

(a)

Figure 28 Flow Patterns with a Tilted Torch, 0°(a).

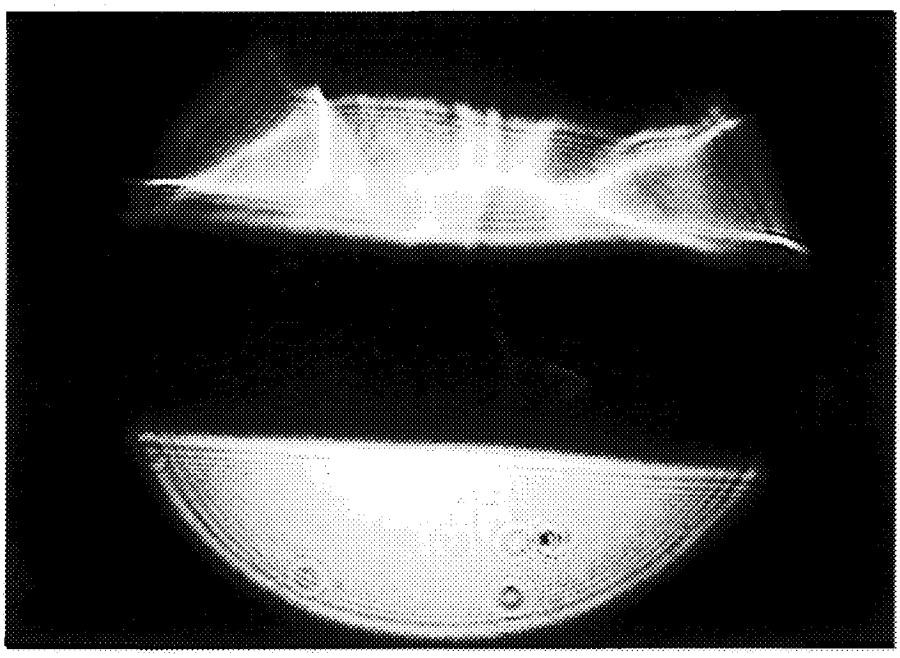

(b)

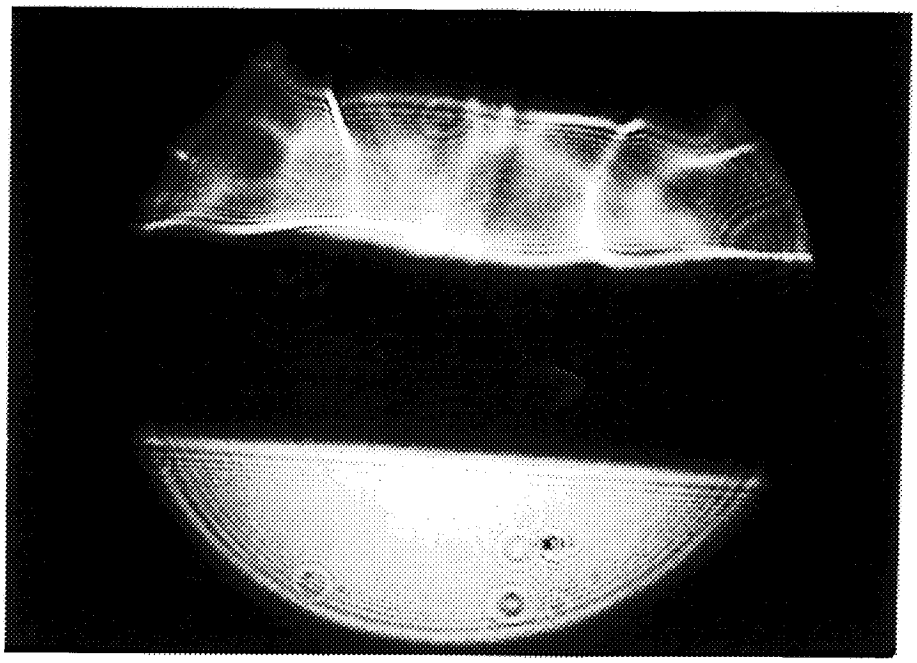

(c)

Figure 28 (continued) Flow Patterns with a Tilted Torch, 1°(b), 2°(c).

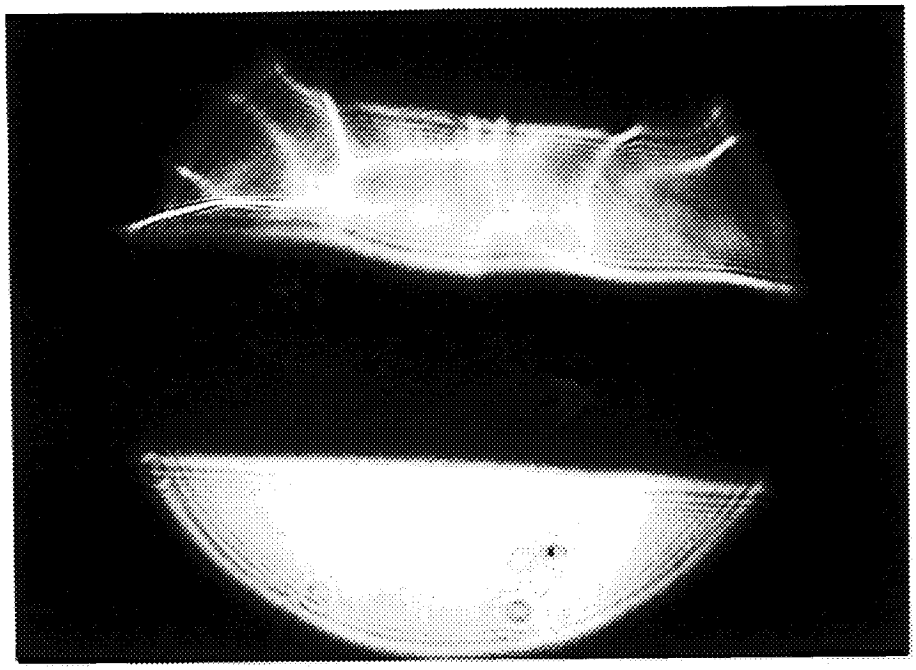

(d)

Figure 28 (continued) Flow Patterns with a Tilted Torch, 3°(d).

13. UNDERCUTTING RESULTS

Figure 29 shows the cross sections of Al 2219 welds with a torch tilt angle ranging from 0 to 4 degree. Figure 30 shows the similar welds made on Al 6061 with the same tilt angle range. The curves in Figure 31 demonstrate the relationship between undercutting and torch tilt angle for these two alloys.

Al 6061 shows an abrupt undercutting increase before 2 degree and slight changes afterwards. While Al 2219 displays a continuous increase with the torch tilt angle.

The results of undercutting on Al 6061 with 3 degree tilted torch at different

commercially clean helium gas flow rates are shown in Figure 32. Figure 33 is the same conditions but with a 4 degree tilted welding torch. After helium contaminated with 650ppm nitrogen was used as shield and the torch was tilted still 4 degree , the resulting undercutting conditions with varying flow rates are given in Figure 34. The results are quantitatively displayed in Figure 35.

When the torch is tilted 3 degree, the undercutting increases moderately with flow rate from 560l/hr (20CFH) to 980l/hr (35CFH) but only slightly beyond 980l/hr (35CFH). When the torch is tilted 4 degree, the undercutting is higher while the flow rate is below 840l/hr (30CFH) and starts to level off with a higher gas flow rate.

Here two factors should be considered to explain the observed phenomena. One is the trace gas contamination in the commercially clean helium shield gas. The amount of this contamination is less predictable and generally will cause the undercutting to go deeper with an increase in gas flow rate. This is the case when the torch is tilted by 3 degree. Another factor is gas contamination from the surrounding atmosphere. This factor can dominate when the tilt angle is larger and shield gas flow rate is lower because poor shielding will exist on the torch side which has a larger standoff. This is also the side which shows the undercutting.

In contrast, the undercutting becomes deeper with gas flow rate when shielding gas with a higher concentration of contaminant is used. This implies that the degree of undercutting is related to the amount of contaminant put into the weld zone.

Helium with a methane contaminant was also used to study the undercutting

issue. In this case the torch was almost perpendicular to the welding plate. The experimental results under four different shielding conditions are shown in Figure 36. The same results are also plotted in Figure 37.

Undercutting is smallest for the case with a flow rate of 560l/hr (20CFH) and a contaminated gas of 250ppm methane. Once the flow rate and gas contamination are doubled, the undercutting shows almost a 7 fold increase. This further shows that undercutting is strongly related to the total contaminant volume which contacts the weld pool.

14. CONCLUSIONS OF UNDERCUTTING STUDY

1. Undercutting increases with increasing torch tilt angle. The amount of increase changes with different alloys.

2. The effect of shielding flow rate on the undercutting shows some complexity due to the combination of the gas contamination within the shielding gas itself and the entrained gas contamination from the surrounding atmosphere.

3. The amount of undercutting is related to the total gas contaminant volume which contacts the weld pool. A minimum shielding gas flow rate consistent with adequate shielding is recommended to minimize the occurrence of undercutting.

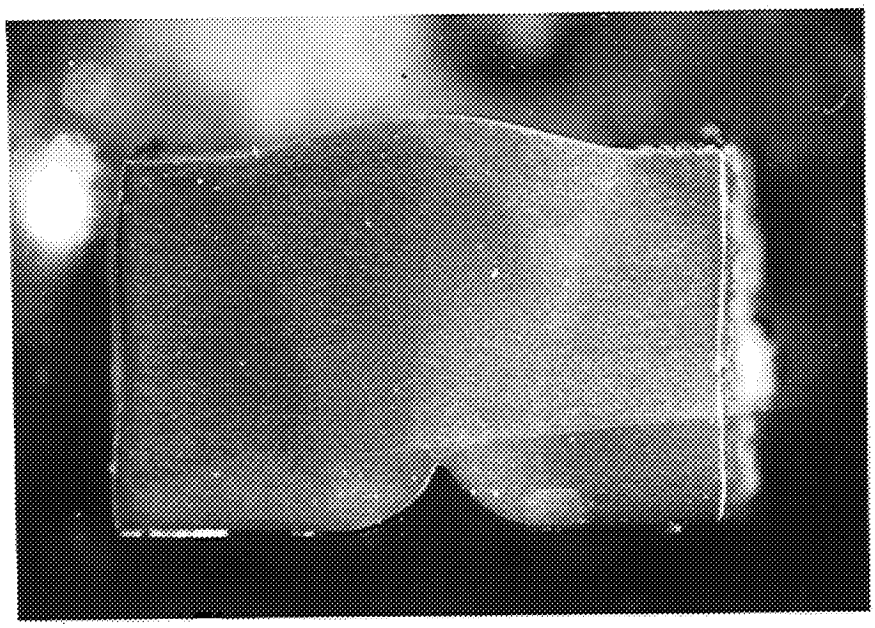

(a)

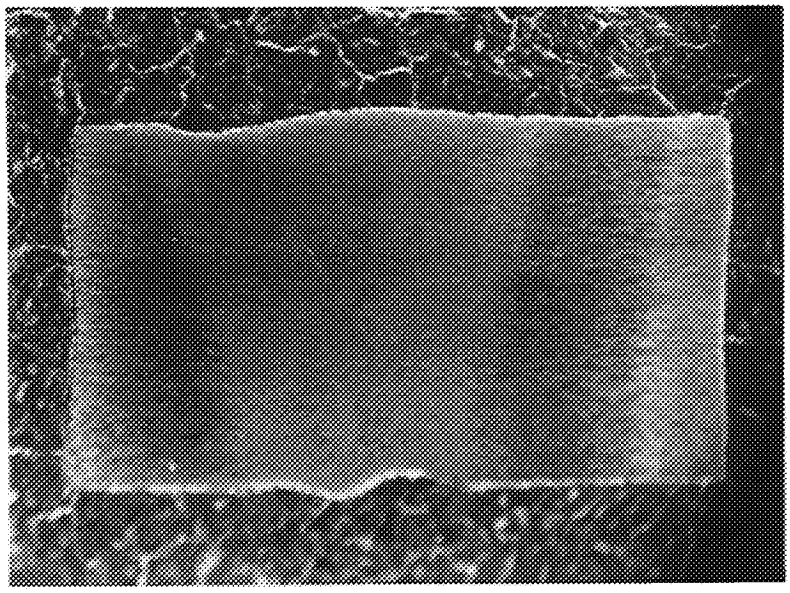

(b)

Figure 29 Undercutting for Al 2219 with a Tilted Torch, 0°(a), 1°(b).

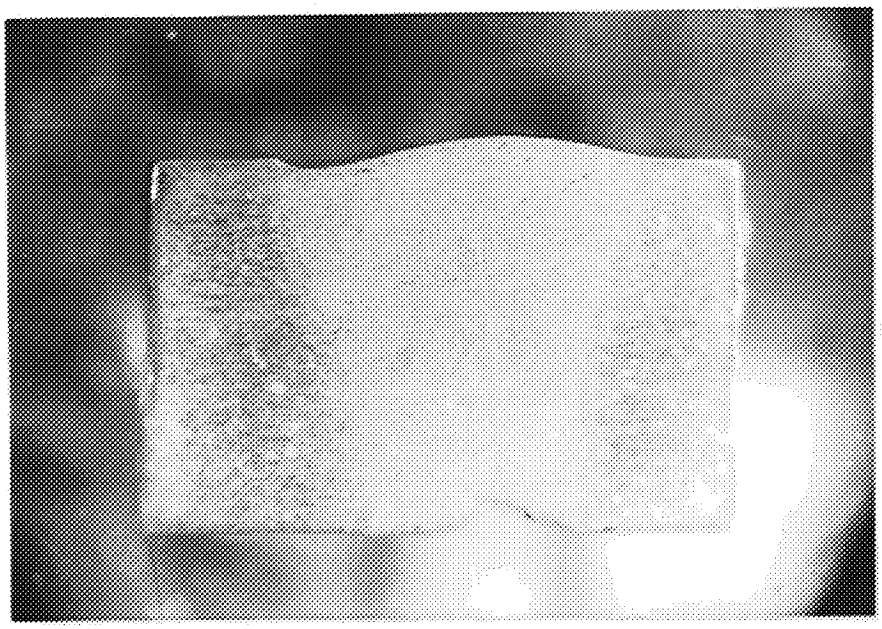

(c)

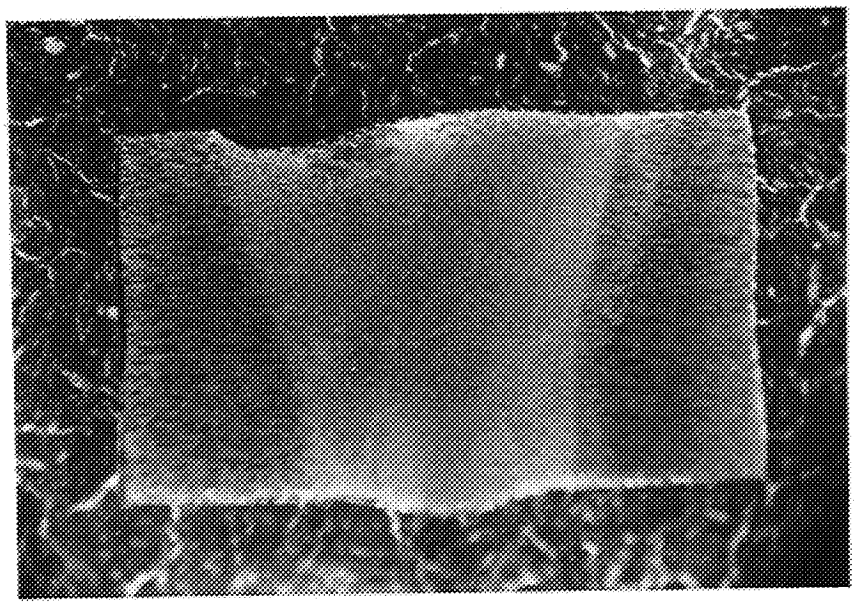

(d)

Figure 29 (continued) Undercutting for Al 2219 with a Tilted Torch, 2°(c), 3°(d).

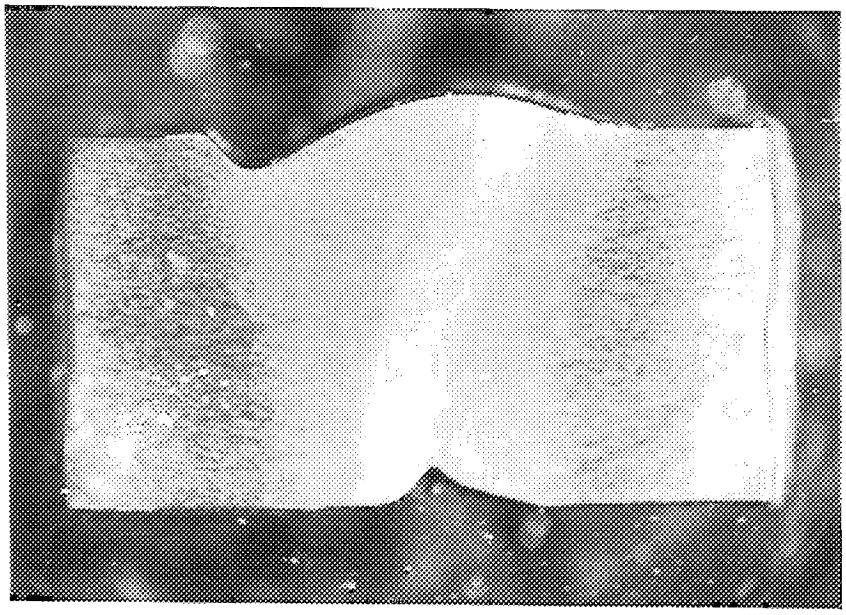

(e)

Figure 29 (continued) Undercutting for Al 2219 with a Tilted Torch, 4°(e).

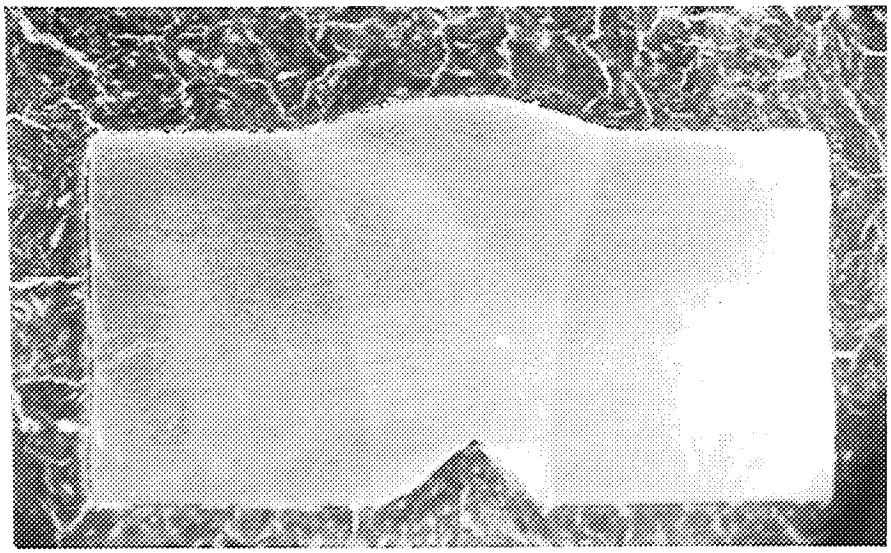

(a)

Figure 30 Undercutting for Al 6061 with a Tilted Torch, 0°(a).

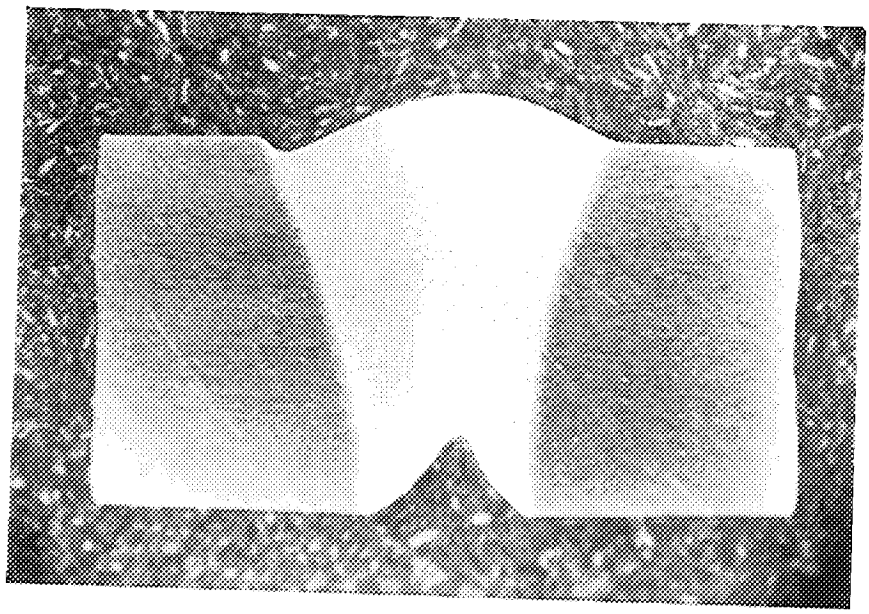

(b)

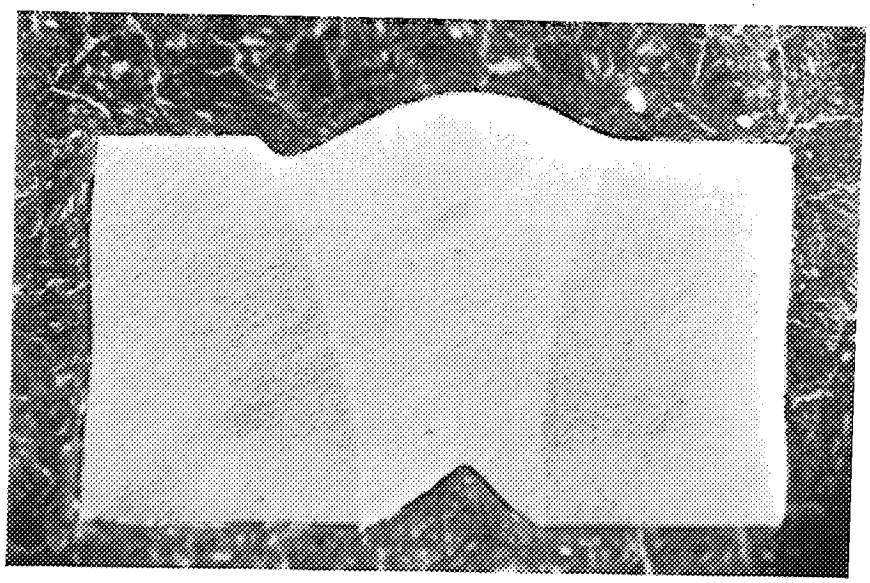

(c)

Figure 30 (continued) Undercutting for Al 6061 with a Tilted Torch, 1°(b), 2°(c).

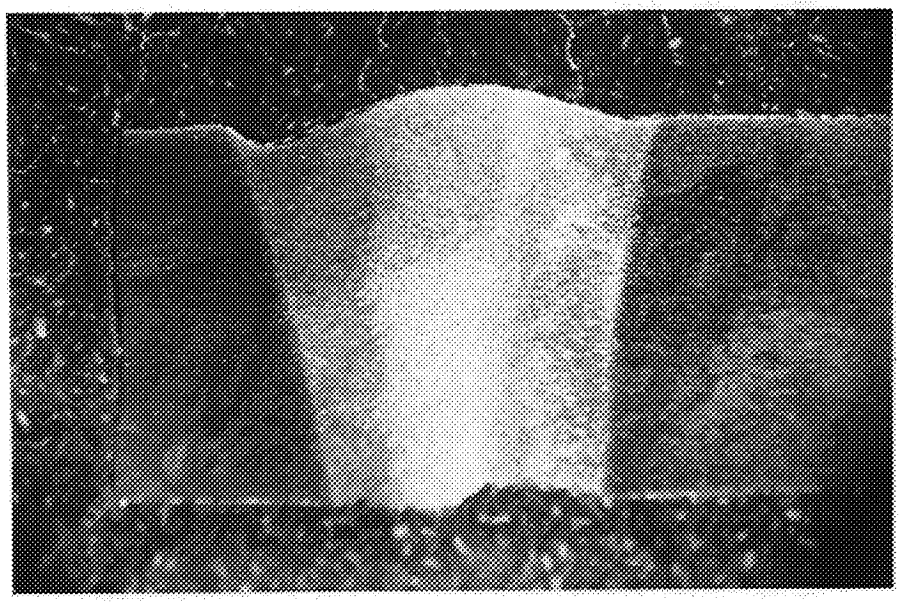

(d)

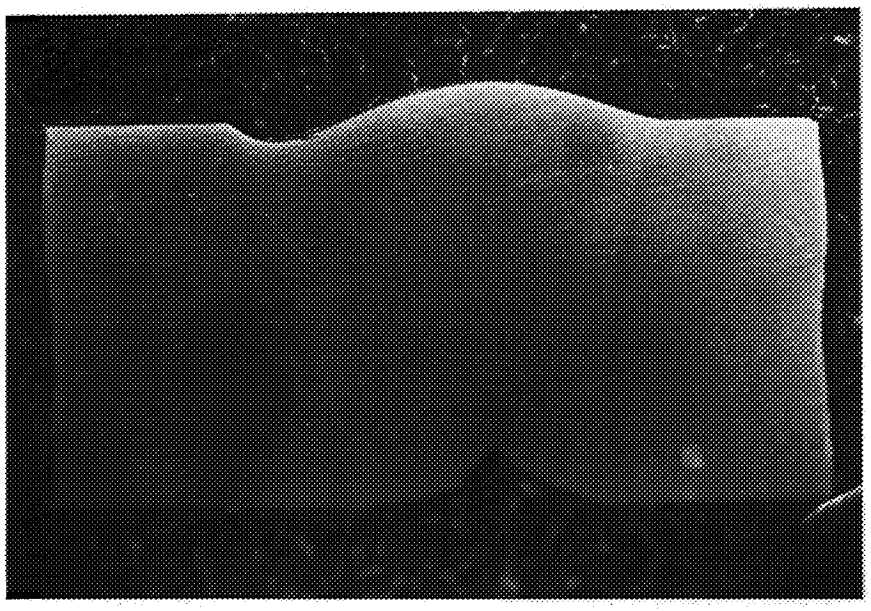

(e)

Figure 30 (continued) Undercutting for Al 6061 with a Tilted Torch, 3°(d), 4°(e).

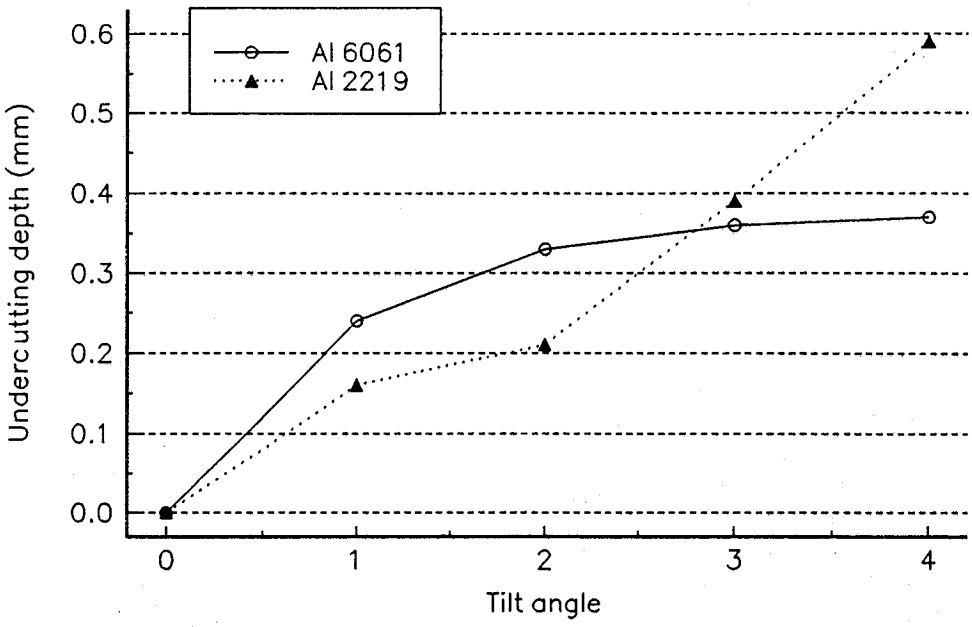

Figure 31 Relationship between Undercutting and Tilt Angle for Al 2219 and Al 6061.

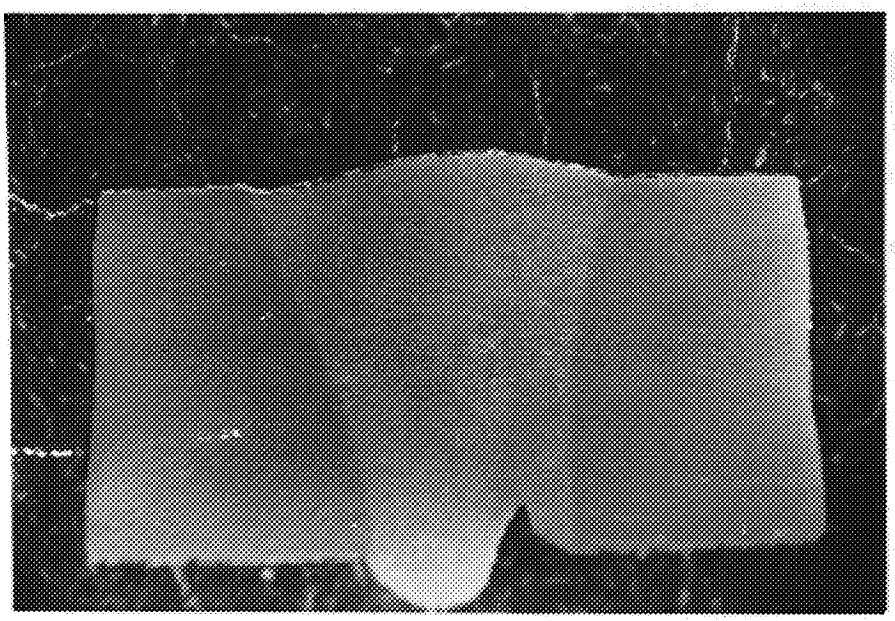

(a)

Figure 32 Undercutting for Al 6061 with a 3° Tilted Torch, 20CFH(a).

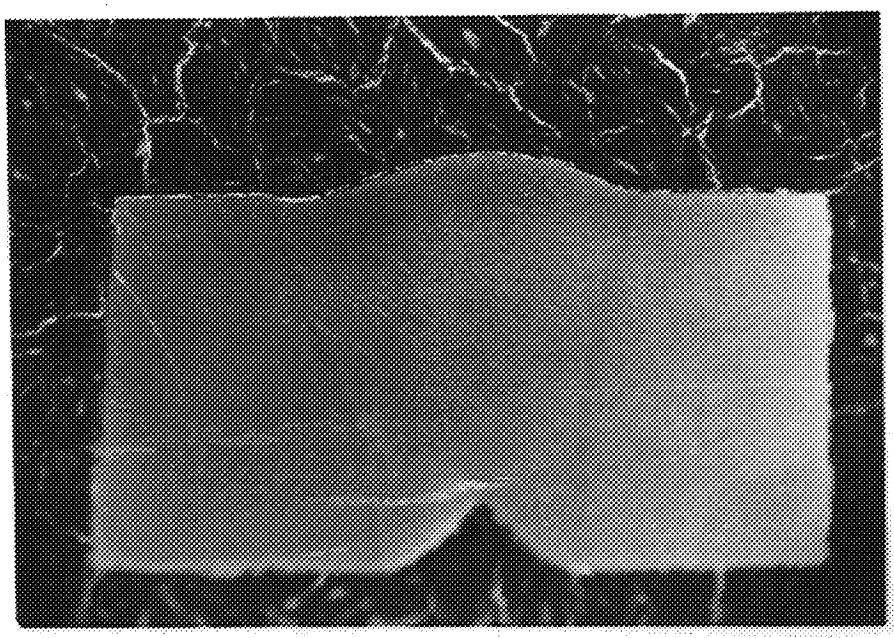

(b)

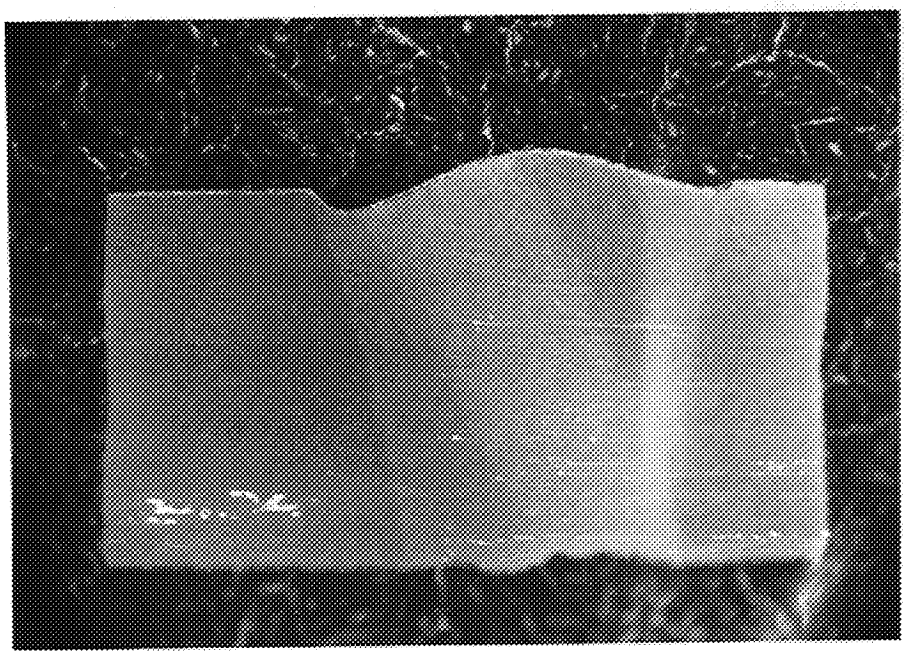

(c)

Figure 32 (continued) Undercutting for Al 6061 with a 3° Tilted Torch, 27CFH(b), 35CFH(c).

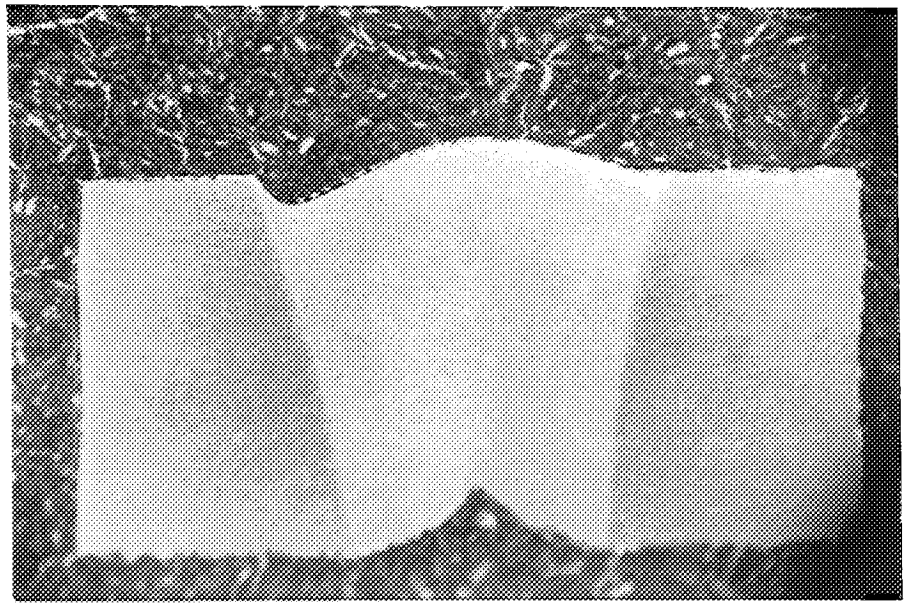

(d)

Figure 32 (continued) Undercutting for Al 6061 with a 3° Tilted Torch, 46CFH(d).

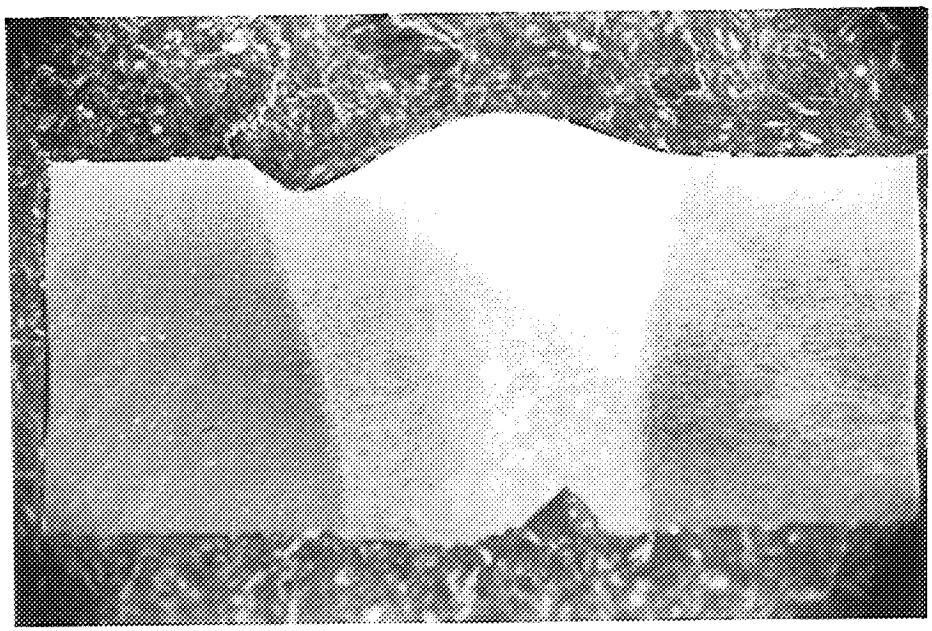

(a)

Figure 33 Undercutting for Al 6061 with a 4° Tilted Torch, 20CFH(a).

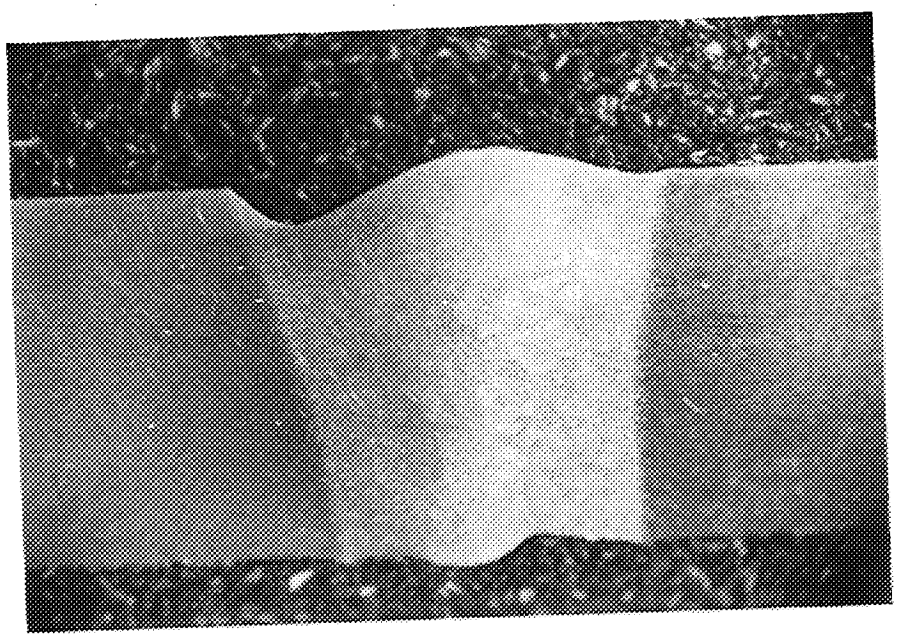

(b)

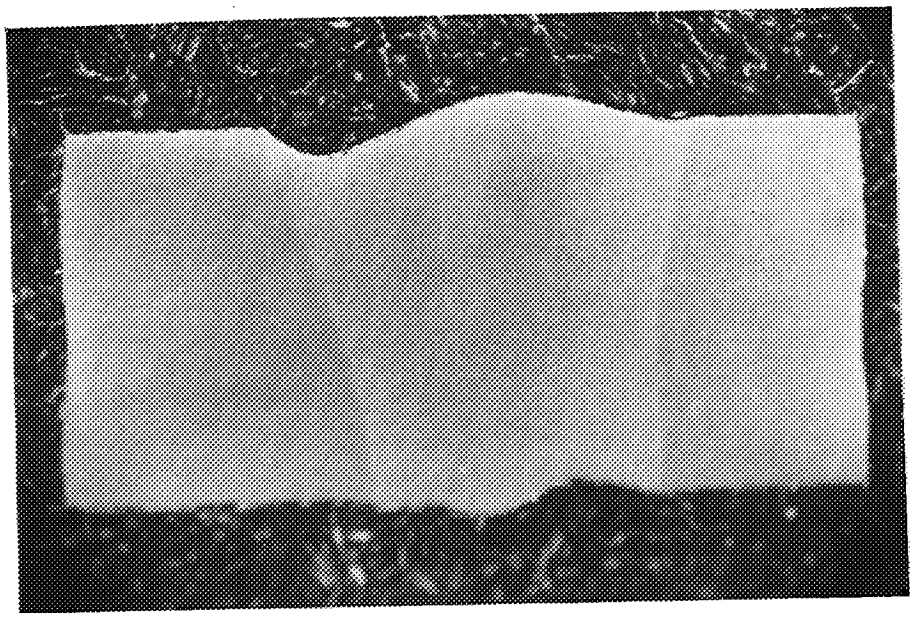

(c)

Figure 33 (continued) Undercutting for Al 6061 with a 4° Tilted Torch, 27CFH(b), 30CFH(c).

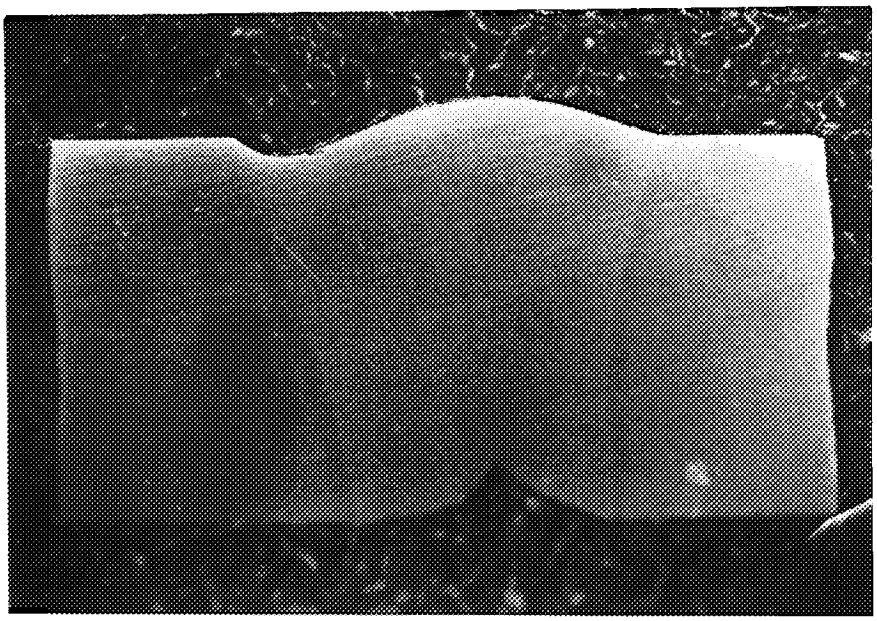

(d)

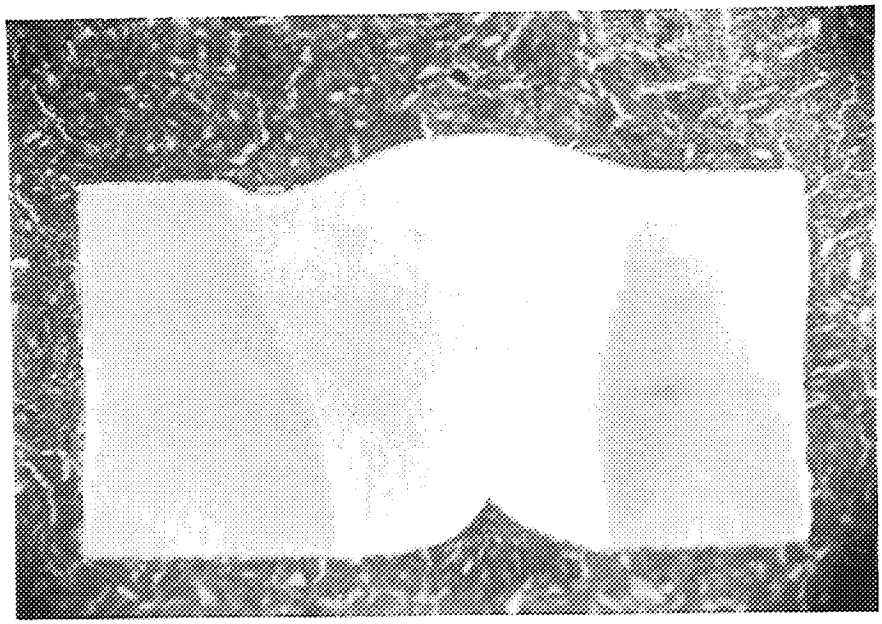

(e)

Figure 33 (continued) Undercutting for Al 6061 with a 4° Tilted Torch, 46CFH(e).

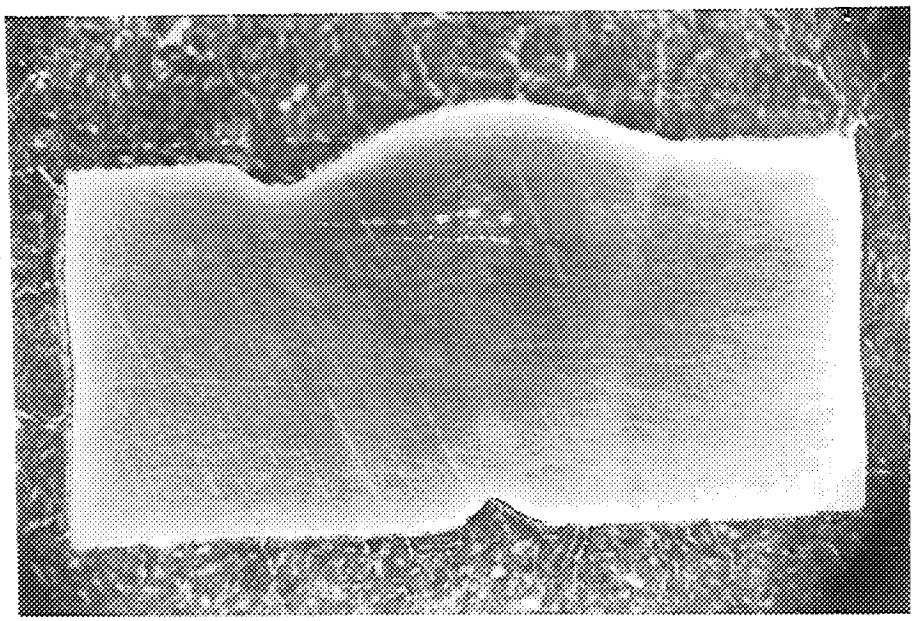

(a)

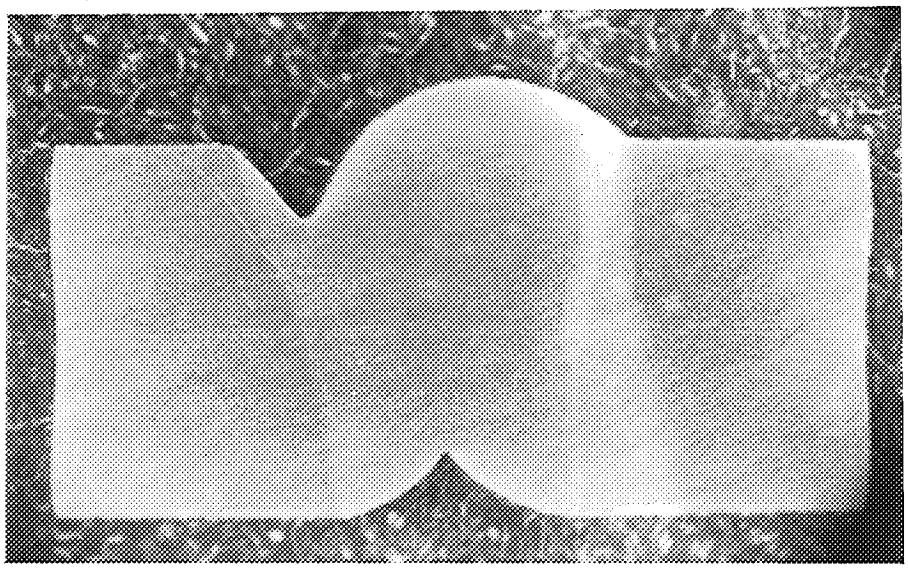

(b)

Figure 34 Undercutting for Al 6061 with a 4° Tilted Torch and 650ppm N_2 Contaminated Shield Gas, 20CFH(a), 27CFH(b).

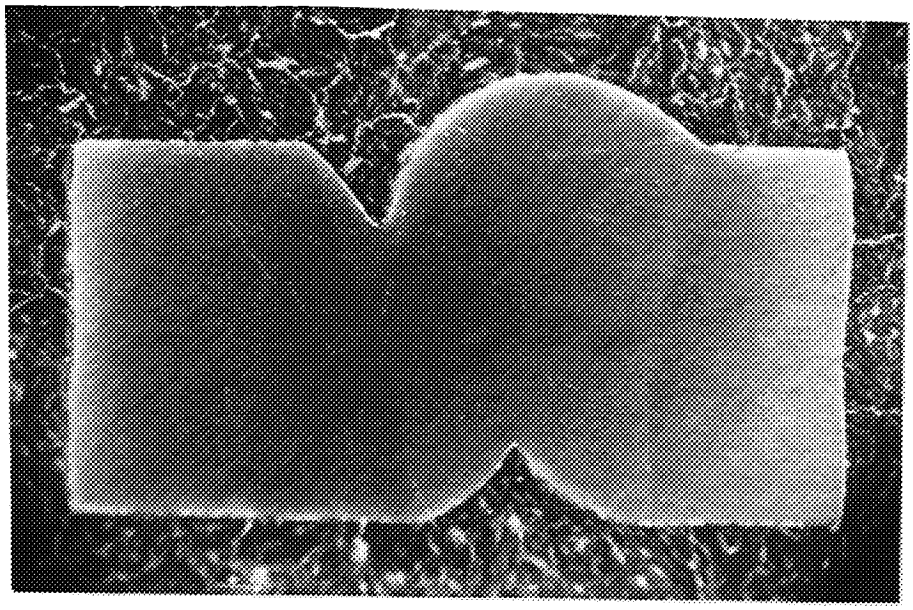

(c)

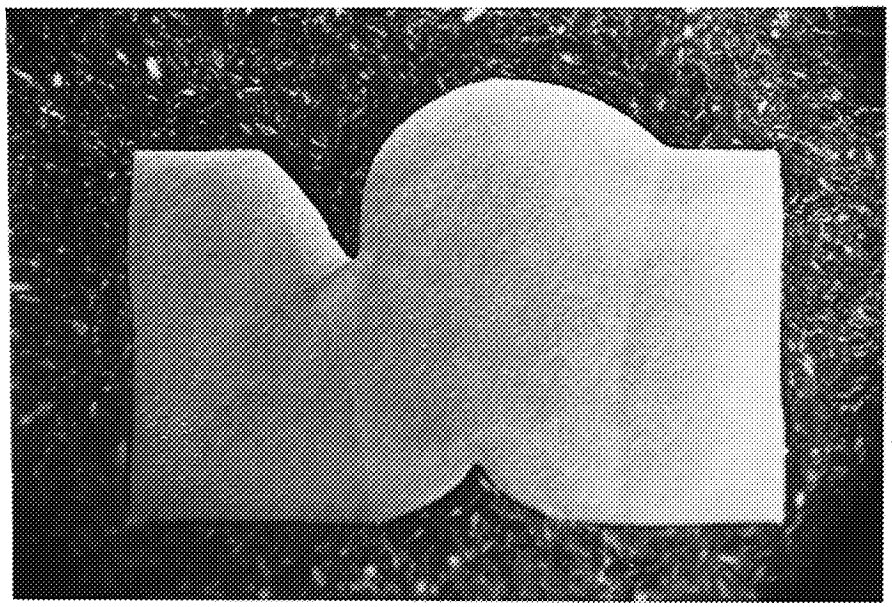

(d)

Figure 34 (continued) Undercutting for Al 6061 with a 4° Tilted Torch and 650ppm N_2 Contaminated Shield Gas, 30CFH(c), 35CFH(d).

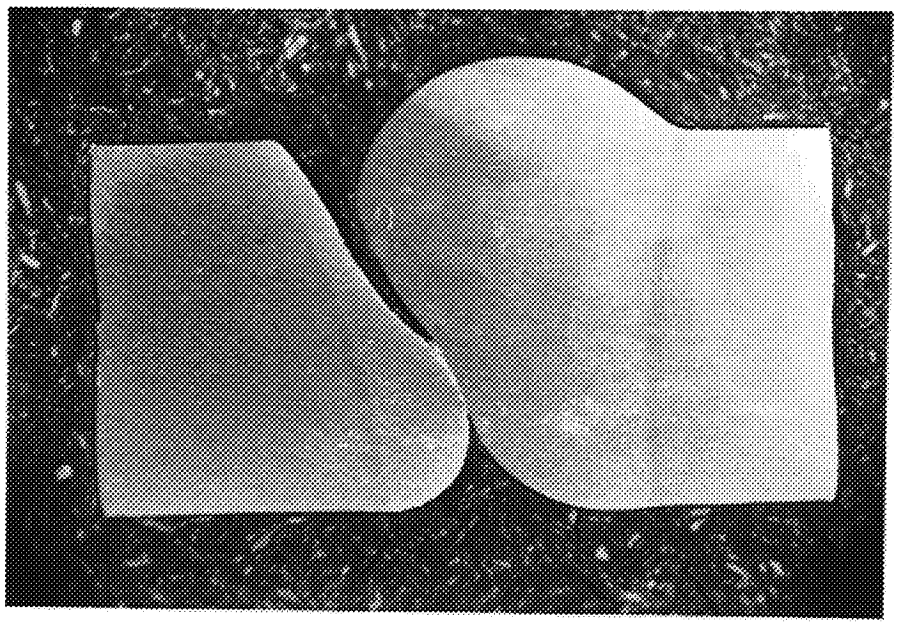

(e)

Figure 34 (continued) Undercutting for Al 6061 with a 4° Tilted Torch and 650ppm N_2 Contaminated Shield Gas, 40CFH(e).

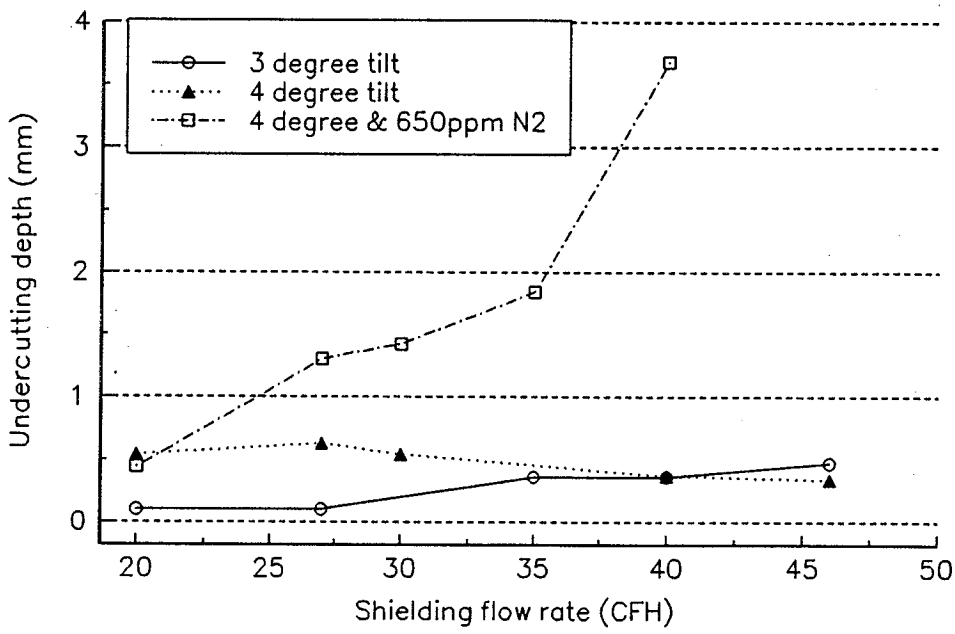

Figure 35 Relationship between Undercutting and Gas Flow Rate for Al 6061.

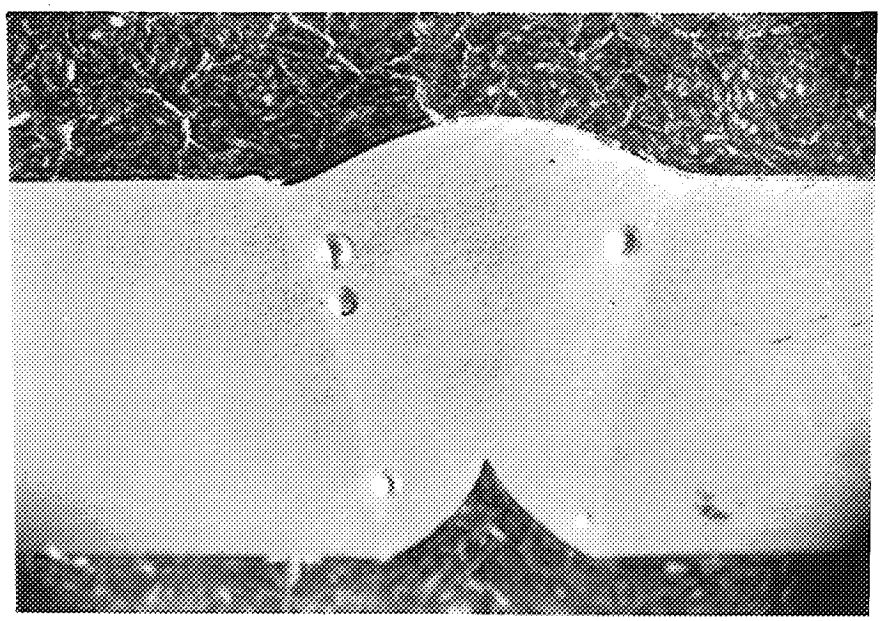

(a)

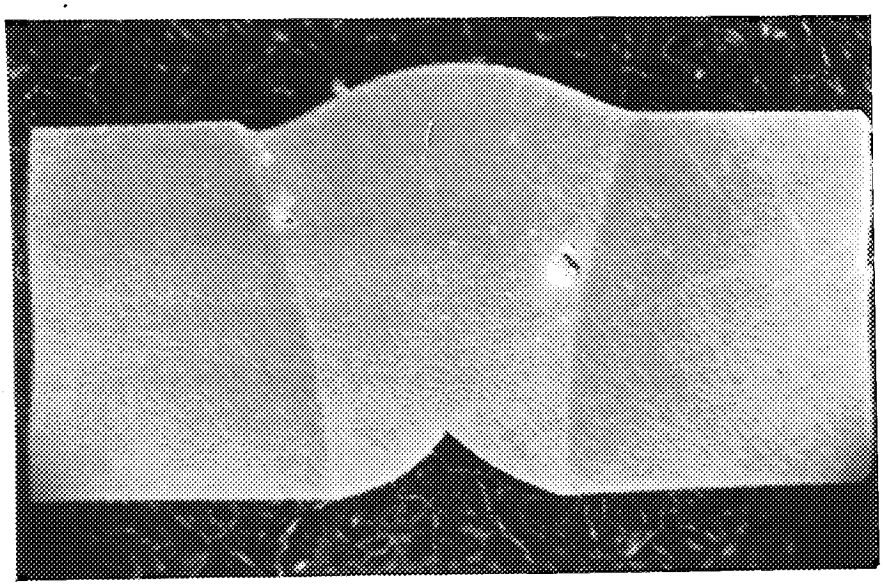

(b)

Figure 36 Undercutting for Al 6061 with a CH_4 Contaminated Shield Gas, 20CFH & 250ppm(a), 20CFH & 500ppm(b).

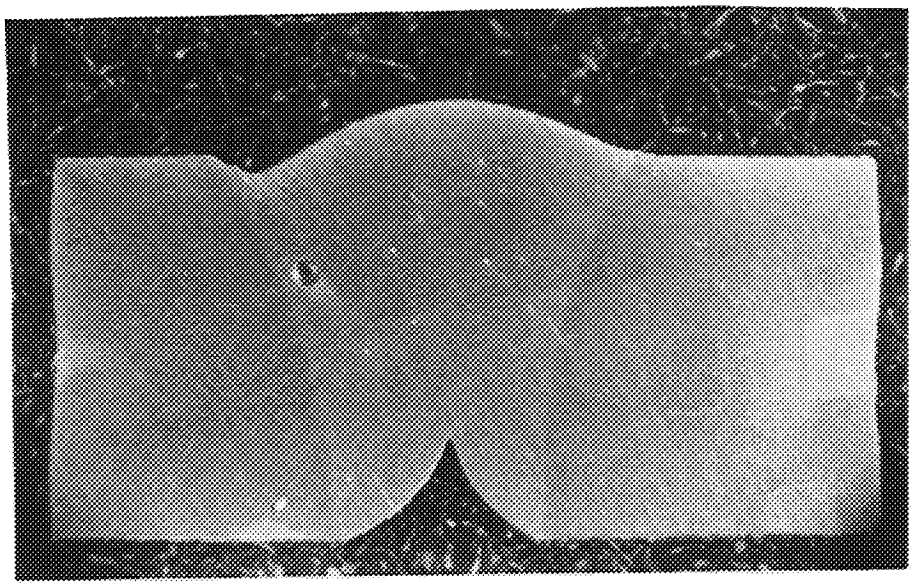

(c)

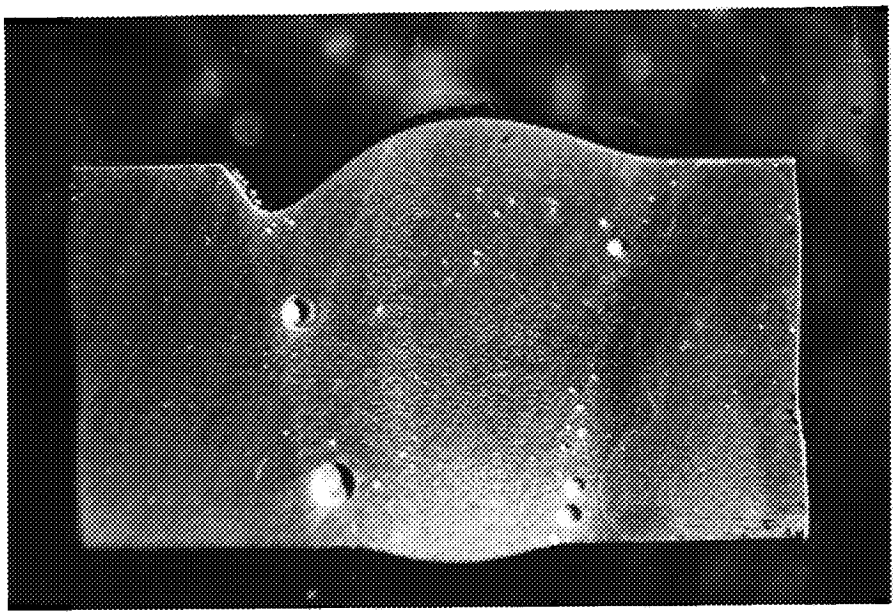

(d)

Figure 36 (continued) Undercutting for Al 6061 with a Contaminated Shield Gas, 40CFH & 250ppm(c), 40CFH & 500ppm(d).

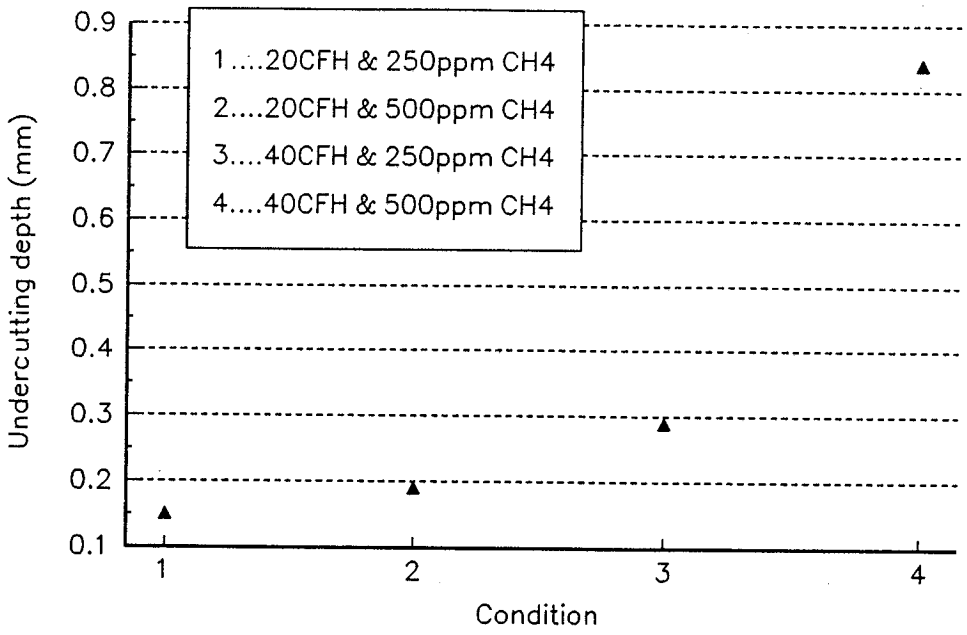

Figure 37 The Relationship between Undercutting and Gas Contamination.

15. MODIFICATION OF SHIELD CUP

A schematic of the VPPA welding torch assembly is shown in Figure 38. The electrode is held in a collet assembly to insure its alignment. The shape of the shield cup is tapered to fit with the nozzle. The top of the cup is on the same plane as the tip of the orifice.

At a fixed standoff, which is the distance between the shield cup and the workpiece, there exists a critical shield gas flow rate below which the shield gas will not successfully protect the weld pool from the atmosphere. When standoff is increased, the critical shield flow rate increases because of the increased length of the shield gas column, as shown in Figure 20.

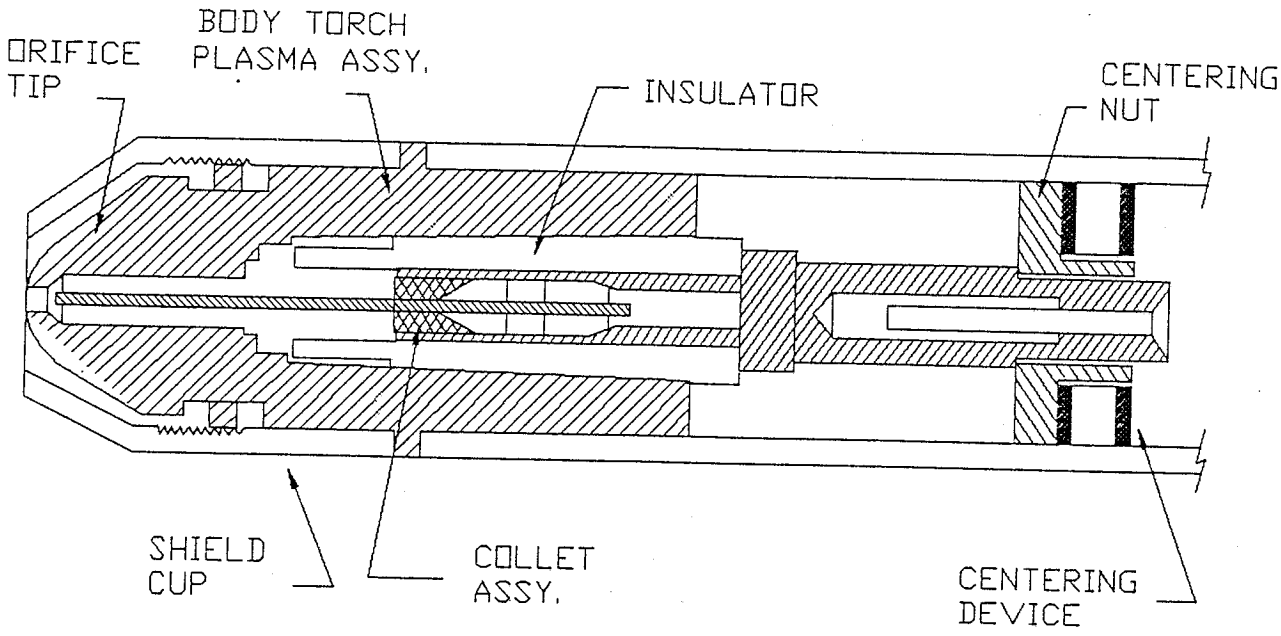

Figure 38 VPPA Welding Torch Assembly.

Figure 39 shows the relationship between the standoff and the effectiveness of shielding. A cover pass weld was made on a 6061 Al plate with a 3° tilted torch, where the plasma and shield gas flow rates were 56 l/hr and 560 l/hr respectively. When the torch is tilted, different standoff conditions exist, e.g., one side will have a larger standoff and the other will have a smaller one. If the total shield gas flow rate is close to the critical value for the non-tilted torch condition, the shield flow rate can be above the critical value on one side while on the other side it is below the critical value. Thus the side which meets the critical rate requirement will have an acceptable weld and the other side will not. Figure 39 illustrates this situation.

The left side of the weld bead (the part away from the tilt) is clearly inadequately shielded while the right half is acceptable.

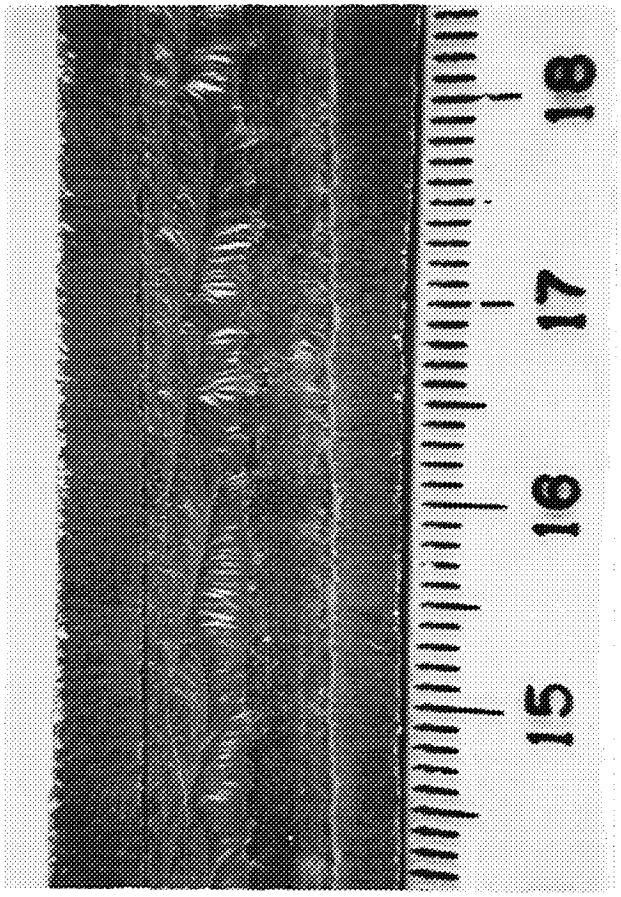

Figure 39 A Cover Pass Weld Made with a Tilted Torch.

Based on these considerations, decreasing the standoff will be advantageous in terms of reducing shield gas consumption. In addition, as shown above, a reduction of the shield flow rate can minimize susceptibility to undercutting since less possibly contaminated gas is needed.

The standoff can be reduced by increasing the length of the shield cup slightly which will make the cup extend beyond the welding nozzle. This increase in length

cannot be large because of the limited distance between the cup and workpiece during welding. However, a small change might make a difference since the critical shield flow rate is very sensitive to the standoff.

Two new shield cups, made of aluminum, were fabricated with the same height of 4.9cm (1.93"), both 1.5mm (0.06") longer than the original one. The original shield cup will be referred to as mode 1. The mode 2 cup was made with a tapered inner shape like the original one, while the mode 3 cup was the same length as the mode 2 cup but did not have the inner taper. Schematics of these cups are shown in Figure 40. Figure 41 shows their flow patterns when plasma flow rate and shield flow rates were 56l/hr (2CFH) and 1120l/hr (40CFH) respectively. Turbulent flow can be observed with the mode 3 cup presumably caused by the sharp corners on the flow path.

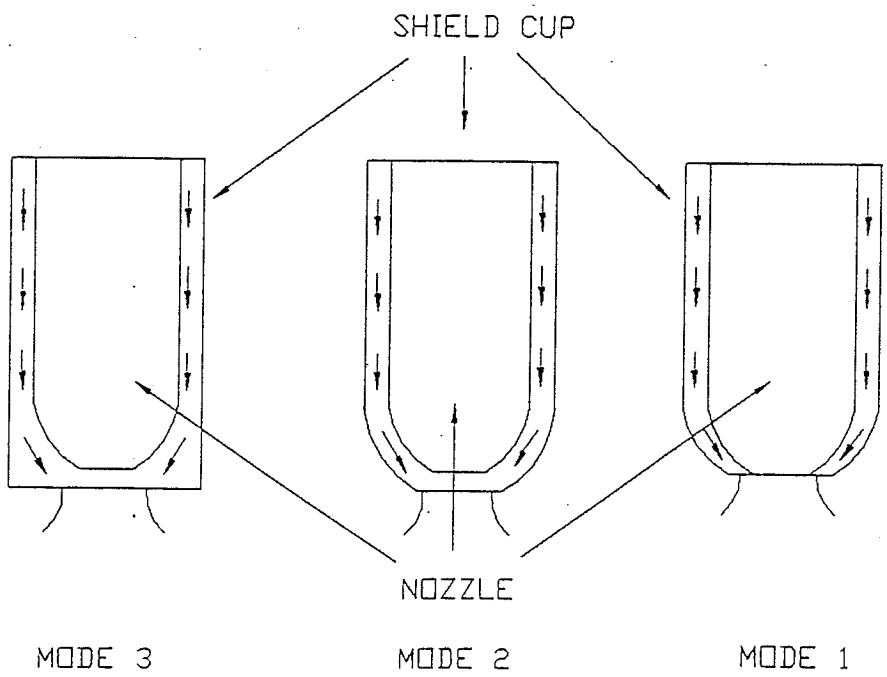

Figure 40 Schematics of Shield Cups.

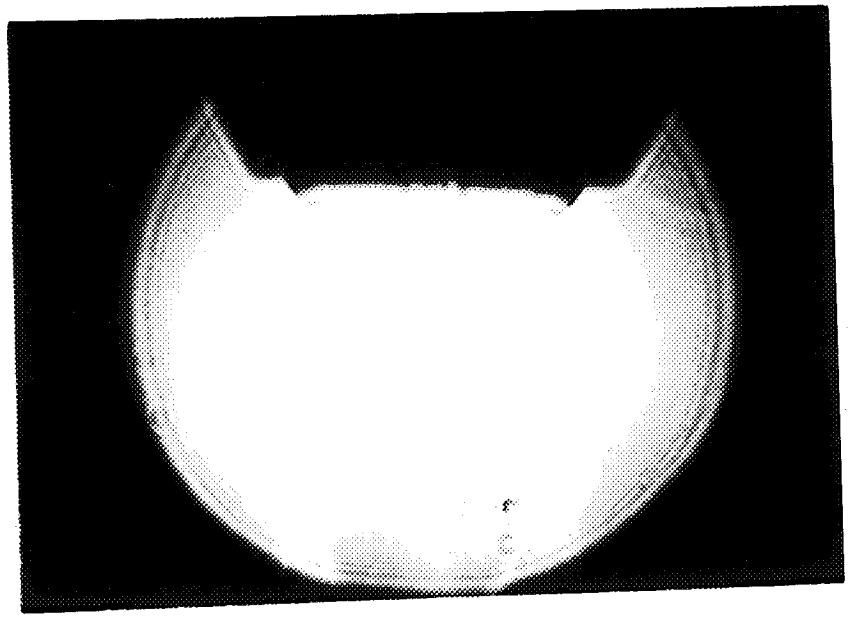

(a)

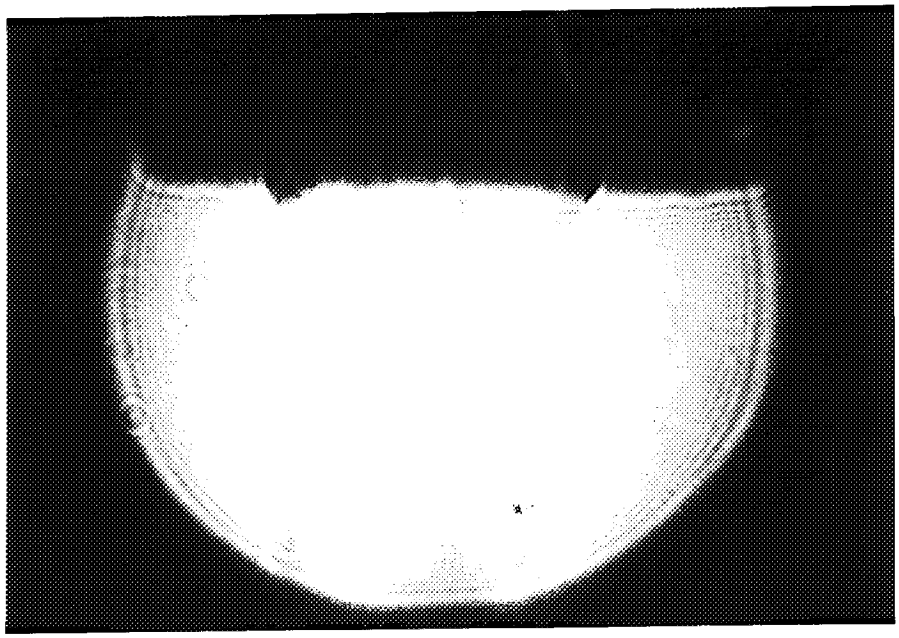

(b)

Figure 41 Flow Patterns for Different Shield Cups, Mode 1(a), Mode 2(b).

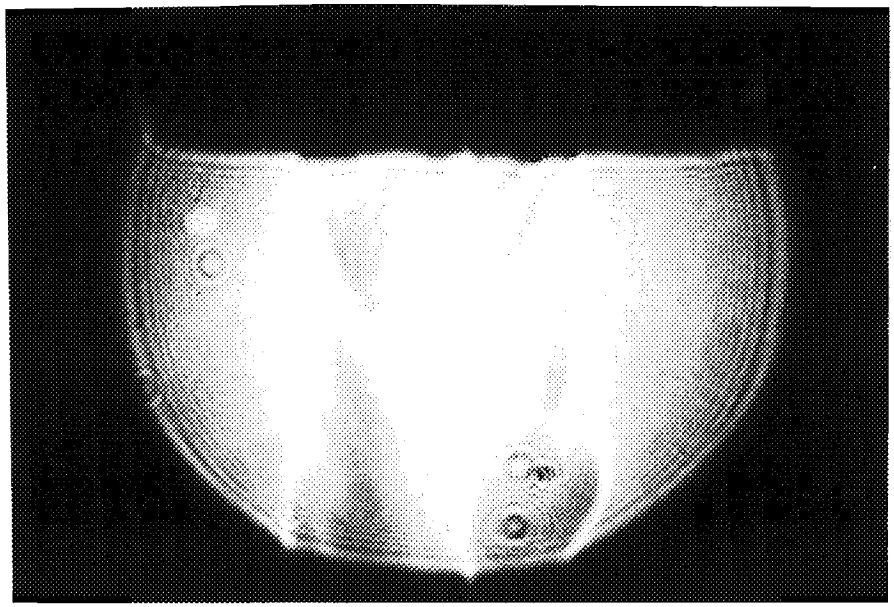

(c)

Figure 41 (continued) Flow Patterns for Different Shield Cups, Mode 3(c).

16. RESULTS WITH NEW SHIELD CUP

Welds were made on 6.35mm (1/4") thick 6061 aluminum plates using the new cups as well as the original one. Welding parameters are listed in Table 2.

Figure 42 shows the weld surfaces of sample 1' and 1 made with the original cup. After the shield flow rate was reduced from 1120l/hr (40CFH, weld 1) to 560l/hr (20CFH, weld 1'), the weld became defective and obviously unacceptable. Weld sample 2 made with cup 2 is shown in Figure 43, and weld 3 with cup 3 is shown in Figure 44. Although welds 2 and 3 only consumed half the shield gas that weld 1 did, their surfaces still look shiny and smooth, indicating adequate shield gas.

Cross sections of sample 1, 2 and 3 are shown in Figure 45. No porosity is found in sample 2 and 3. The aspect ratio (weld depth/weld length) as well as the molten area of sample 1, 2 and 3 are shown in Figure 46. The molten area was calculated by assuming a parabolic shape and using 2/3 X depth x width of the weld[16]. Sample 3 shows a smaller aspect ratio and molten area than sample 1 while sample 2 shows a slightly larger aspect ratio and molten area than sample 1. This implies that the tapering of the cup is necessary to concentrate the heat on the workpiece. Cup 3, which has no tapering, generates more turbulent flow and hence dissipates more heat by faster gas convection. Weld quality with the mode 2 shield cup is as good as that with mode 1 (original cup), but used only half the shield gas.

Table 2 Welding Conditions with 3 Different Shield Cups

Weld Sample	1'	1	2	3
Shield Cup (mode)	1	1	2	3
Welding Mode	cover		pass	
Welding Current (A)	120	120	120	120
Welding Voltage (V)	30	30	30	30
F/R Time	19/4	19/4	19/4	19/4
Plasma Flow Rate (l/hr)	56	56	56	56
Shield Flow Rate (l/hr)	560	1120	560	560
Torch Speed (mm/sec)	4.13	4.13	4.13	4.13

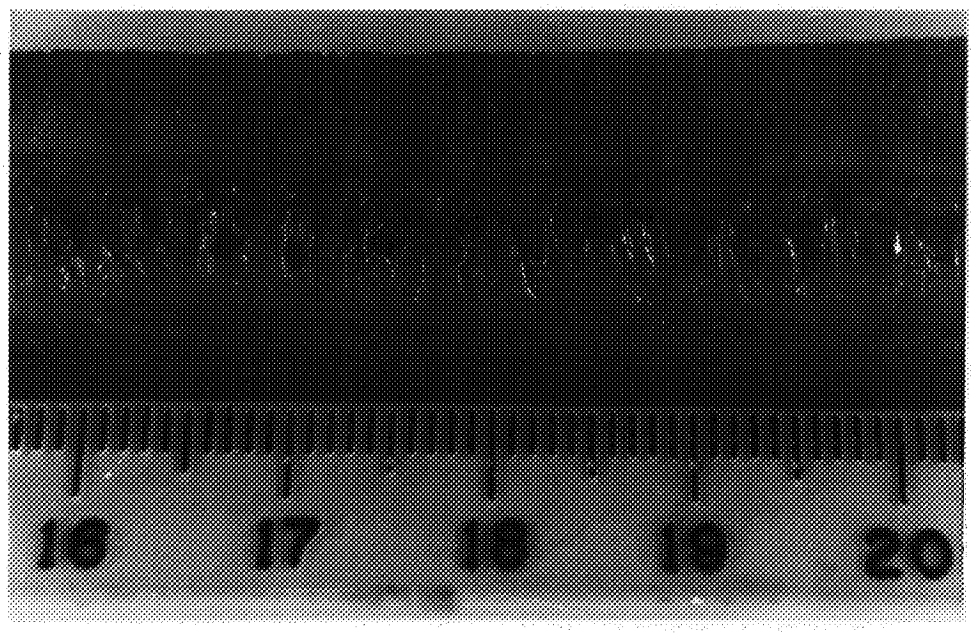

(a)

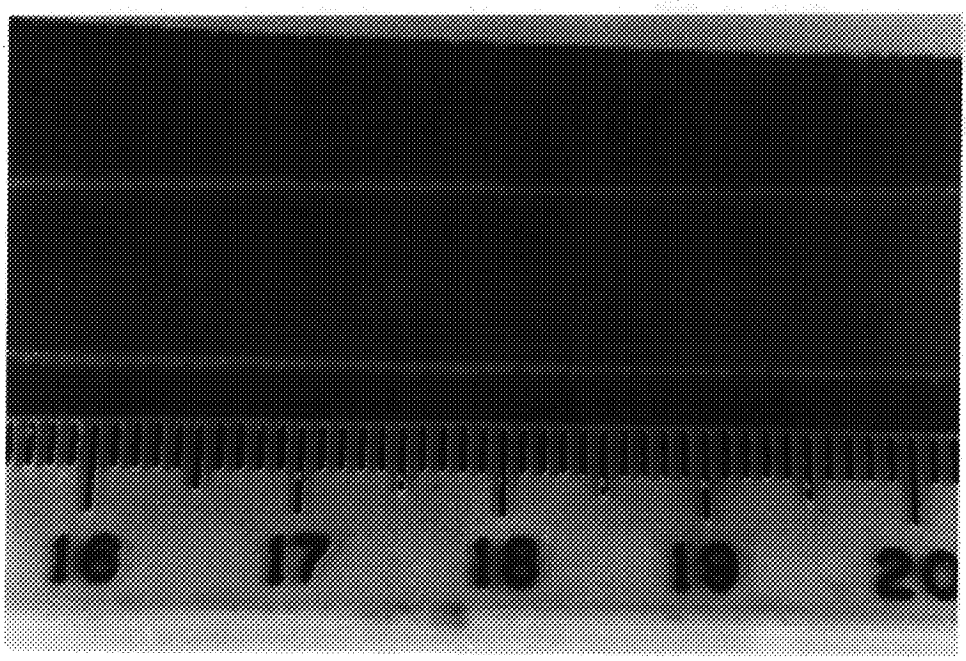

(b)

Figure 42 Surfaces of Weld 1' and 1 Made with Current Cup (mode 1), Shield Flow Rate, 20CFH(a) and 40CFH(b).

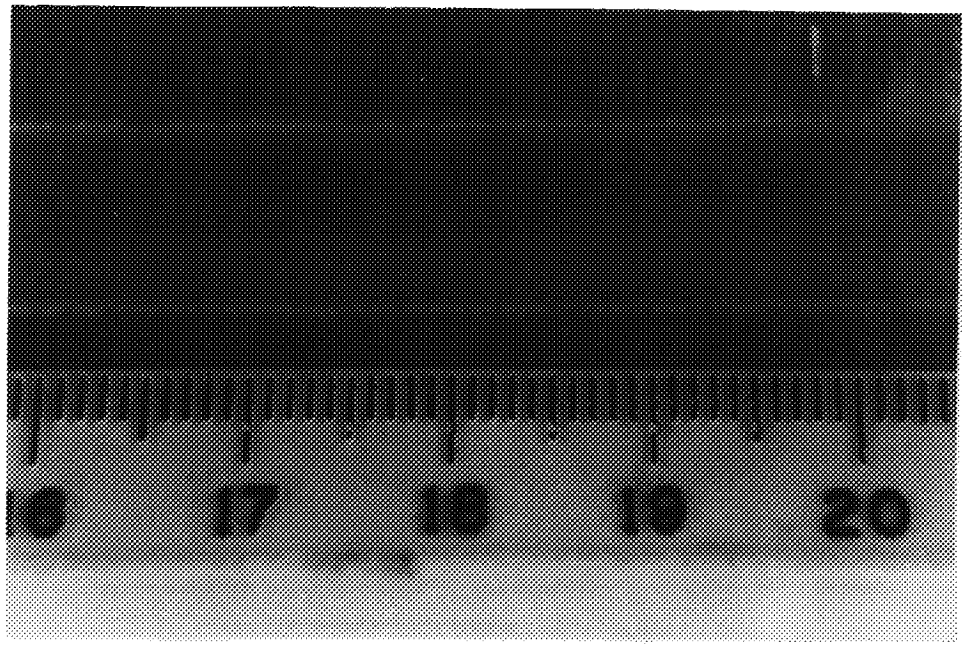

Figure 43 Surface of Weld 2 Made with Cup 2.

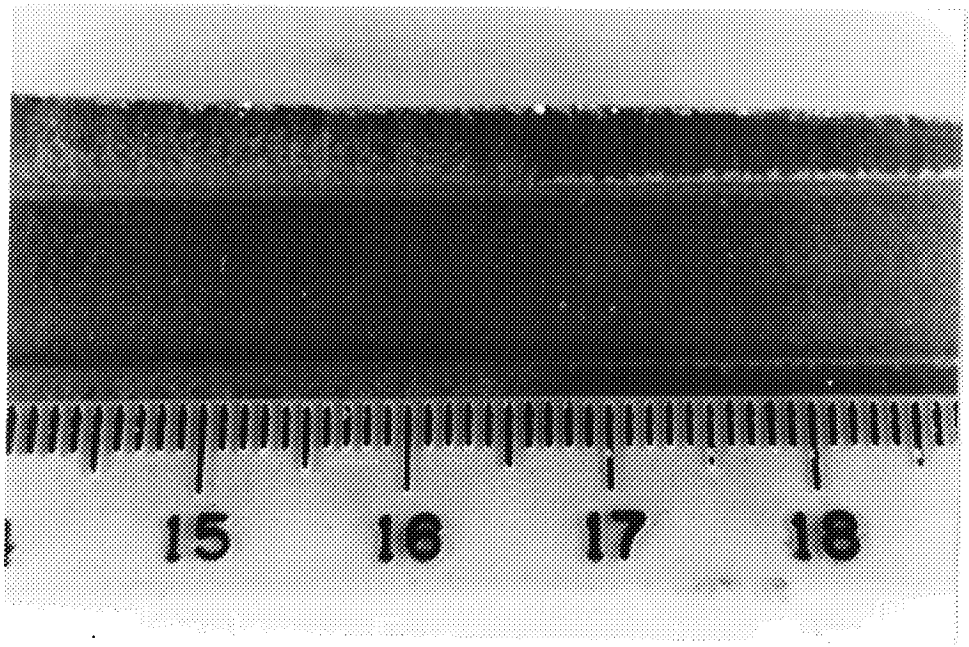

Figure 44 Surface of Weld 3 Made with Cup 3.

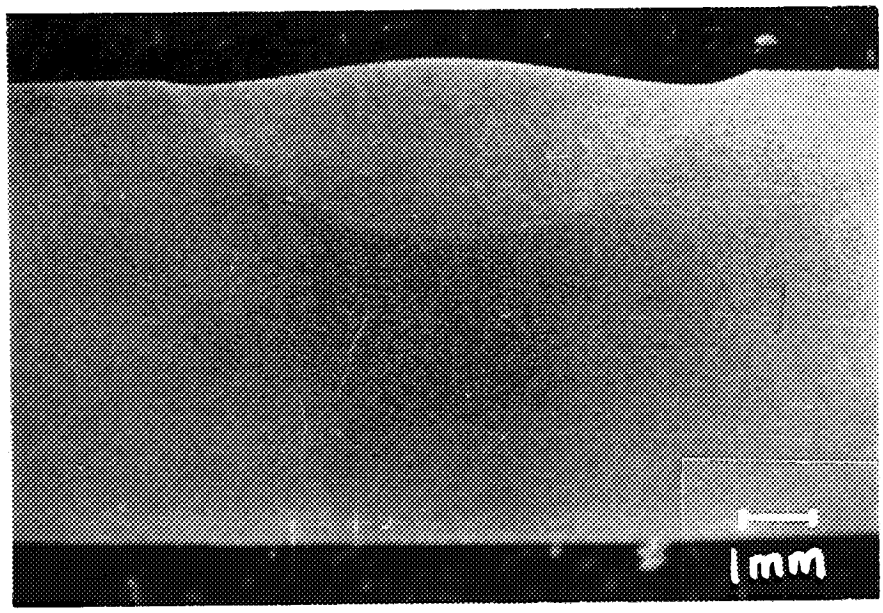

(a)

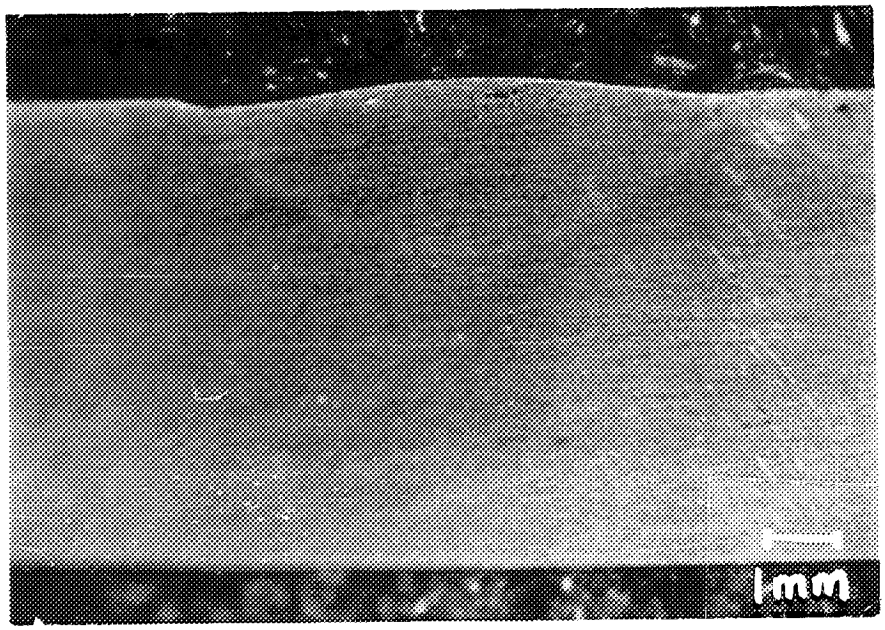

(b)

Figure 45 Cross Sections of Weld Samples, Weld 1(a), Weld 2(b).

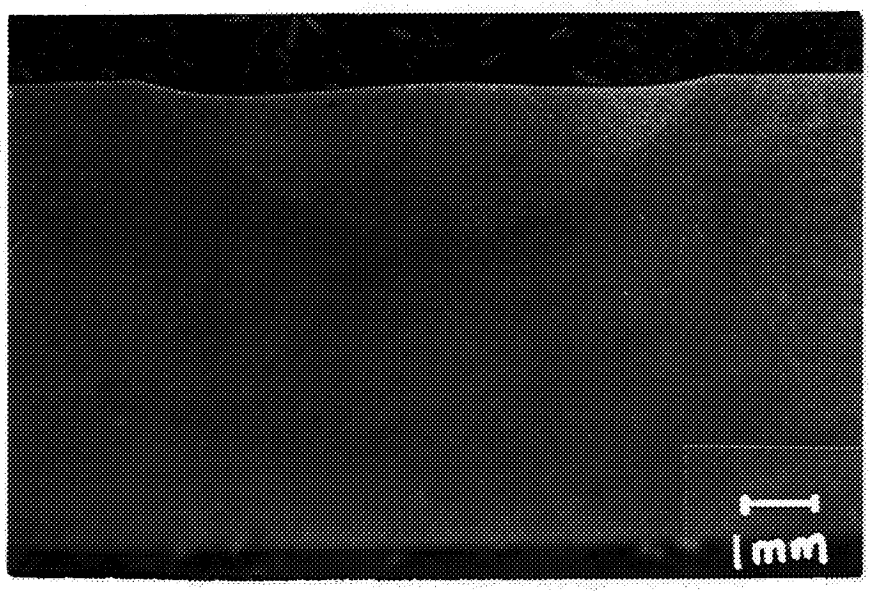

(c)

Figure 45 (continued) Cross Sections of Weld Samples, Weld 3(c).

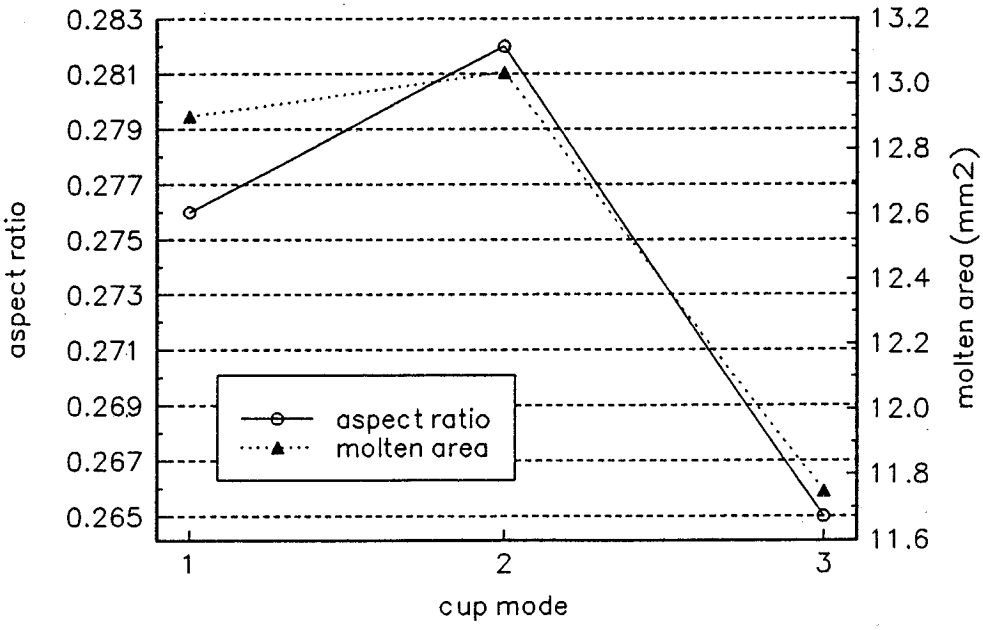

Figure 46 Aspect Ratio and Molten Area vs. Shield Cup.

17. CONCLUSIONS ON NEW SHIELD CUP

The Mode 2 shield cup, which has a tapered inner shape and is 1.5mm longer than the original cup, can reduce the shield gas flow distance and thus the shield gas consumption while maintaining the required weld quality. This cup is also believed to reduce the tendency to undercut.

18. WELDING TORCH MODIFICATION FOR AL-LI WELDING —— INTRODUCTION

The aluminum-lithium alloy family shows promise as a structural alloy because of its lower density combined with a higher stiffness and excellent fatigue properties and cryogenic toughness. Its use in the aircraft and space industries will yield significant weight saving without, and more efficiently with, redesign. The extensive use of Al-Li can lead to structural weight reductions of up to 15% in commercial airliners[17].

Recent reviews[18-20] have indicated that difficulties such as hot cracking and weld porosity are encountered when incorrect filler alloys were employed in either gas-metal or gas-tungsten arc welding of Al-Li based alloys. Welding with high energy density heat sources, such as electron beams or lasers, at high welding speeds can eliminate the need for a filler alloy, reduce the heat input to the workpiece, give a fine-scale, rapidly solidified weld pool microstructure and minimize weld cracking. But cracks are still observed perpendicular to the welding direction and close to the top surface, and, more seriously type I (spherical) pores and type II (irregular) pores

occur in either partial or full penetration welds[21].

VPPA welding, another high energy density heat source welding technique, has shown advantages in the Al-Li welding[22]. This section will discuss some problems found in welding of Al-Li. The material used in this study was aluminum-lithium alloy 2095 plate with a thickness of 8.5mm (1/3"), provided by NASA Marshall Space Flight Center. Plates were shaved from 9.5mm (3/8") to remove surface contamination.

19. SENSITIVITY OF Al-Li TO SHIELD GAS FLOW

The lithium in Al-Li alloys can easily be removed during melting since lithium is a particularly active element. Therefore welding on Al-Li alloy will be very sensitive to the shield gas, which protects the weld from the surrounding atmosphere.

Two cover pass welds were made consecutively with the same welding parameters except the voltage. Because the standoff is directly related to voltage, the standoffs were therefore different in the two welds. The specific welding parameters are listed in Table 3.

Figure 47 shows the surfaces of weld 1 (right side) and 2 (left side). Their cross sections are shown in Figure 48. Both indicate no porosity in the welds. Due to the higher energy input of weld 2, its cross section shows a higher penetration. However, its surface is dull, indicating oxidization at the weld surface, while the surface of weld 1 is smooth and shiny. Since the total shield flow rate was kept constant in both cases, weld 2, which had a larger standoff and therefore poorer

shielding, is more easily oxidized. This occurred after the standoff had changed only 1.7mm (0.066"). Welding of Al-Li is so sensitive to the standoff (voltage) that care must be taken to assure the correct standoff (voltage) is used so that the shielding is adequate.

Table 3 Welding Conditions for Al-Li 2095

Weld Sample	1	2
Welding Mode	cover pass	cover pass
Welding Current (A)	165	165
Welding Voltage (V)	23	25
F/R Time	19/4	19/4
Plasma Flow Rate (l/hr)	56	56
Shield Flow Rate (l/hr)	1400	1400
Torch Speed (mm/sec)	2.96	2.96
Electrode Size	3/16"	3/16"
Orifice Size	5/32"	5/32"
Standoff (mm)	1.37	3.05

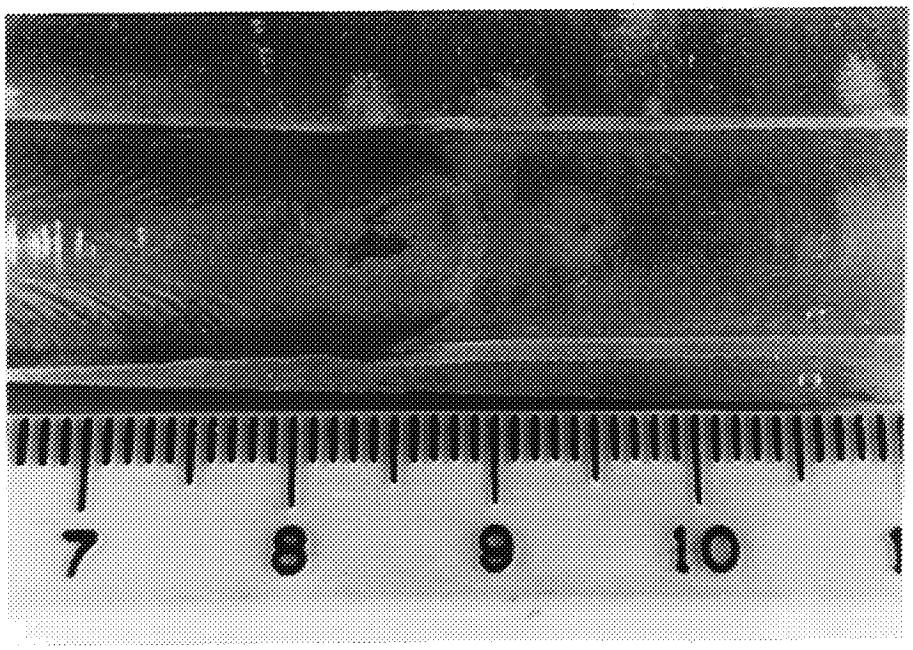

Figure 47 Comparison of Al-Li Weld Surfaces with Different Standoff (Voltage), Smaller Standoff(right) and Bigger Standoff(left).

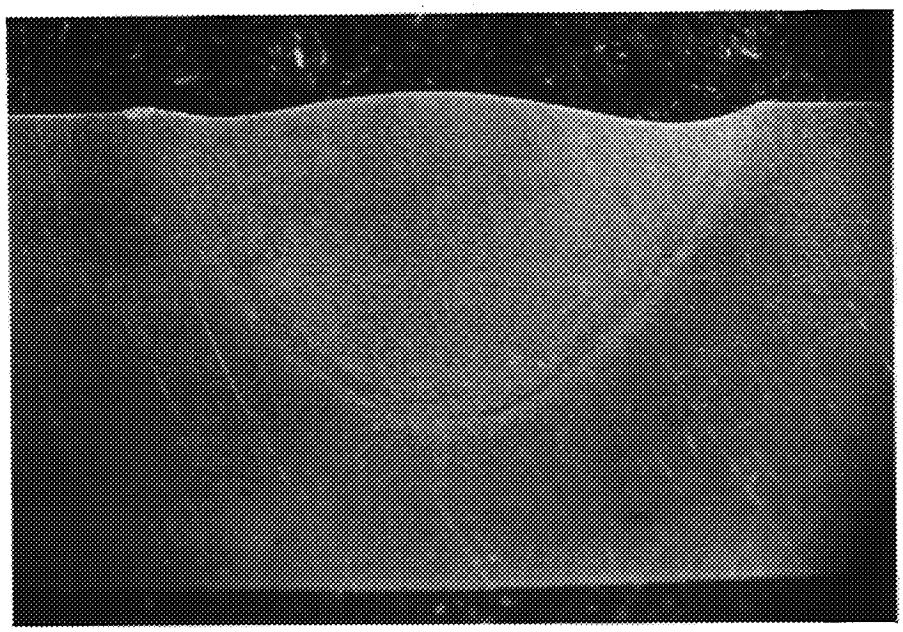

(a)

Figure 48 Comparison of Al-Li Weld Cross Sections with Different Standoff (Voltage), Weld 1, standoff 1.37mm(a).

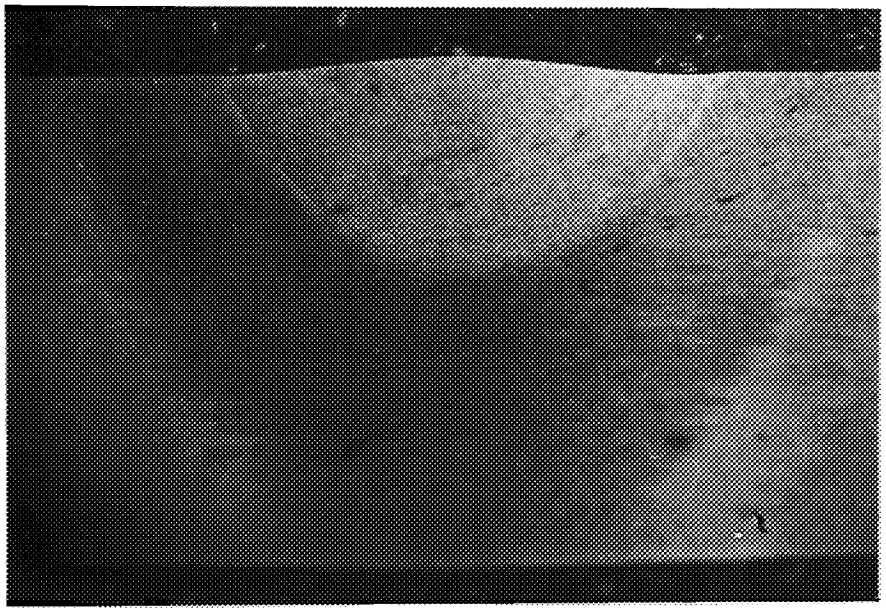

(b)

Figure 48 (continued) Comparison of Al-Li Weld Cross Sections with Different Standoff (Voltage), Weld 2, standoff 3.05mm(b).

20. HOT CRACKING IN 2095

Transverse weld cracks, longitudinal weld cracks, and crater cracks, can all occur during welding. Transverse weld cracks are perpendicular to the axis of the weld and are more common in joints having a high degree of restraint. Longitudinal weld cracks are predominantly within the weld metal and are usually confined to the center of the weld. Such cracks may occur as the extension of crater cracks formed at the end of the weld. They may also occur as extensions after successive weld passes of a crack that existed in an earlier pass. The final extension of the crack to the weld surface may occur during the cooling of the weld after welding operations

have been completed. Crater cracks are usually star-shaped and occur in the crater that is formed at the end of the weld. They can be initiation points for longitudinal weld cracks. These cracks are all associated with the solidification of the molten metal and are classified as solidification cracking.

During welding, a partially molten, i.e. two-phase, zone surrounds the moving weld pool. The partition and rejection of alloying elements at columnar grain boundaries and ahead of the advancing solid-liquid interface causes marked segregation. The segregant forms low melting phases or eutectics to produce a highly wetting films at grain boundaries. These films weaken the structure to the extent that cracks form at the boundaries under the influence of the tensile residual stresses that occur during cooling. These tensile stresses are actually the residual stresses caused by inhomogeneous thermal expansion (or contraction) and thus are termed "thermal stresses".

Thus, cooling rate is critical in avoiding hot cracking. Some studies have found that a slower cooling rate promotes segregation of insoluble constituents during solidification of 8090 Al-Li alloy[23]. On the other hand, cooling can also affect the temperature gradient and the thermal stresses cross the weld. Any measures which can improve the cooling process during welding may be helpful to minimize hot or solidification cracking.

21. MODIFICATION OF THE WELD TORCH WITH A GAS TRAILER

A torch trailer was used to help reduce the temperature gradient behind the

weld pool and thus the thermal stress. It was anticipated that the trailer would decrease the segregation tendency of undesirable constituents. The trailer was made of a polyethylene tube with a 1.27cm (1/2") O.D.. The tube was fixed at the bottom of the cylindrical torch. A schematic is shown in Figure 49 and a photograph is shown in Figure 50. Helium was used as the trailer gas because of its high thermal conductivity. A shadowgraph image of the plasma, shielding, and trailer cooling flow is shown in Figure 51.

Weld samples were made with the parameters listed in Table 3. Two passes were performed on each weld to build up enough stresses to insure hot cracking at the final crater.

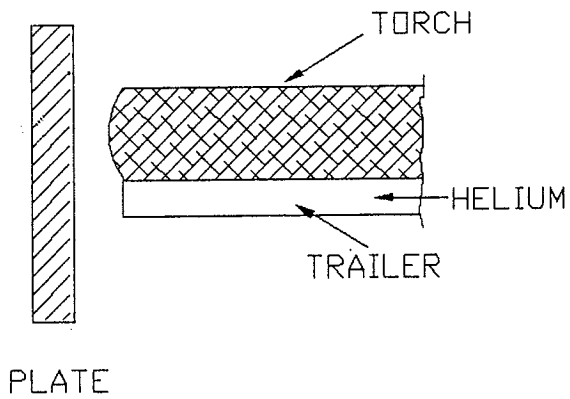

Figure 49 Schematic of Trailer and Torch.

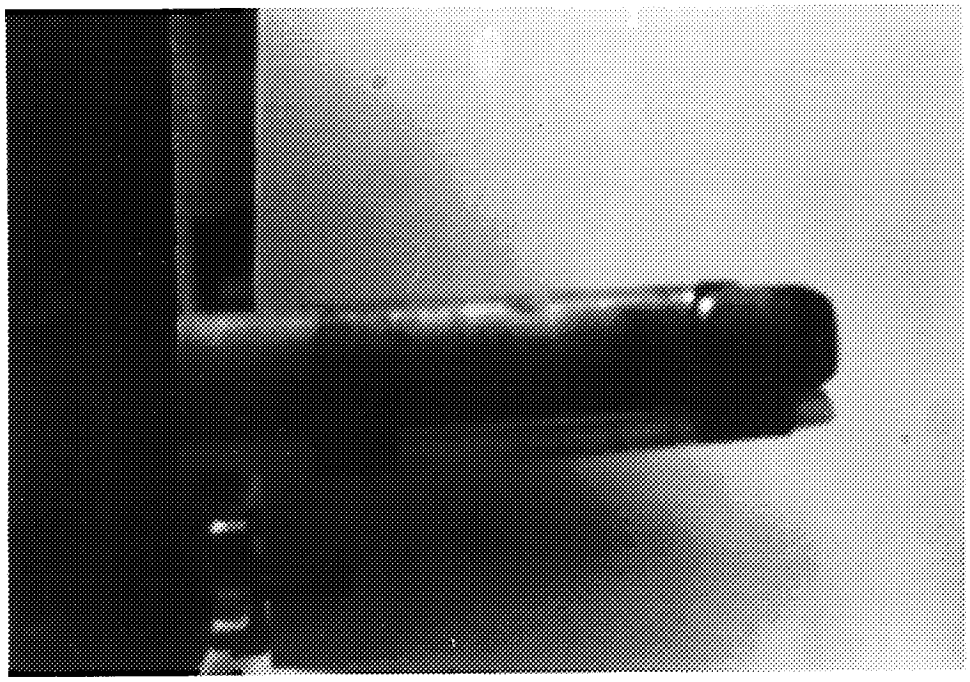

Figure 50 Photograph of Trailer and Torch.

Figure 51 Shadowgraph image of the Modified Torch.

Table 3 Comparison of Welding Conditions for Two Different Al-Li Welds

Weld Sample	1	2
Welding Current (A)	165	165
Welding Voltage (V)	23	23
F/R Time	19/4	19/4
Plasma Flow Rate (l/hr)	56	56
Shield Flow Rate (l/hr)	1400	1400
Torch Speed (mm/sec)	2.96	2.96
Pass Number	2	2
Trailer	no	yes
Flow Rate From Trailer (l/hr)	0	140

The surface of weld 1 (without trailer) is shown in Figure 52. It shows crater cracks and a longitudinal crack which starts from one crater crack and extends downward. While, Figure 53 shows the surface of weld 2 (with trailer). In this case, only moderate crater cracks can be observed. To further examine the crack, the welds were sectioned just below the crater. After being hot mounted, the sample was polished to a 1 μm finish. Keller's etch was used on the sample surface before photographs were taken. A cross section of each sample is shown in Figure 54. It is found that some small cracks are still present below the surface on the sample with the trailer. But, compared with the sample without trailer, the cracking is much less

pronounced. It is possible that an even better result could be obtained with an additional backside trailer and this is recommended for further study.

An optical micrograph of the crack in weld 1 is shown in Figure 55. Figure 56 is an SEM image of the same sample. They both indicate a brittle transgranular fracture mode.

22. CONCLUSIONS ON TORCH MODIFICATION FOR Al-Li

1. The quality of Al-Li welds is very sensitive to the standoff or adequacy of shield gas.

2. The application of a gas trailer to the original welding torch may improve the thermal stress conditions and decrease the segregation tendency. This modification can reduce hot cracking, which is a critical problem with Al-Li alloy welding.

3. An additional backside trailer is recommended for further study.

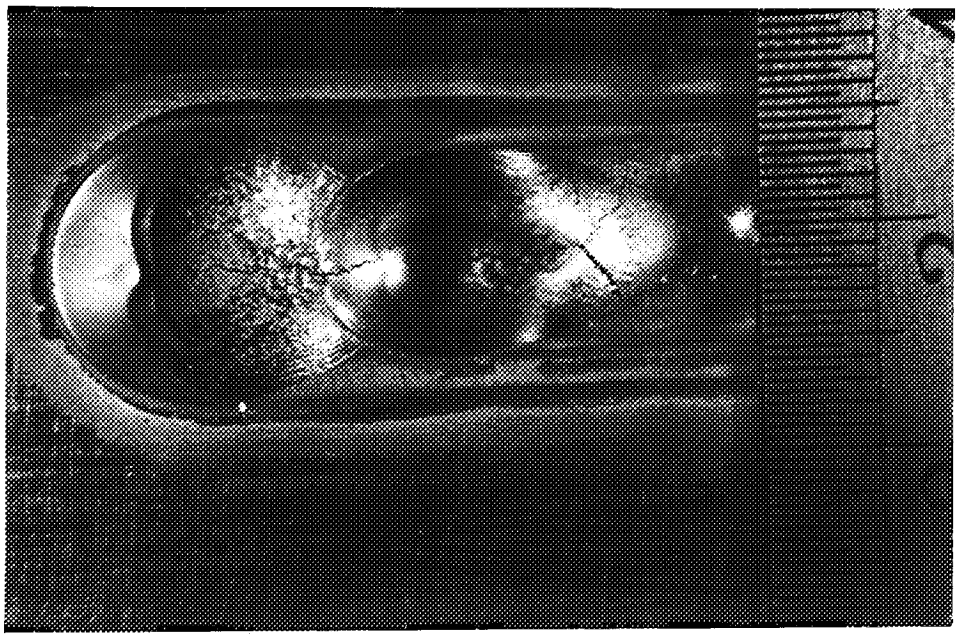

Figure 52 Surface of Al-Li Weld without Trailer.

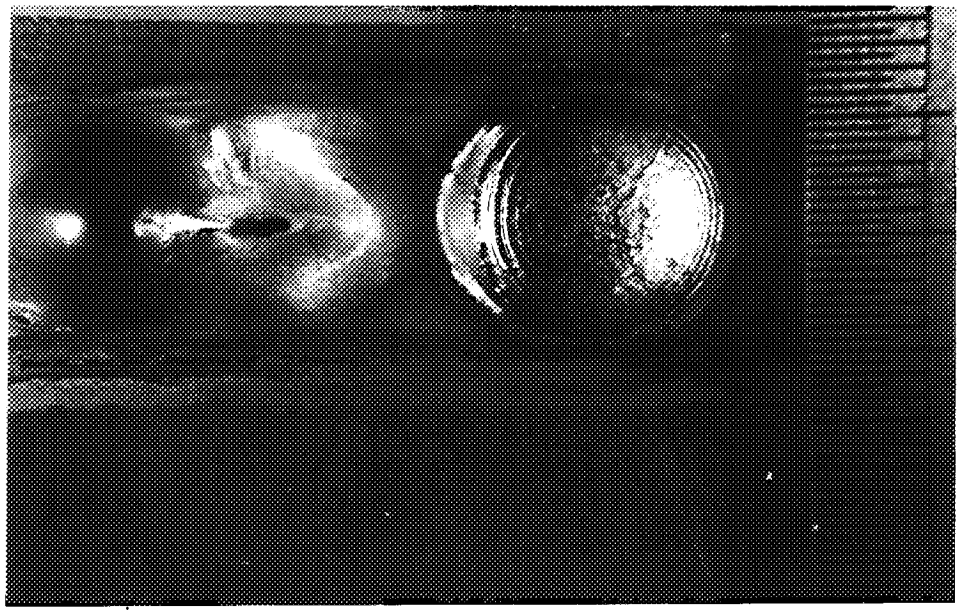

Figure 53 Surface of Al-Li Weld with Trailer.

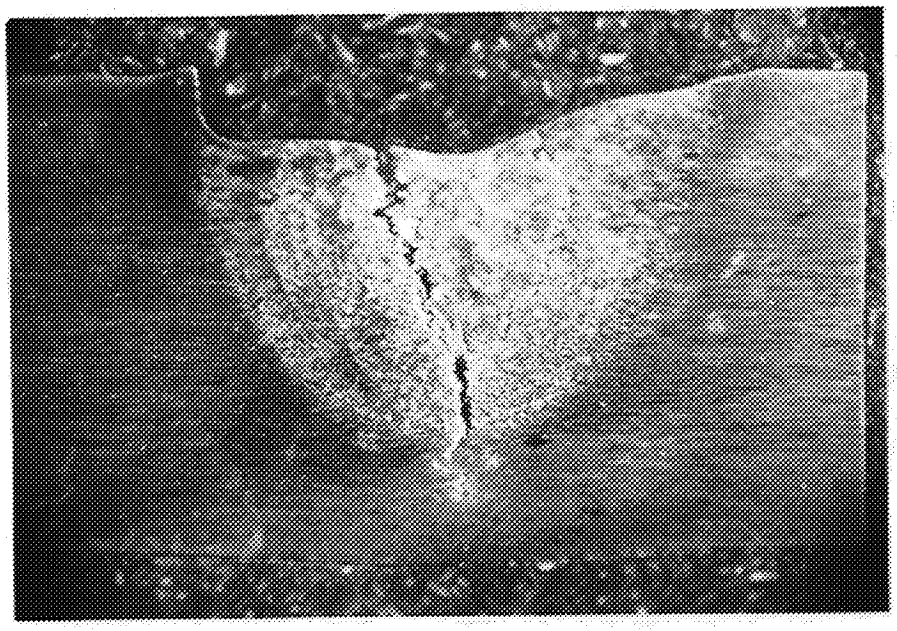

(a)

Figure 54 Cross Sections for Al-Li Welds, without Trailer(a).

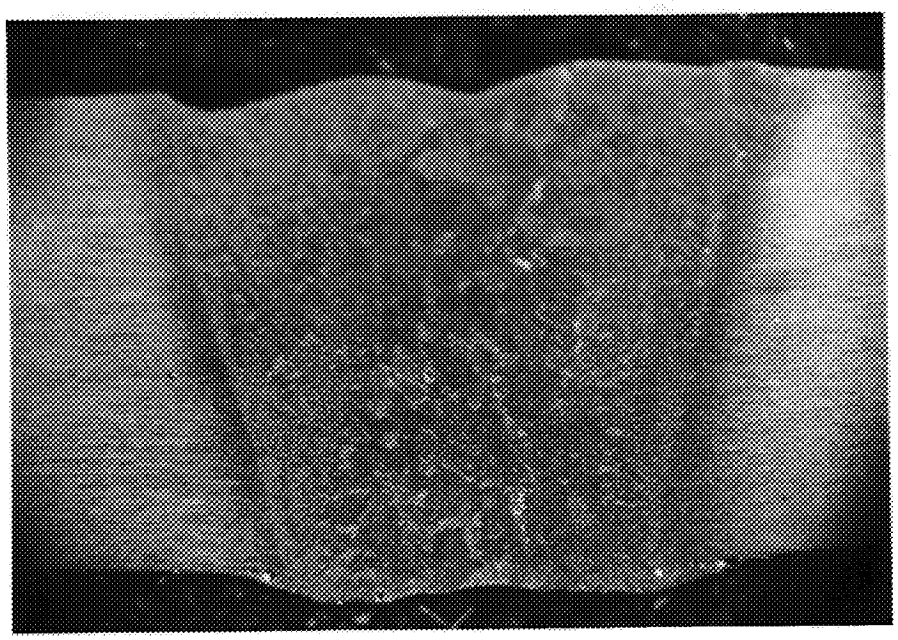

(b)

Figure 54 (continued) Cross Sections for Al-Li Welds, with Trailer(b).

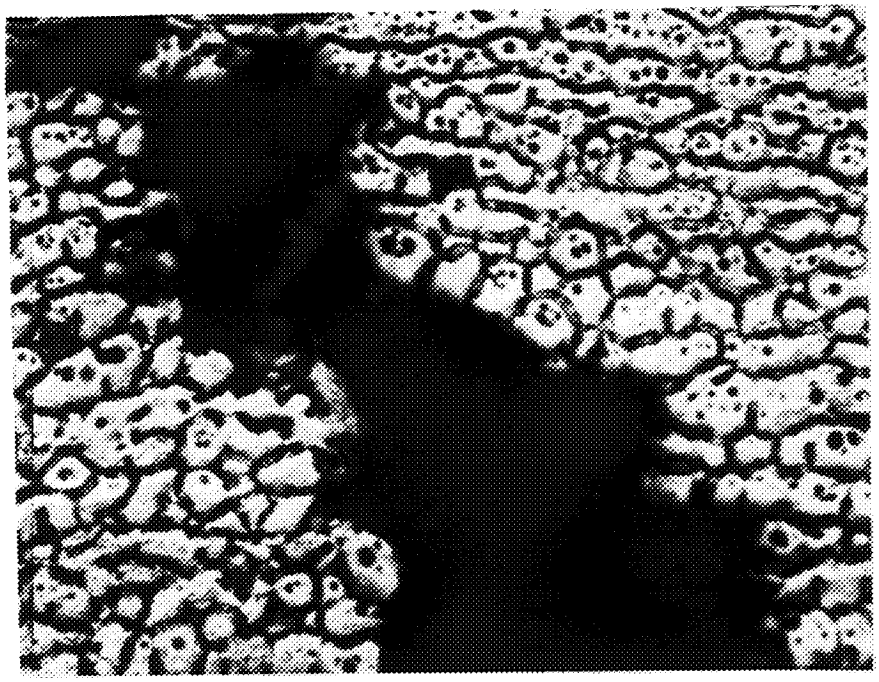

Figure 55 Optical Micrograph of Al-Li cracking (without trailer) (600X).

Figure 56 SEM Image of Al-Li cracking (without trailer).

23. SUMMARY CONCLUSIONS

1. The plasma gas plays a dominant role on the overall flow pattern. The shield gas can reduce the turbulence caused by the plasma gas and maintain the stability of the plasma arc. The presence of a high density of electrons in the plasma arc greatly affects the appearance of flow pattern in VPPA welding.

2. Undercutting in VPPA welding increased with increasing torch tilt angle. The undercutting sensitivity to torch tilt angle changes with different alloys. The effect of shielding flow rate on undercutting shows some complexity due to a combination of gas contamination within the shielding gas itself and the entrained gas contamination from the surrounding atmosphere. The degree of undercutting is strongly related to the total gas contaminant volume which contacts the weld pool. A minimum shielding gas flow rate consistent with adequate shielding is recommended to minimize the occurrence of undercutting.

3. The new mode 2 shield cup, which has a tapered inner shape and is slightly longer than the current cup, can reduce the welding standoff and thus the shield gas consumption while maintaining the required weld quality. This cup is also believed to reduce the tendency to undercut.

4. The quality of Al-Li welds is very sensitive to the standoff or shield adequacy. The application of a gas trailer to the original welding torch may improve the thermal stress condition and decrease segregation tendency. This modification can reduce hot cracking, which is a critical problem for Al-Li alloy welding. An additional backside trailer is recommended for further study.

REFERENCES

1. A.C. Nunes et al., "Variable Polarity Plasma Arc Welding on the Space Shuttle External Tank", *Welding Journal*, **36**(9), 1984, pp15-25.

2. T. Okada, H. Yamamoto and S. Harada, *Arc Physics and Weld Pool Behavior*, The Welding Institute (ed.), Cambridge, 1980, pp203.

3. G.J. Gibson, "Gas Flow Requirements for Inert-Gas-Shielded Arc Welding", *Welding J.*, **34**(4), 1953, pp198s-208s.

4. Wolfgang Merzkirch, *Flow Visualization, 2nd Edition*, Academic Press, Inc., 1987, pp124-128.

5. N.B. Vargaftok, *Tables on the Thermophysical Properties of Liquids and Gases, 2nd Edition*, John Wiley & Sons, Inc., 1975.

6. R.A. Alpher, and D.R. White, "Optical refractivity of high temperature gasses. II: Effects resulting from ionization of monatomic gases", *Phys. Fluids*, **2**, 1959, pp162-169.

7. R.H. Huddlestone and S.L. Leonard, Editor, *Plasma Diagnostic Techniques*, Academic Press, 1965, pp434.

8. A.C. Nunes, O.E. Bayless et al., "The Variable Polarity Plasma Arc Welding Process: Its Application to the Space Shuttle External Tank --- First Interim Report", NASA TM-82532, *NASA Technical Memorandum*, June, 1993, pp2.

9. T. Hashimoto, F. Matsuda, "Piercing Mechanism of the WeldPool in Electron Beam Welding", *Trans. Nat. Res. Inst. Met.*, **7**, 1965, pp117-185.

10. A. Matsunawa, "Role of Surface Tension in Fusion Welding", *Trans. IWRI*, **11**(2), 1982, pp145-154.

11. M.G. Velarde, C. Normand, "Convection", *Scientific American*, **7**, 1980, pp93-108.

12. Takamichi Iida and Roderick I.L. Guthrie, *The Physical Properties of Liquid Metals*, Clarendon Press, Oxford, 1988, pp134.

13. J.K. Brimacombe, F. Weinberg, "Observations of Surface Movements of Liquid Copper and Tin", *Metall. Tans.*, **3**, 1972, pp2298-2299.

14. M.R. Torres, *The Effect of Impure Gases on Variable Polarity Plasma Arc*

Welded 2219 Aluminum, M.S.Thesis, The University of Texas at El Paso, 1990, pp55.

15. L.F. Martinez, *Spectroscopic Measurements of Contaminants during VPPA Welding of Aluminum Alloys*, M.S.Thesis, The University of Texas at El Paso, 1992, pp34.

16. J.T. Liu, D.C. Weckman, H.W. Kerr, "The Effects of Process Variables on Pulsed Nd:YAG Laser Spot Welds : Part I AISI409 Stainless Steel", *Metall. Tans.*, **24B**(6), 1993, pp1065-1076.

17. G.L. Roy, "Status of Al-Li Development at Pechiney", *Aluminum-Lithium alloys ——— Design, Development and Application Update*, Edited by Ramesh J. Kar and Suphal P. Agrawal, ASM, 1988, pp79.

18. P.A.Molian and T.S.Srivatsan, "Weldability of Aluminum-Lithium Alloy 2090 Using Laser Welding", *J. Mater. Sci.*, **25**(7), 1990, pp3347-3358.

19. J.R. Pickens, "Review Recent Developments in the Weldability of Lithium-Contained Aluminum Alloys", *J. Mater. Sci.*, **25**, 1990, pp3035-3047.

20. I.J. Polmear, *Light Metals*, Edward Arnold, 1981, pp94.

21. I.R. Whitaker, D.G. McCartney, N. Calder, and W.M. Steen, "Microstructural characterization of CO2 laser welds in the Al-Li based alloy 8090", *J. Mater. Sci.*, **20**, 1993, pp5469-5478.

22. L.F. Martinez, J.C. McClure, and A.C. Nunes, "The Effect of Gas Contamination during Welding of Aluminum-Lithium Alloy", *Welding and Joining Processes*, PED - Vol. **50**, ASME, 1991, pp235-243.

23. Y.L. Liu, Z.Q. Hu, Y. Zhang, and C.X. Shi, "The Solidification Behavior of 8090 Al-Li Alloy", *Metall. Trans.* **24B**(10), 1993, pp857-865.